January 2024

UNoN / UNEP
MALAWI-Climate Change Adaptation

Search and Rescue operations in Malawi, 14 March 2023, following flooding caused by Tropical Cyclone Freddy. Photo: DoDMA Malawi

Flood Assessment in Malawi
UNON/UNEP Adaptation

References: Report ARIA /2023.050_V2
Related documents: -
Type of document: Associated study report
Document progress: Version 2
Accessibility: Restricted

ARIA Technologies	**Titre :** MALAWI-Climate Change Adaptation – **Flood Assessment in Malawi**						
ARIA Report. Number	23.050 V3						
ARIA Project Number	22.014						
Number of pages	95	**Figures**	73	**Tables**	19	**Appendix**	5
Author(s)	Hydroscience : Jean ALBERGEL AAA : ARIA /ACTERRA / AGRER : Lawrence FLINT- Céline DEANDREIS						
Subcontractors	Hydroscience : Jean ALBERGEL						

Documentary Interest				Accessibility	Confidential		Free	
Yes		No			ARIA Technologies		Restricted	

Document Status	Writter Nom/Date	Review Nom/Date
Version V1	Jean ALBERGEL (Hydroscience) 28/01/2024	
Version V2	Jean ALBERGEL (Hydroscience) 02/11/2023	
Version V3	Jean ALBERGEL (Hydroscience) 28/11/2023	

DIFFUSION	Date	Recipient	Number
e-mails	03/11/2023	AAA	1
Paper	-	-	-

TABLE OF CONTENT

LIST OF TABLES

LIST OF ILLUSTRATIONS

1. INTRODUCTION

This flood risk assessment supports the Malawi NAP-CRA task undertaken on behalf of the Government of Malawi, which sets out to:

i) to support the Department of Climate Change and Meteorological Services (DCCMS) of Malawi in its efforts to conduct climate change modelling, specifically in developing downscaled projections for eight selected districts, together representing the eight Agricultural Development Divisions of the country, distributed amongst the 3-4 agro-ecological zones of the country;

ii) to conduct a Climate Risk Assessment (CRA) for the country and amongst the eight selected districts.

It is envisioned that this flood risk assessment (FRA) will be conducted at a national level with the objective of risk zoning and compiling a more detailed risk assessment of three selected water basins in coordination with the relevant Malawian authorities for the survey on “Advancing the NAP process: Climate resilience for sustainable development in Malawi”. This FRA is based on available data, observed trends and on the information and knowledge produced by the climate downscaling/scenario projections. This assessment will enjoined by soil erosion projections in the same three water basins.

At the request of the surface water division and in consultation with the Environmental Affairs Department (EAD) and the Department of Water Resources of the Government of Malawi (GoM) and the Department of Disaster Management Affairs (DoDMA), the specific study takes into account the following water basins:

- Catchment 6: Dwangwa catchment, concentrating on Sub-catchment 6C: Dwangwa, Livulezi and Rupashe Rivers, Mpasadzi.
- Catchment 4: Linthipe Catchment, concentrating on Sub-catchment 4B: Lifidzi River.
- Catchment 7: South Rukuru, with a focus on Sub-Catchment 7E: South Rukuru.

This document, Version 3 (V3), builds upon the foundational knowledge presented in the previous edition, which was formulated based on bibliographic elements and the ERA5 climatic archives. Following the provision of data by the DCCMS, additional complementary work has been incorporated. This includes insights derived from weather station data and their subsequent climatic projections considering the DCCMS data.

2. FLOOD RISK ASSESSMENT AT NATIONAL SCALE

The general flood risk assessment data used in this work comes from:

- The Malawi Department of Disaster Management Affairs (DoDMA), which is responsible for responding to and managing disasters in the country including floods and provides information and updates on their website;
- The European Centre for Medium-Range Weather Forecasts (ECMWF), which provides current forecasts, climate reanalyses and specific datasets. These are available via the web, through point-to-point dissemination, data servers and broadcasting;
- The ESA (European Space Agency) Climate Office. Across the European Space Agency's Climate Change Initiative (CCI) programme, there are 26 Essential Climate Variable (ECV) projects;
- The Malawi Department of Climate Change and Meteorological Services (DCCMS);
- The United Nations Office for the Coordination of Humanitarian Affairs (OCHA), which provides updates and reports on the impact of floods in the country;
- International news agencies such as the BBC and Reuters, which provide coverage of natural disasters such as floods in Malawi;

- International non-governmental organizations (NGOs) such as Oxfam, Red Cross (IFRC) and ACT (Action by Churches Together International), which provide humanitarian assistance to those affected by floods in the country and also have reports and updates on their website;
- Climate Change and Development in Africa (CCDA), which provide detailed information on the impact of climate change on the continent and specifically in Malawi;
- The Asian Disaster Reduction Center (ADRC);
- Extension for Community Healthcare Outcomes (ECHO).

2.1 Context and historical floods in Malawi

Flood risk assessment in Malawi involves analysing various factors such as weather patterns, topography, land use and infrastructure to determine the likelihood and potential impact of flooding in specific areas. This information can be used to develop flood management plans and strategies to protect communities and infrastructure. Factors that contribute to flood risk in Malawi include heavy rainfall, inadequate drainage systems and deforestation. Climate change is also increasing the risk of flooding in the country.

Malawi is located in south-eastern Africa and is prone to seasonal heavy rainfall. The rainy season runs from December to April. The country experiences a mostly unimodal rainy season from November to April with the northernmost parts of the country experiencing peaks at the beginning and end of the season, a vestige of the twin rainy season phenomenon experienced in East Africa, the climate drivers of which, are shared in northern Malawi. These heavy rainfall events can cause flash floods and riverine flooding.
The country also experiences tropical storms/cyclones (low-pressure systems bringing heavy cyclonic rainfall and strong winds) that form over the Indian Ocean, affecting most especially Southern Malawi and the Central Region. Such weather patterns, combined with the country's topography and land use, can make certain areas particularly susceptible to flooding.
Malawi has several rivers that can cause significant damage during heavy rainfall events and floods.

The main rivers that have been known to cause damage in the past include (Figure 1):

1. **The Shire River:** The Shire River is the longest river in

2. Malawi and is a major tributary of the Zambezi River. The Shire is known to overflow its banks during heavy rainfall events. These heavy rainfall events cause flash floods and can result in riverine (fluvial) flooding, especially in the southernmost, low-lying, Lower Shire Valley (Chikwawa and Nsanje being two of the districts most affected).

3. **The Dwangwa River:** The Dwangwa River is located in the Central Region of Malawi and is known to cause flooding in the surrounding areas. During heavy rainfall events, the river can overflow its banks. Large volumes of water can cause flash floods that can damage homes, infrastructure and crops.

4. **The South Rukuru River:** The South Rukuru River is located in the Central and Northern region of Malawi and has caused significant damage in the past from flooding. The river can overflow its banks during heavy rainfall events, causing riverine flooding.

5. **The Lilongwe River:** The Lilongwe River is located in the central region of Malawi. Heavy rainfall events cause the river to swell its banks which may lead to flooding, affecting both urban and rural areas.

In general, the southern Lower Shire basin of Malawi is highly prone to flooding due to its low elevation and flatness and to its proximity to the Shire River, which is the major river of the country and only outlet of Lake Malawi, and its tributary, the Ruo River, both of which are known to overflow their banks during heavy rainfall events. The shoreline areas around the Lake also experience flooding due to overflow of water from the lake and heavy rainfall in the catchment areas of streams that flow into the Lake bringing heavy loads of silt, made worse by deforestation and poor farming methods which gets deposited near to river mouths as flow reduces, blocking channels and causing overbanking in lakeshore areas.

Malawi has experienced several severe floods in recent years. A striking set of floods occurred during the rainy season, November 2021 to April 2022, where heavy rainfall caused severe flooding and landslides in several parts of the country. In late January 2022, Cyclone Ana exacerbated this succession of events, already exceptional in their severity. Ana heavily affected Southern Malawi. Throughout the country, 37 people were reported dead with another 22 remaining missing as of 31 January, while 158 people were injured. 200,000 had to leave their homes and 109,359 people were forced to relocate to temporary emergency relief camps. Most of the country lost electricity as floodwaters damaged the Kapichira Hydroelectric Power Station, which provides 30% of the country's electricity. The nationwide electricity supply remained intermittent long after the storm passed. Access to clean water and sanitation deteriorated significantly and, to date, Malawi is experiencing the largest cholera outbreak in its history. It has affected more than 54,300 people, of whom 1,671 have died (from 2 March 2022 to 11 April 2023), a situation which worsened considerably in the aftermath of the next tropical storm to hit southern Malawi - Cyclone Freddy in March 2023[1].

Another severe flood occurred in March 2019 that affected over 1 million people and caused widespread damage to homes, infrastructure and crops in the wake of Cyclone Idai. Heavy rainfall with several rivers overflowing caused flooding in many parts of the country. The worst affected areas were the districts of Chikwawa, Nsanje, Phalombe and Thyolo. Before these events, a devastating flood hit Malawi in 2015. The flood affected over 1.5 million people and caused widespread damage to homes, infrastructure and crops. The flooding caused by heavy rainfall and the overflowing of several rivers resulted the in loss of human lives and displacement of thousands of people.

It is worth noting that these are just a few examples of the floods that have occurred in recent years. Floods are recurrent events in the country and often have severe impacts on the population. Table 1 gives the main floods in the country since 2000 with their characteristics. The table highlights the vulnerability of Malawi to flooding and shows the importance of preparedness measures to reduce the impact of such disasters.

An analysis of the floods that have hit Malawi since the beginning of the 21st century offers two types of meteorological phenomena that cause these disasters

i) atmospheric blocking over the range of ITCZ that will oscillate several days in a row and can create heavy rainfall often accompanied by hail and strong winds,

ii) tropical storms of cyclonic type that are born in the Indian Ocean and arrive in Malawi after having crossed Madagascar and recharged in moisture over the Mozambique Channel (such as Tropical Storm Ana - Figure 2a) or those born on the Mozambique Channel and arriving in Malawi (such as Tropical Storm Idai - Figure 2b). When a tropical storm follows heavy front rains, it can lead to catastrophic impacts such as occurred during the rainy season 2021-2022.

1 https://reliefweb.int/report/malawi/malawi-africa-cholera-outbreak-operation-update-1-dref-operation-ndeg-mdrmw017

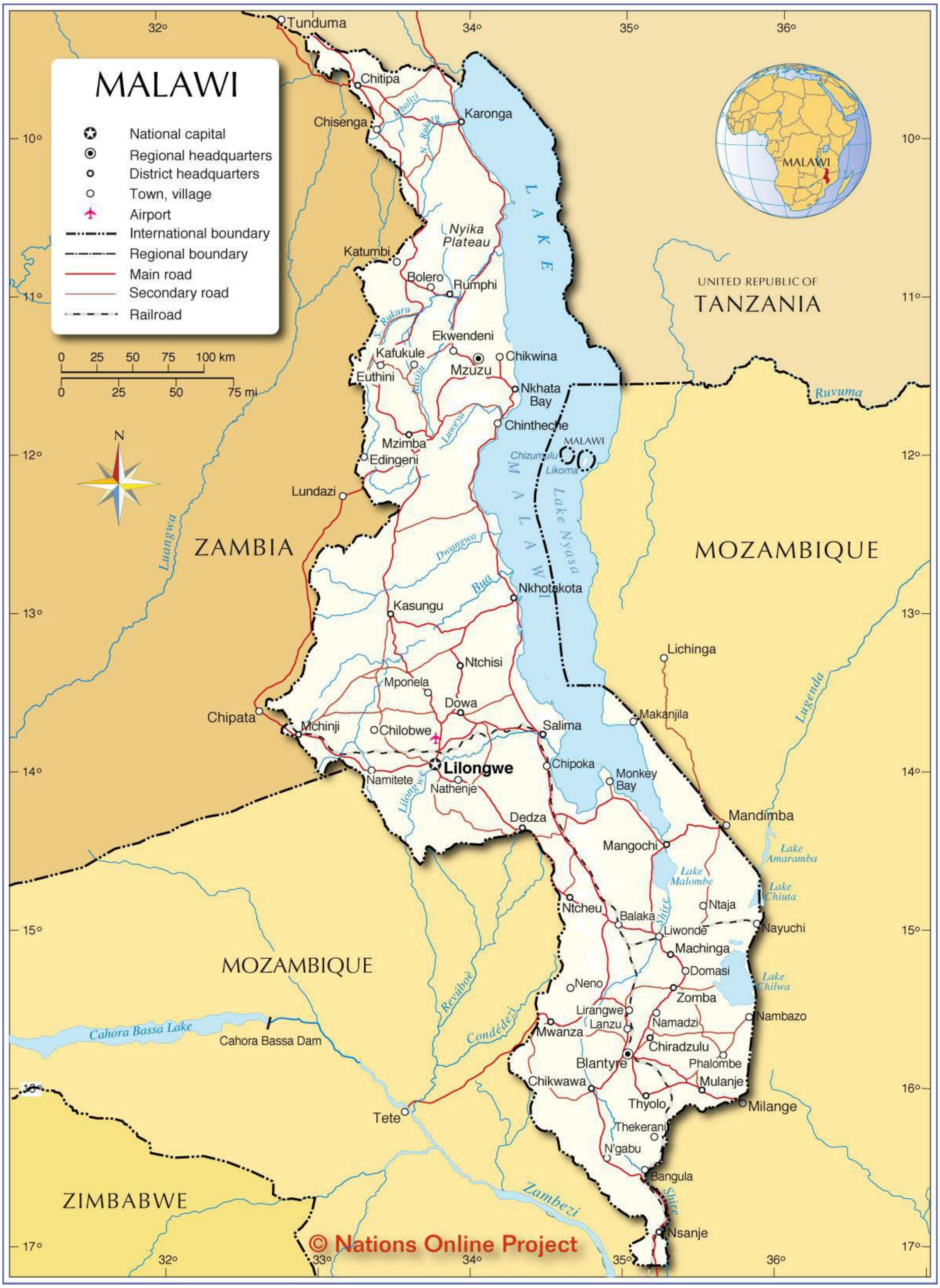

Figure 1: Map of Malawi with main rivers. Source: nations online project maps

Event	Meteorological conditions	Most affected districts	Damage estimation	Remarks
February 2001	Heavy downpour with unique intensity; ITCZ oscillating over Southern Malawi.	Nsanje, Chikwawa, Salima, Nkhotakota	Farmland affected: ha 55,859 People affected: 312,530 in 62,506 households	Source: UN RC Malawi
January 2003	Heavy rains falling, Tropical Storm Delfina	Rumphi, Ntchisi, Karonga.	People killed, at least 7 People displaced, thousands of Landslides in Salawi River Catchment, Critical food shortages, Damages at power station at Nkula & power rationing.	Source: UN RC Malawi. ADRC, DCCMS
January 2007	Heavy rains, ITCZ oscillating over Southern Malawi.	Chikwaka, Nsanje, Mangochi, Ntheu, Salima, Karonga.	Households affected: 25,400 Houses Collapsed: 2,333 Farmland affected: ha 9,552 - Livestock lost: 837	Source: IFRC
January 2008	Heavy rains linked to the 'La Nina' phenomenon since December affecting Mozambique Malawi, Zambia, Zimbabwe	Chikwaka, Nsanje.	3 deaths confirmed 16,845 people displaced 523 Houses destroyed Farmland affected: ha 471.7	Source: ACT (Action by Churches Together International)
December 2014, January 2015	Heavy Rains in December Tropical Storm Chedza in January	15 out of 28 Districts, more affected: Nsanje, Chikwawa, Phalombe.	106 deaths confirmed, 172 reported missing, 230,000 people displaced, Infrastructure damages: roads, bridges railway line, power lines, water points	Source: DCCMS; ECHO; IFRC
February to April 2017	Locally heavy thunderstorms and rain showers. Easterly waves over most areas of Malawi coupled with ITCZ	Koranga, Lilongwe, Nkhotakota Chitipia, Nkhata Bay	16 deaths confirmed, 9,000 people displaced, 5,520 households affected 1075 ha of crops fields Bridge of Jalawa washed away, Flooding in Lilongwe, Malawi Capital Infrastructures affected.	Source: DCCMS, ECMWF
March 2019	Tropical Cyclone Idai (tropical disturbance over the Mozambique Channel) - highest recording: 255.5mm at Mpemba Met Station during 24h	13 districts, Chikwawa, Nsanje, Phalombe, and Thyolo most affected	Over 60 deaths and 577 injuries reported, 162,240 households affected and about 87,000 displaced people, Infrastructures affected: transport, energy, water supply & sanitation, water resources.	Source: OCHA, UN RC Malawi, World Bank, GFDRR
February 2020	Heavy Rainfalls, ITCZ oscillating over Northern - Central Malawi	Lilongwe, Dowa, Salima	3 people died in the Lilongwe River, Streets of the capital flooded up to 1.5 metres deep, major damage to infrastructures: Kamuzu Central Hospital, Corporate Mall, Biwi Township	Source: ECHO

Event	Meteorological conditions	Most affected districts	Damage estimation	Remarks
November 2021 January 2022	Heavy rain and hail around 18 November, 21 december, Tropical Storm Ana lashed the Southern and Central Districts of Malawi from Monday 24 January	Lilongwe, Mulanje, Mangochi, Chikwawa, Ntcheu, Machinga, Balaka, Zomba, Chiradzulu, Phalombe, Salima, Mzuzu and Blantyre	Period July to 19 November: 11,100 households affected with 13 registered deaths and 51 injuries Period 9 December to January: total number of affected people has increased to 42,684 people. A total of 12,955 people were displaced and 87 injured. With Tropical Storm Ana January: 37 people reported dead with another 22 remaining missing as of 31 January. 158 people were injured. Most of the country lost electricity, and 200,000 had to leave their homes. 109.359 people were forced to reside in emergency camps. Floods damaged the Kapichira Hydroelectric Power Station, which provides 30% of the country's electricity. The country experienced an outbreak of cholera. It has affected over 33,600 people, of whom 1,093 have died to date	Source: OCHA, IFRC, DCCMS.
March 2023	Cyclone/Tropical Storm Freddy	14 districts of Malawi, the whole of Southern Region, especially the districts of Blantyre, Chikwawa, Chiradzulu, Mulanje, Mwanza, Neno, Nsanje, Thyolo, Phalombe and Zomba	12-15 March 2023, heavy cyclonic rains and strong winds, pluvial/flash and fluvial flooding, land/rock/mudslides causing damage to infrastructure such as roads, buildings and electricity plants and lines. As of 6 April 2023: 2,267,458 people affected, 676 killed with 537 more missing, 2171 injured, 659,278 displaced people in 767 camps,[2] and flooded an area equivalent to 400 km2 flooded. Power lost across country as turbines in hydroelectric stations had to be shut down because of debris entering. Concern over further spread of cholera and other water-borne diseases. Schools turned into centres for displaced persons.	Sources: UK.gov and bbc.co.uk, msf.org, DoDMA AA News Agency, Turkey

Table 1: Main floods occurred in Malawi since year 2000

[2] https://reliefweb.int/report/malawi/wfp-malawi-cyclone-freddy-response-update-6-april-2023-0800-cat

a) Tropical Storm Ana 2022	b: Tropical Stotm Idai 2019

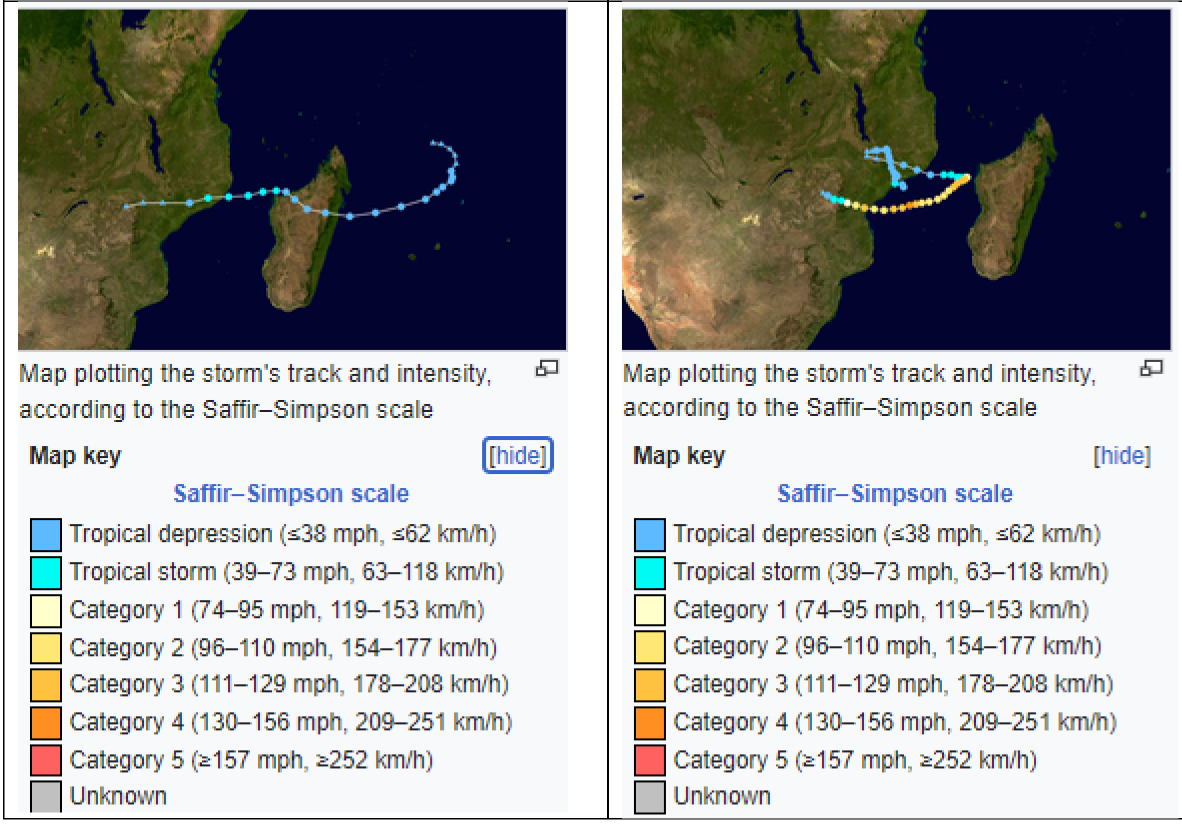

Figure 2: Tropical depressions arriving on Malawi (Source : Created by Meow using WikiProject Tropical cyclones/Tracks . The background image is from NASA. Tracking data is from NRL and NO

At the time of writing this report (March 2023), a new tropical storm has hit the country: Storm Freddy. Very Intense Tropical Cyclone Freddy was an exceptionally long-lived, powerful, and deadly storm that traversed the southern Indian Ocean for more than five weeks in February and March 2023. Freddy is both the longest lasting and highest ACE (Accumulated Cyclone Energy)-producing tropical cyclone ever recorded. It was the fourth named storm of the 2022–23 Australian region cyclone season, and the second very intense tropical cyclone of the 2022–23 South-West Indian Ocean cyclone season. Tropical Storm Freddy led to people being swept away by raging waters, and being buried under landslides. It killed at least well over 1000 peopleeople in Malawi alone.[3] Blantyre, the hilly commercial capital of Malawi, wasworst affected, with residents dying in landslides and homes crumbling into floodwaters.[4]

The histogram in Figure 3 shows an increase in the number of cyclones recorded in the NOAA cyclones database since the post-war period. We can observe 7 significant cyclones from 1944 to 1983 and 11 cyclones from 1984 to 2023 (considering the cyclone season ended at the time of writing).
It seems that tropical storms are linked to a weak Oceanic Niño Index[5] during the cyclone period (December to February) corresponding mostly to La Niña events, while during El Niño events (strong Oceanic Niño

[3] https://www.reuters.com/world/africa/cyclone-freddy-death-toll-jumps-over-1000-malawi-president-says-2023-04-12/ and https://en.wikipedia.org/wiki/Cyclone_Freddy

[4] "Cyclone Freddy Survivors Dig with Bare Hands for Victims as Death Toll Reaches 326," CNN March &6, 2023 https://www.reddit.com/r/worldnews/comments/11t3uyb/cyclone_freddy_survivors_dig_with_bare_hands_for/

[5] https://www.climate.gov/news-features/understanding-climate/climate-variability-oceanic-ni%C3%B1o-index

Index), the climate is drier and calmer over the Indian Ocean[6]. La Niña, which is the cold phase of the El Niño-Southern Oscillation (ENSO), can potentially have an impact on the formation of depressions in the Indian Ocean. During La Niña, changes in large-scale atmospheric circulation patterns can create favourable conditions for the development of low-pressure systems including depressions in the Indian Ocean region. The Indian Ocean Dipole (IOD), which is a sea surface temperature pattern in the Indian Ocean, can also play a role in the formation of depressions in the region. During a positive IOD phase, which can sometimes occur during La Niña, sea surface temperatures (SSTs) are warmer in the western Indian Ocean and cooler in the eastern Indian Ocean. This can create conditions that are favourable for the development of low-pressure systems in the region including depressions that are capable of producing severe tropical storms.[7]

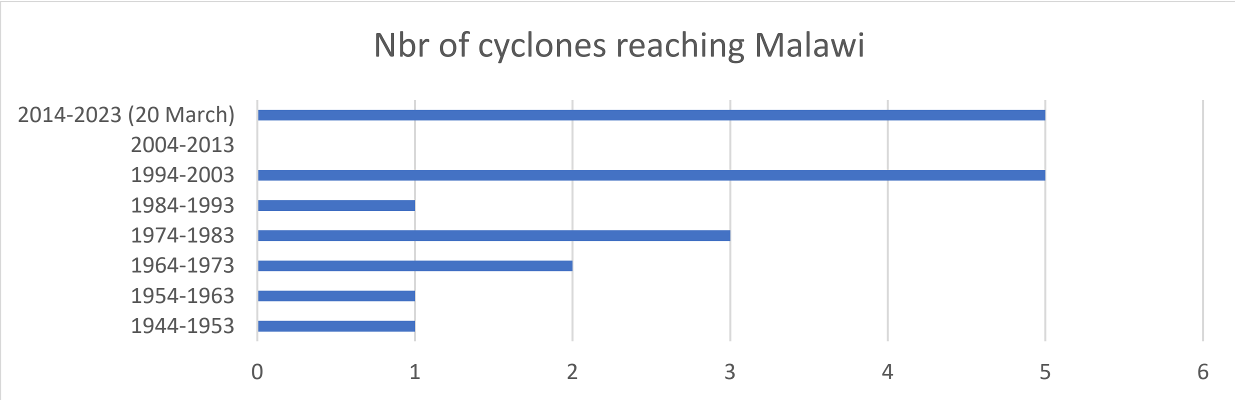

Figure 3: Ten-year interval number of significant cyclones reaching Malawi (source NOAA)

However, it is important to note that the relationship between La Niña, the IOD and depression formation in the Indian Ocean is complex and not well understood. Many other factors can influence the formation of low-pressure systems in the region including local sea surface temperatures (SSTs), atmospheric humidity and wind patterns.

It's also important to consider that even if La Niña or the IOD creates favourable conditions for the formation of depressions in the Indian Ocean, the specific path and intensity of a depression can still be influenced by a number of other factors, including upper-level wind patterns and SSTs.

Therefore, it is important for communities in the Indian Ocean influenced region, including Malawi, to be prepared, especially in terms of Disaster Risk Reduction and Management (DRR and DRM) for extreme weather events, regardless of the evolution of La Niña or IOD events.

Looking at the focus districts and the location of the floods, we can distinguish three types of floods:

6. **Lakeshore flooding**. Lakeshore flooding in Malawi is a frequent occurrence that occurs due to heavy rains in watershed areas of steams flowing into Lake Malawi or the overflow of the lake, which is one of the largest freshwater lakes in the world. The flooding can cause significant damage to infrastructure, homes and crops, as well as displacing local communitiesleading to the spread of waterborne diseases.

7. **Riverine floods**. Riverine floods in Malawi occur when rivers overflow their banks and flood nearby areas. These floods are often caused by heavy rains, poor drainage systems and deforestation, which can lead to soil erosion and an increase in runoff. Riverine floods can, as with lakeshore

[6] Astier N. Plu M. Claud C. (2015) Associations between tropical cyclone activity in the Southwest Indian Ocean and El Niño Southern Oscillation Atmospheric Sciences Letters. RMets Volume16. Issue4. October/December 2015 Pages 506-511. https://doi.org/10.1002/asl.589

[7] Wu. X.. Okumura. Y. M.. & DiNezio. P. N. (2019). What Controls the Duration of El Niño and La Niña Events?. Journal of Climate. 32(18). 5941-5965.. https://journals.ametsoc.org/view/journals/clim/32/18/jcli-d-18-0681.1.xml

flooding, cause significant damage to infrastructure, homes and crops, as well as displacing local communities, leading to the spread of waterborne diseases.

8. **Flash Floods**. Flash floods in Malawi are sudden and intense floods that occur because of heavy rainfall over a short period. They can cause widespread damage to infrastructure, homes and crops, resulting in loss of life and displacement of local communities. The country's geography and topography, combined with poor drainage systems and deforestation, make it particularly vulnerable to flash floods. The deposition of eroded sediments in low-lying, slower-flowing areas of the river system, caused by soil erosion upstream and the collapse of embankments of streams due to human activity lead to flooding in lakeshore communities and lands and reduce drainage.

2.2 Land use and flood risk

While weather conditions are the cause of flooding and weather forecasting is the best means of flood warning, land use is a factor that can exacerbate or mitigate the risk. Among the factors aggravating floods, three are considered for which human activity is responsible:

1. Deforestation and land-use changes that reduce the ability of natural ecosystems to absorb and retain water;
2. Urbanization and urban development that can reduce the capacity of natural waterways to absorb excess water;
3. Climate change, which can alter precipitation patterns and increase the frequency and severity of extreme weather events.

At the country level, we studied the variation over time of deforestation and urbanization.

Climate Data Sets provide global maps allotting the land surface into 22 classes, [8] which have been defined using the United Nations Food and Agriculture Organization's (UN FAO) Land Cover Classification System (LCCS). In addition to land cover (LC) maps, four quality flags are produced to document the reliability of the classification and change detection. In order to ensure continuity, these LC maps are consistent with the series of global annual LC maps from the 1990s to 2015 produced by the European Space Agency (ESA) Climate Change Initiative (CCI), which are also available on the ESA CCI LC viewer.[9]

We divided land cover datasets for Malawi over the period 1992-2020 into 6 categories: Forest, Crops, Shrubs, Wetlands, Urban (which includes bare surfaces) and "Other," which corresponds mainly to areas covered by water bodies. Land cover areas in km² are given for each of these classes in Annex 1 and are represented in Figure 4.

[8] https://cds.climate.copernicus.eu/

[9] Copernicus Climate Change Service, Climate Data Store, (2019): Land cover classification gridded maps from 1992 to present derived from satellite observation. Copernicus Climate Change Service (C3S) Climate Data Store (CDS). (Accessed on 23-Nov-2023), 10.24381/cds.006f2c9a

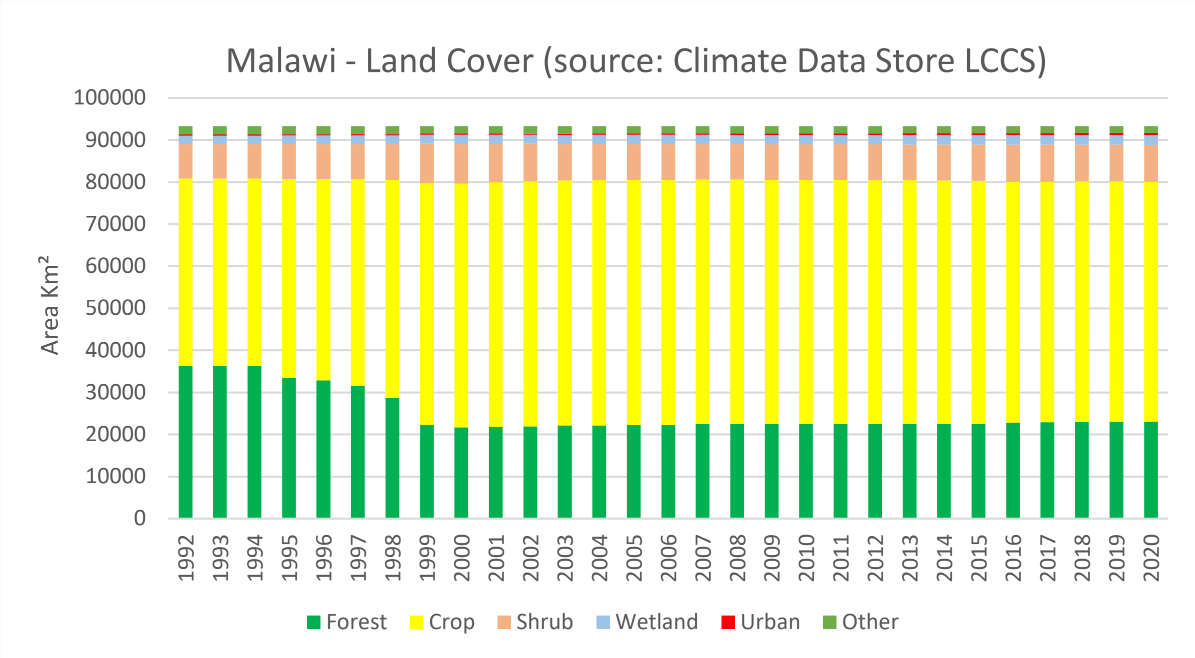

Figure 4: Stacked bar plot of Land Cover in km²

Heavy deforestation can be observed at the end of the 1990s in favour of increased cultivation throughout the country (Figure 5). Forest and cultivated areas have remained constant since the early 2000s. There has been a slight decrease in agricultural activity in recent years, which is related to the increase in degraded land (shrubs) and wetlands. Deforestation is a factor aggravating the floods.

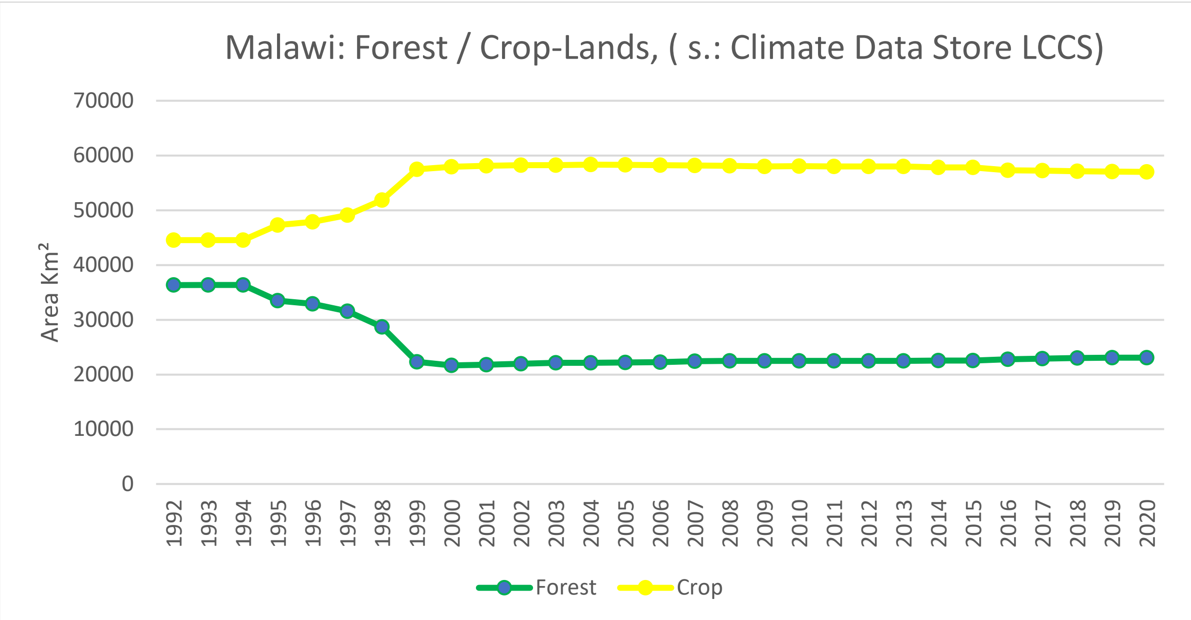

Figure 5: Evolution of forest cover and cultivated cover

Although remaining relatively moderate at the country scale, the urbanized areas are increasing in areal extent (Figure 6). Considering the importance of infrastructure in the city, this increase in urban land cover with low permeability increases flood as well as health risks and danger of damage to buildings, and infrastructure as well as to lives and livelihoods.

.

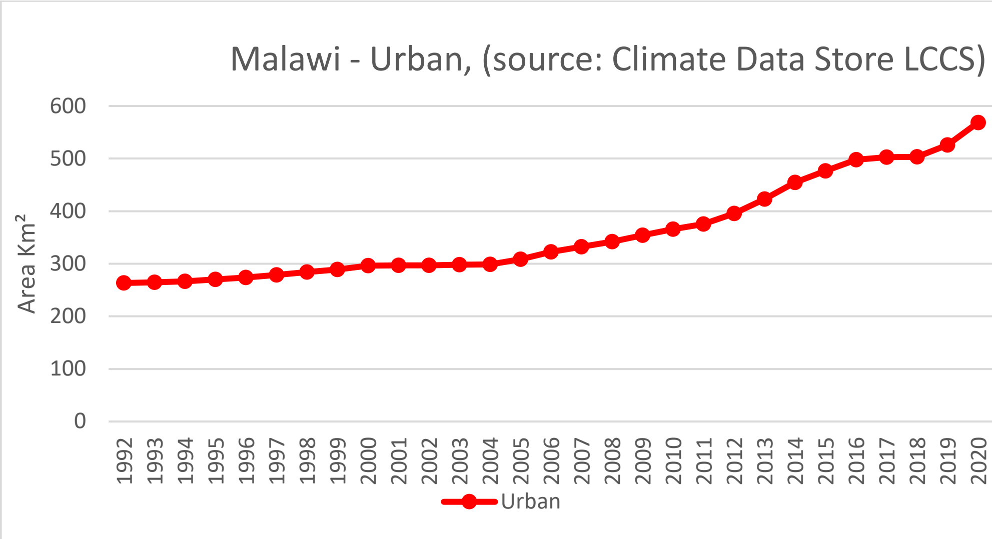

Figure 6: Urban area growth

Deforestation and increasing urbanization have led to increased loss of life and property in the history of flooding events (see Table 1).

We have selected three dates to compare the evolution of land cover (Figure 7):

1. 1992, which marks the commencement of available satellite observations.
2. 2000, corresponding to the peak of deforestation and the onset of the increase in urbanized areas.
3. 2020, representing the current situation, the latest available year on the Copernicus platform when we conducted this study (corresponding to version 1 of this report).As can be seen deforestation decreased substantially in the period 1992-2000.

Land cover 1992	Land Cover 2000	Land Cover 2020
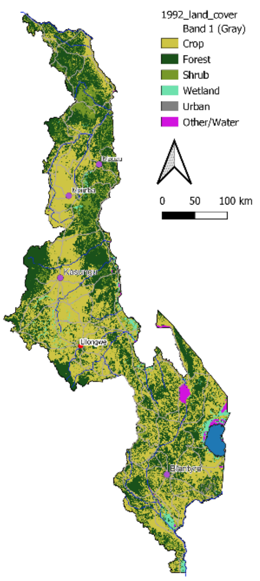	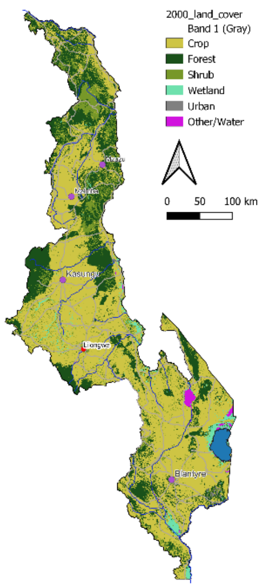	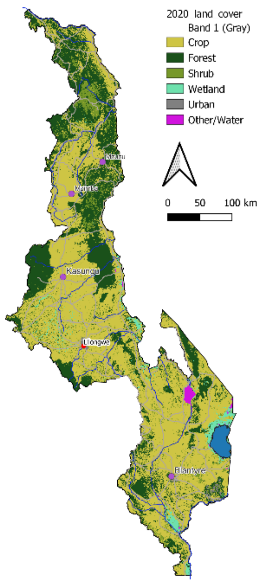

Figure 7: Land cover evolution, 1990, 2000, 2020

Regions with Most Deforestation in Malawi are:

- Southern Malawi: Historically, the Southern region of Malawi has seen significant deforestation. This is partly due to the high population density in this area, leading to increased land clearing for agriculture and charcoal production.
- Central Malawi: The Central region, particularly areas surrounding Lilongwe, the capital city, has also experienced notable deforestation. Urban expansion and the need for agricultural land are primary contributors here.
- Deforestation Hotspots: Specific districts like Chikwawa, Nsanje, and parts of the Shire Valley are deforestation hotspots due to the prevalence of commercial agriculture and the use of wood for fuel. In addition to this very few trees grow in the floodplains of the Lower Shire and are very much in demand for fuel.

The scale of the maps does not allow for an easy comparison of the growth of urbanized areas. Later in this report, we will review maps at a smaller scale for urban centres in the targeted watersheds for this study: Lilongwe and other urban centres in the Linthipe watershed, Mzuzu in the South Rukuru watershed.

At the country scale, a closer examination of regions where the expansion of urbanized areas poses a risk of infrastructure loss due to flooding particularly highlights the agglomeration of Lilongwe, Blantyre (which is not in a watershed targeted by this study), and Mzuzu.

1. Lilongwe: As the capital and one of the fastest-growing cities in Malawi, Lilongwe has seen substantial urban expansion. This growth often comes at the expense of surrounding forested and natural areas (See § on Linthipe watershed).
2. Blantyre: The commercial and industrial hub of Malawi, Blantyre, has also experienced significant urban growth, leading to increased pressure on nearby land and resources.
3. Mzuzu: Mzuzu, as the capital of Malawi's Northern Region, has seen rapid urban expansion. This growth is primarily due to rural-urban migration, economic opportunities, and its role as a commercial and administrative centre.

2.3 Lakeshore flooding

The European Space Agency (ESA) Lake project is a satellite-based initiative that monitors the world's largest lakes. This project has as its objective a better understanding of lake dynamics and the impact of climate change on these important freshwater resources. The data provided by the ESA Lake project includes the landmark and distance to land dataset of more than two thousand lakes in the world.

Lake level data: ESA's Climate Change Initiative (CCI) provides global satellite-derived lake level data for more than 60 large lakes, including Lake Malawi selected for their size, importance for freshwater resources, and their susceptibility to climate change impacts. The data are available from 1992 to the present and can be used for various applications, such as water resource management and climate studies. The data provided by CCI includes lake-level time series, derived from radar altimetry measurements from the ESA’s Sentinel-3 satellite, which allow for monitoring of lake level changes over time. This information is critical for understanding the impacts of climate change on freshwater resources and for managing these resources sustainably.

Lake surface temperature data: ESA's CCI also provides satellite-derived lake-surface temperature data for more than 30 lakes around the world, including Lake Malawi, Lake Tanganyika and the Great Lakes of North America. The data are available from 1981 to the present and can be used for various applications, such as fisheries management and climate studies. The temperature of lake water is measured using infrared sensors on board the satellite.

Lake water quality data: ESA's Sentinel-2 satellite provides high-resolution optical imagery to monitor water quality parameters, such as chlorophyll-a concentration in lakes. This data can be used to support the management of freshwater resources and the monitoring of harmful algal blooms. The concentration of chlorophyll-a, a pigment found in algae, is used to estimate the level of primary productivity in the lake.

Lake ice: Changes in the extent and thickness of ice cover on the lake surface are measured using microwave sensors. This data is not relevant for low altitude sub-tropical lakes.

The data obtained from these measurements are processed and analysed to create detailed maps and time series of lake properties. This includes identifying seasonal patterns, trends over time, and comparisons between different lakes. The data can also be used to develop models to predict future lake behaviour under different climate scenarios. Overall, the ESA Lake project provides valuable information for water resource management, ecosystem monitoring, and climate change research.
The data can be accessed through various online platforms, such as the ESA Climate Change Initiative,[10] and the Copernicus Open Access Hub.[11]

Here we use water heights observed by different satellites (Figure 8). A chronicle of these water heights recorded manually on water level gauges would be necessary to validate these data.

Figure 9 shows the evolution of the maximum annual height of Lake Malawi recorded by the satellites. This height is strongly dependent on the downstream hydraulic control of Kamuzu Barrage on Shire River at Liwonde, constructed in 1965 and upgraded in 2015. This barrage controls water flow to generate electricity for the country but also connects Liwonde and Balaka townships. It controls water levels upstream and increases the storage capacity of the lake.

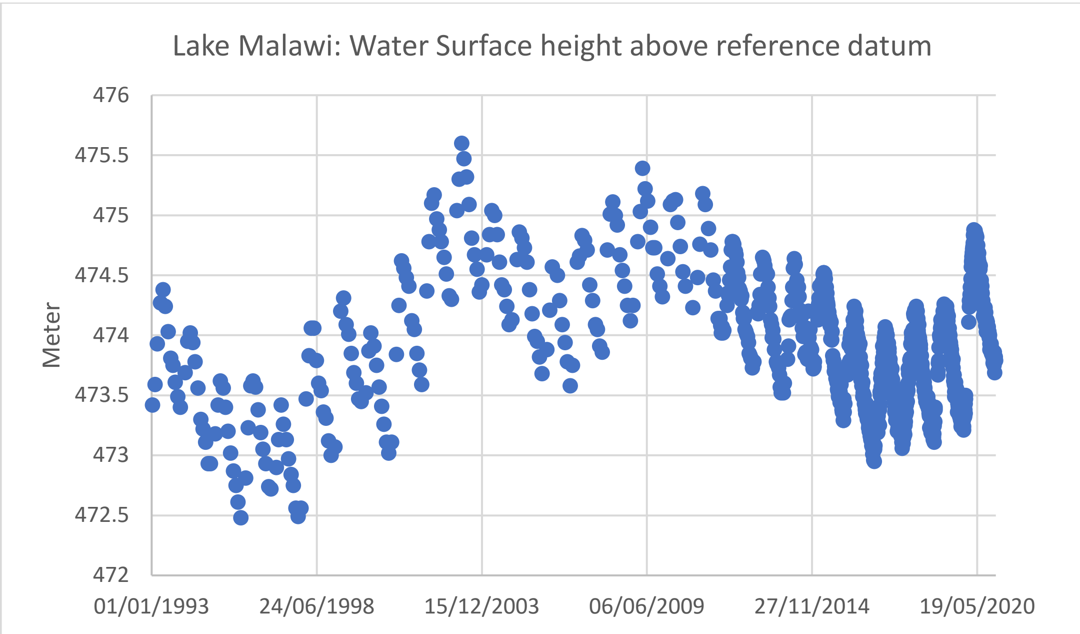

Figure 8: Variation of the lake level

[10] https://climate.esa.int/en/projects/lakes/

[11] https://scihub.copernicus.eu/

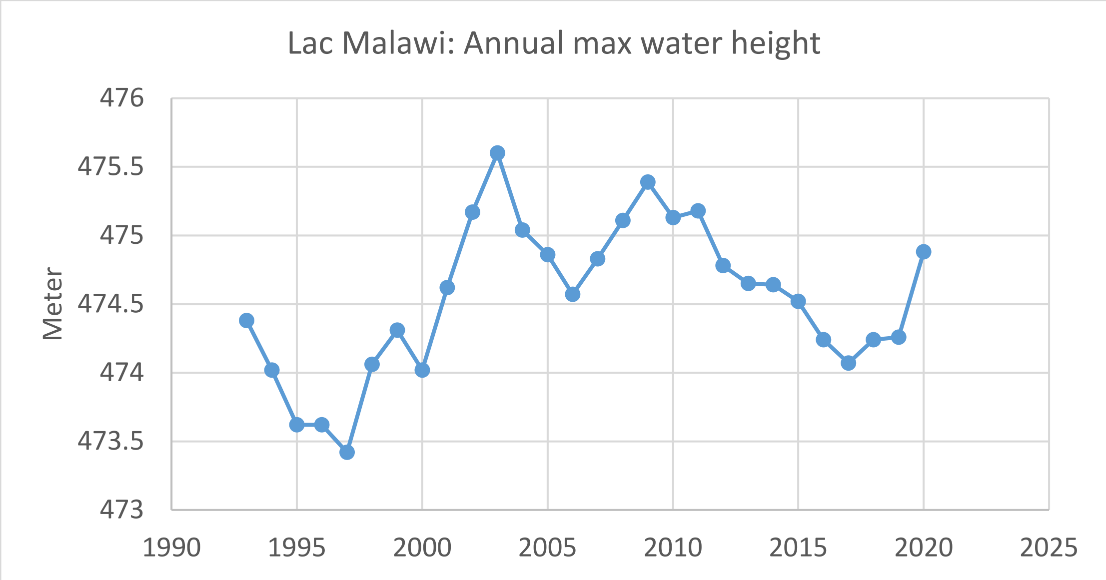

Figure 9: Evolution of the annual maximum lake water levels

To give an idea of settlements and infrastructure to be prioritized in preparation for lake flooding scenarios, we used a digital elevation model (DEM) based on the *World Geodetic System 1984 ensemble* (EPSG:6326) to extract 1m topographic contours for the whole country. The DEM dataset has a limited accuracy of 2m at best. We then used a GIS to “vectorize” the DEM by drawing contour lines to approximate the topography of the land surface after which the contour representing an elevation 1m above the lake surface was used to select towns and settlements situated below this elevation.

The GIS found the lakeshore to sit at ~477m geodesic elevation. Given that the satellite imagery used to compile the DEM was collected in 2009 when satellite altimetry showed the lake level to be closer to 475m, this suggests a precision error of ~2m. The extracted contour representing 1m above the lake surface (Figure 10) is thus meant to approximate 476m geodetic height. Figure 9 and the accompanying table show the towns and settlements to be protected from lakeshore flooding given their elevation relative to this 476m topographic contour line.

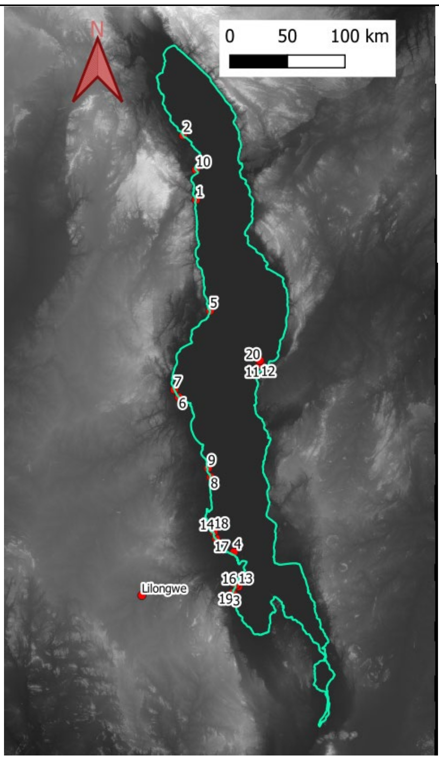

Figure 10: Infrastructure to be protected around the lake between elevation 475.6m and 476m

	Towns around lake below 476m
1	Rukuru Point
2	Ngara
3	Ndindi
4	Kachulu
5	Chisi Point
6	Ngala
7	Kasitu
8	Sani
9	Kawerama
10	Hara
11	Chiguluwindi
12	Chiponde
13	Mzunza village
14	Mwanjowa Village
15	Makho Village
16	Mkwaila village
17	Mpilingidzo GVH
18	Makho GVH
19	GVH Ntika
20	Chipyela

2.4 Riverine and flash floods.

Flood risk indicators are usually developed by using both the Topographic Wetness Index (TWI) and the average annual rainfall. Incorporating multiple variables is often necessary to develop a more comprehensive understanding of flood risk in a given area.

TWI provides information about the relative moisture availability in a given area based on local topography, while the average annual rainfall provides information about the overall amount of precipitation that an area receives. By combining these two variables, it is possible to identify areas that are more susceptible to flooding due to a combination of high rainfall and a high potential for surface runoff or infiltration.
The formula for calculating TWI, as defined by Beven and Kirkby (1979)[12], is

$$\boldsymbol{TWI = ln\left(\frac{a}{\tan(b)}\right)}$$

where :

- ***a*** is the local upslope area draining through a given pixel and
- ***tan(b)*** is the local slope in radians.

The formula combines information on slope, aspect, and elevation. The upslope contributing area (*a*) is a measure of the area upstream of a given point that contributes flow to that point. The slope angle (*b*) is used to estimate the water-holding capacity of the soil and the potential for runoff. Overall, $\boldsymbol{TWI}$ can be a valuable tool in flood risk assessment, providing information about the relative moisture availability in a

[12] Beven, K. J., and Kirkby, M. J. (1979). A physically based, variable contributing area model of basin hydrology. *Hydrological Science Bulletin*, 24 (1): 43–69. doi:10.1080/02626667909491834.

given area and the potential for surface runoff and infiltration of water into the soil. $\boldsymbol{TWI}$ is a dimensionless index that ranges from 0 to 1, with higher values indicating areas with greater moisture availability.

One approach to developing a flood risk indicator using $\boldsymbol{TWI}$ and average annual rainfall is to create a composite index that combines both variables. We have developed this indicator using a regression analysis where we first normalize the average annual precipitation values for the whole country on a 0 to 1 scale. These normalized precipitation values are then multiplied by the $\boldsymbol{TWI}$ values such that :

$$\boldsymbol{FRI_n = 10.\frac{FR - \min_n(FR_i)}{\max_n(FR_i) - \min_n(FR_i)}}$$

Where $\boldsymbol{FRI_n}$ is the flood risk index normalized on a scale of 0 to 10. $\boldsymbol{FR}$ represents the non-normalized flood risk index and is equivalent to:

$$\boldsymbol{FR = \frac{P - \min_n(P_i)}{\max_n(P) - \min_n(P_i)} * TWI}$$

Where ***P*** is the average annual precipitation (in m) in a given pixel.

One drawback to using such an approach is that since the precipitation values are normalized using only ERA rainfall data within the country's borders, the calculated index is not necessarily of absolute flood risk, but rather of the *relative* flood risk, i.e. the flood risk for certain parts of the country compared to others. This may, nevertheless, be helpful for planning and management purposes.

Alternatively, TWI and average annual rainfall can be used separately to develop flood risk maps for different types of flooding. For example, areas with high TWI values may be more susceptible to flash flooding, while areas with high rainfall may be more susceptible to river flooding.

For rainfall we used the ERA5 database. ERA5 is a global atmospheric reanalysis dataset of fifth generation, produced by the European Centre for Medium-Range Weather Forecasts (ECMWF). It provides comprehensive information on atmospheric conditions such as temperature, wind, precipitation, and pressure at different levels of the atmosphere, from the surface up to 80 km altitude. It provides also a wide range of hydrological data, including:

- Precipitation: ERA5 provides estimates of precipitation at the surface and at various vertical levels in the atmosphere, including snowfall and rainfall.
- Evaporation: ERA5 provides estimates of evaporation from the land surface and from water bodies, including lakes and oceans.
- Soil moisture: ERA5 provides estimates of soil moisture content in different soil layers.
- Runoff: ERA5 provides estimates of runoff from land surfaces and river basins.
- Snow cover: ERA5 provides estimates of snow depth and snow cover fraction.
- River discharge: ERA5 provides estimates of river discharge at various locations across the globe.
- Water vapour: ERA5 provides estimates of water vapor content in the atmosphere.

ERA5 combines observational data from various sources including satellite measurements, ground-based weather stations, and buoys, with the latest advancements in weather forecasting models to create a consistent global record of the Earth's climate since 1979. The dataset is updated every month and is freely available for download from the ECMWF website.

The area of an ERA5 grid cell varies with latitude due to the convergence of meridians at the poles. At the equator, an ERA5 grid cell has an area of approximately 0.25 degrees of longitude by 0.25 degrees of latitude, which corresponds to about 27.8 km² (10.7 square miles).

ERA5 data has a high spatial and temporal resolution, making it valuable for a wide range of applications, including weather forecasting, climate research, and environmental monitoring. The dataset has been widely used by scientists, researchers, and policymakers to better understand and predict the Earth's climate system.

ERA5 data can be displayed on maps using a variety of software tools, including Geographic Information Systems (GIS) software, online mapping tools, and scientific visualization software. Maps can show various types of data, such as precipitation, temperature, wind speed, and atmospheric pressure, at different spatial and temporal scales.

For this study, we downloaded rainfall data, evaporation data, total runoff and sub-surface runoff at a daily resolution from the Climate Data Store (CDS) website, [13] which is operated by the European Centre for Medium-Range Weather Forecasts (ECMWF) (Annex 2).

The data on the map (Figure 11) gives an average precipitation of 1778 mm (70 in) with a standard deviation of 186 mm for the whole country. In much of the country, annual precipitation is between 800 and 2000 mm, and it's generally more abundant in the north, where, March and April are very rainy with more than 3,000 mm on the Nyika Plateau, but also on the southern slopes of Mount Mulanje.

The map in Figure 12 is a visual representation of the TWI values across the country. It has been created using Geographic Information System (GIS) software and digital elevation models (DEMs) of the country. The TWI values are calculated (in %) for each pixel in the DEM and represented as a colour gradient, where drier areas are typically shown in shades of yellow, and wetter areas are shown in shades of blue. This map is useful for identifying areas of high soil moisture, potential wetlands, and predicting the location of stream channels. It shows high soil moisture in some places on the lakeshore and mostly in the valley of the Shire River, but also in the other valleys.

The resulting composite index can be used to identify areas that are more at risk for flooding based on both the TWI and average annual rainfall (Figure 13). The most sensitive places for flooding are:

1. Nyika plateau, most of which sits at over 2100 m contains a high flood hazard. Mudslides, local flooding, and the occurrence of swampy ground during the rainy season are frequent. The foot of the escarpments is particularly at risk, but very little infrastructure is found in this area.
2. Lakeshore areas: Lake Malawi is the country's largest body of water and is prone to flooding during periods of heavy rain. The lakeshore areas, particularly in the northern and central parts of the country, are vulnerable to flooding.
3. Lower Shire Valley: This area is situated in the southernmost part of the country and is particularly vulnerable to flooding due to its low-lying floodplain terrain and proximity to the Shire River, which is prone to overflowing its banks in the aftermath of heavy rainfall events upriver in the portions of the Lower Shire Basin into which substantial tributaries flow such as the Mwanza and Ruo Rivers or when the lake levels (Malawi and Malombe) surge.
4. Karonga District: This district, located in the northern part of Malawi, is often affected by floods due to its location in a low-lying area that is prone to heavy rainfall. The town of Karonga (capital of Karonga District) is situated at an elevation of 478 m.
5. Chikwawa and Nsanje Districts: These districts, located in the Lower Shire Valley, are particularly vulnerable to flooding due to location and proximity to the Shire River.

[13] https://cds.climate.copernicus.eu/#!/home

6. Lilongwe District: The capital city of Malawi, Lilongwe, is located in this district, which is prone to flooding due to its location near several rivers and streams.

The exact locations and severity of floods can vary from year to year, depending on factors such as rainfall patterns and infrastructure development.

We noted very high rainfall on the Nyika Plateau, but it was not possible to verify these values. The country has no rain gauge station in this area, which is problematic as the rainfall on the Plateau presents ramifications for the water budget potential of the larger region. Nor do we have details of the algorithm that enables ERA5 to extrapolate annual rainfall close to 3 m in this region. We take these values but warn that they may be exaggerated. With regard to the analysis of the flood hazard, these high values imply a strong hazard, as the plateau has no significant slopes allowing concentrations of run-off water to be evacuated.

From the ERA5 data we looked at whether precipitation and runoff (water that flows over the land surface and into rivers, lakes, and other bodies of water) showed a trend over the period 1958 - 2021. The trend graph lines fitted to the data show an increasing trend in these values (Figure 14). But this increase is smaller than the standard deviation of the sample and is not significant in both cases. We can therefore consider this sample of values as a random selection within a population.

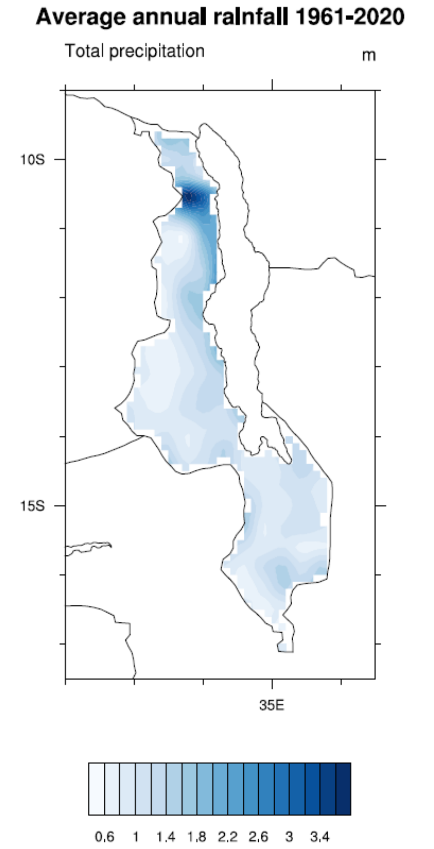

Figure 11: Annual rainfall 1961-2020

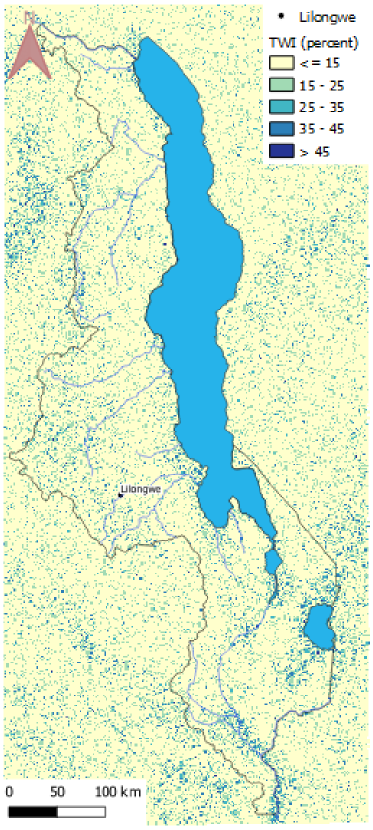

Figure 12: Topographic Wetness Index

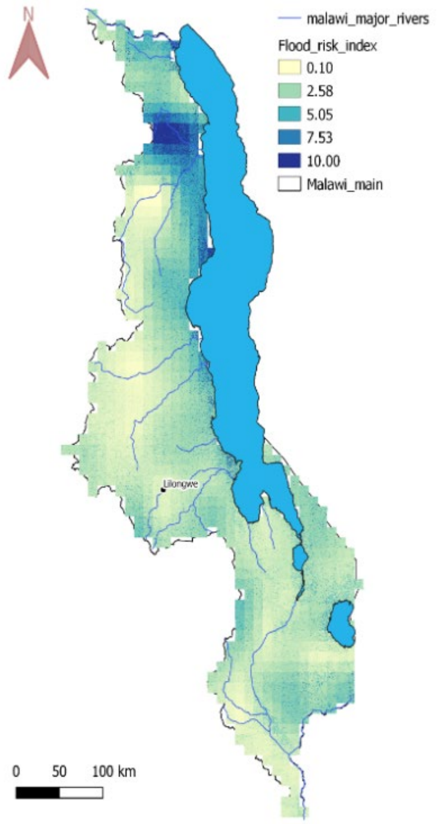

Figure 13: Normalized flood risk index

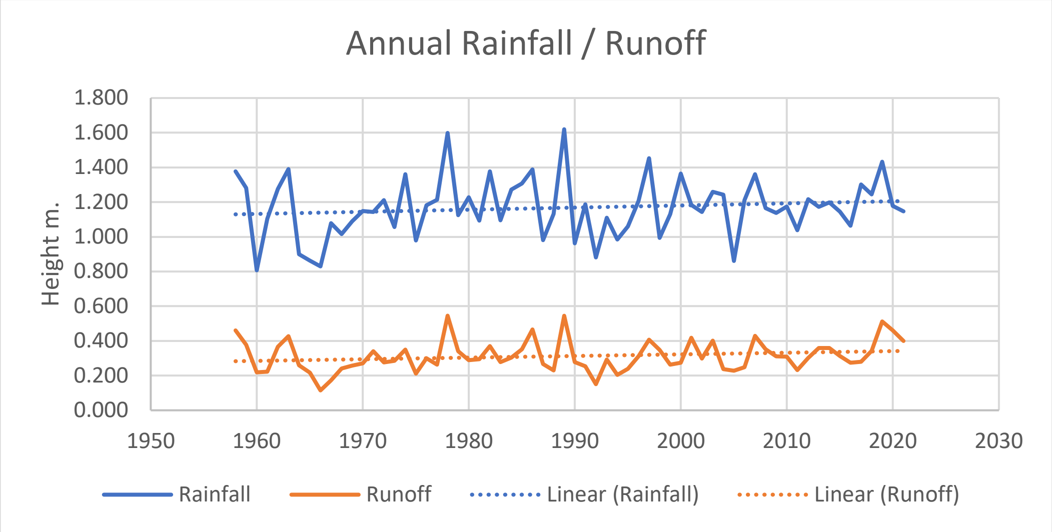

Figure 14: Malawi; Annual rainfall and runoff trends (source CDS - ECMWF)

The correlation between precipitation and annual runoff is significant (Figure 15).

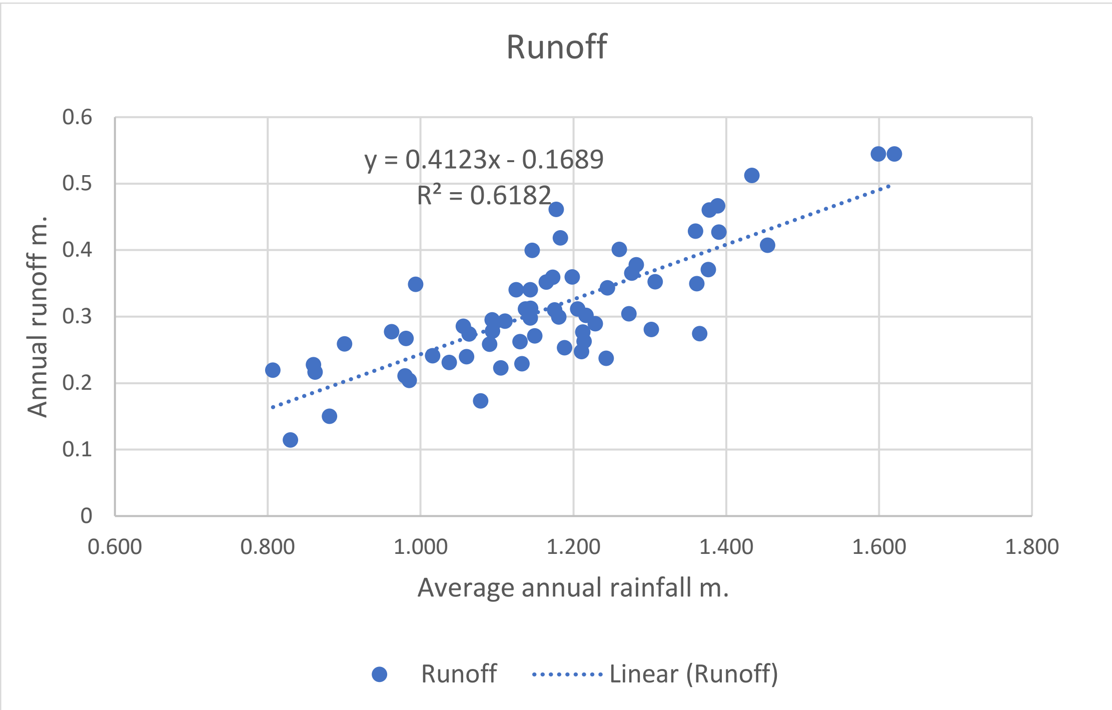

Figure 15: Malawi; Correlation between annual rainfall and runoff (source CDS - ECMWF)

A search for values of rainfall and runoff of rare occurrences was carried out using a software adapted for statistics on geophysical chronicles. DIXLOI is a software written in FORTRAN 77, [14] allowing for a selection of continuous statistical distributions on samples of observed values. This software allows making the best fit of ten statistical distributions, to compute all the parameters of these distributions and the fit tests. It also gives the graphical representations of these fits. Figure 16 shows the fit of the statistical distributions

14 Lebel Thierry, Boyer Jean-François. (1987). Notice utilisateur du logiciel DIXLOI : un ensemble de programmes FORTRAN 77 pour l'ajustement de lois statistiques et leur représentation graphique. Montpellier : ORSTOM, 42 p. multigr. https://www.documentation.ird.fr/hor/fdi:010014668

not rejected by the software (χ^2 test =0) but the one that fits best (Brunet Moret's test) is the Gumbel distribution. The data are represented on a Gaussian scale.

The Gumbel distribution is named after the French mathematician Emil Gumbel, who introduced it in the early 20th century. It is widely used in various fields, including hydrology, engineering, finance, and environmental sciences, to model extreme events and estimate their probabilities.

The Gumbel distribution is characterized by two parameters: location parameter (μ) and scale parameter (β). The location parameter determines the location of the maximum or minimum value, while the scale parameter controls the spread of the distribution. The probability density function (PDF) of the Gumbel distribution is given by:

$$f(x;\mu,\beta) = \frac{1}{\beta} e^{(-z-e^{-z})}$$

where $z = \frac{x-\mu}{\beta}$

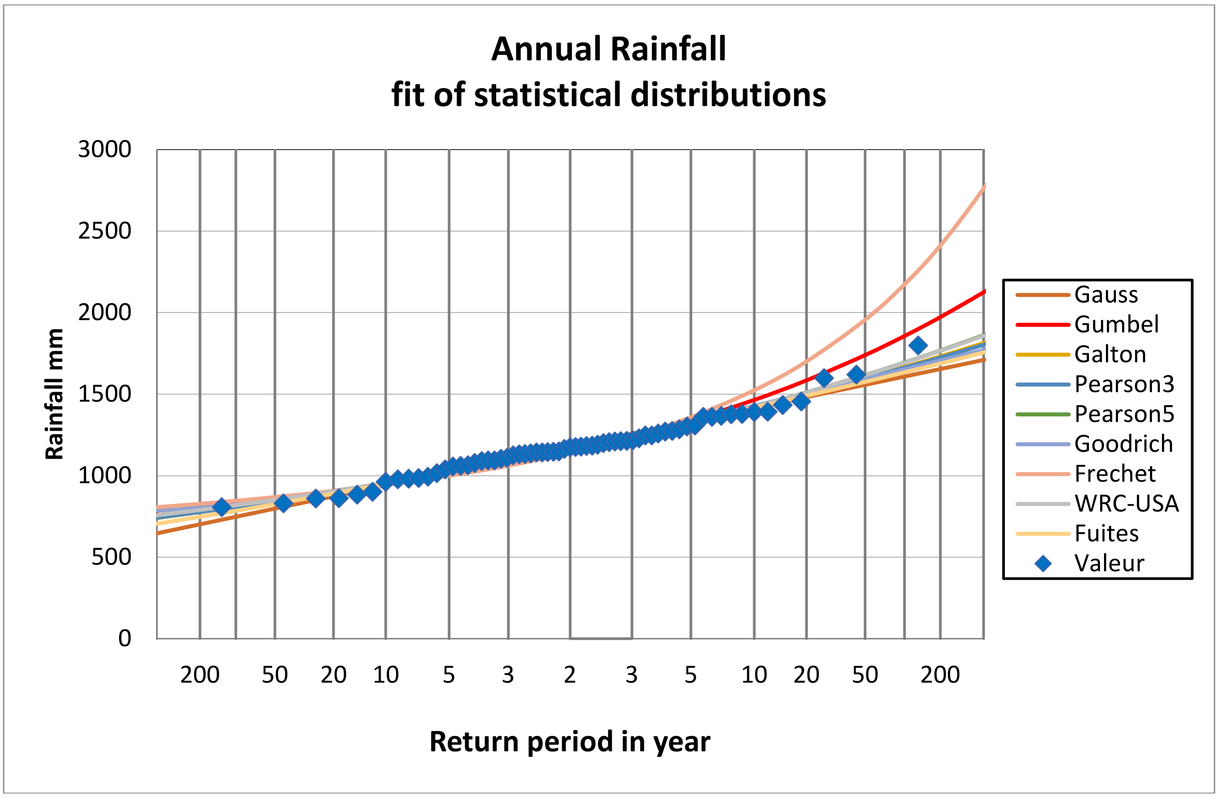

Figure 16: Statistical distributions annual rainfall in Malawi

	Dry years			Median			Wet years		
Frequency	0.002	0.01	0.1	0.2	0.5	0.8	0.9	0.99	0.998	0.999
Return period	500	100	10	5	2	5	10	100	500	1000
Value (mm)	784.7	834.7	950.2	1010	1150	1339	1464	1856	2124	2240

Table 2: Statistical distributions annual rainfall in Malawi

We performed the same type of statistical analysis of the average annual runoff over the entire country. Figure 16 shows the fit of the statistical distributions not rejected by the software (χ^2 test =0) but the one that fits best (Brunet Moret's test) is the Goodrich distribution. The data are represented on a Gaussian scale.

The Goodrich distribution is a probability distribution used in statistics to model continuous data. The Goodrich distribution can model a wide variety of shapes and can be used as an alternative to other distributions, such as the normal, exponential, and Weibull distributions.
The probability density function (PDF) of the GED is given by:

$$\boldsymbol{f(x;\alpha,\beta,\gamma)=\frac{\alpha}{\gamma}e^{-\left(\left(\frac{|x-\beta|}{\gamma}\right)^{\alpha}\right)}}$$

where parameter α controls the tail behavior of the distribution, while β and γ control the location and scale, respectively.

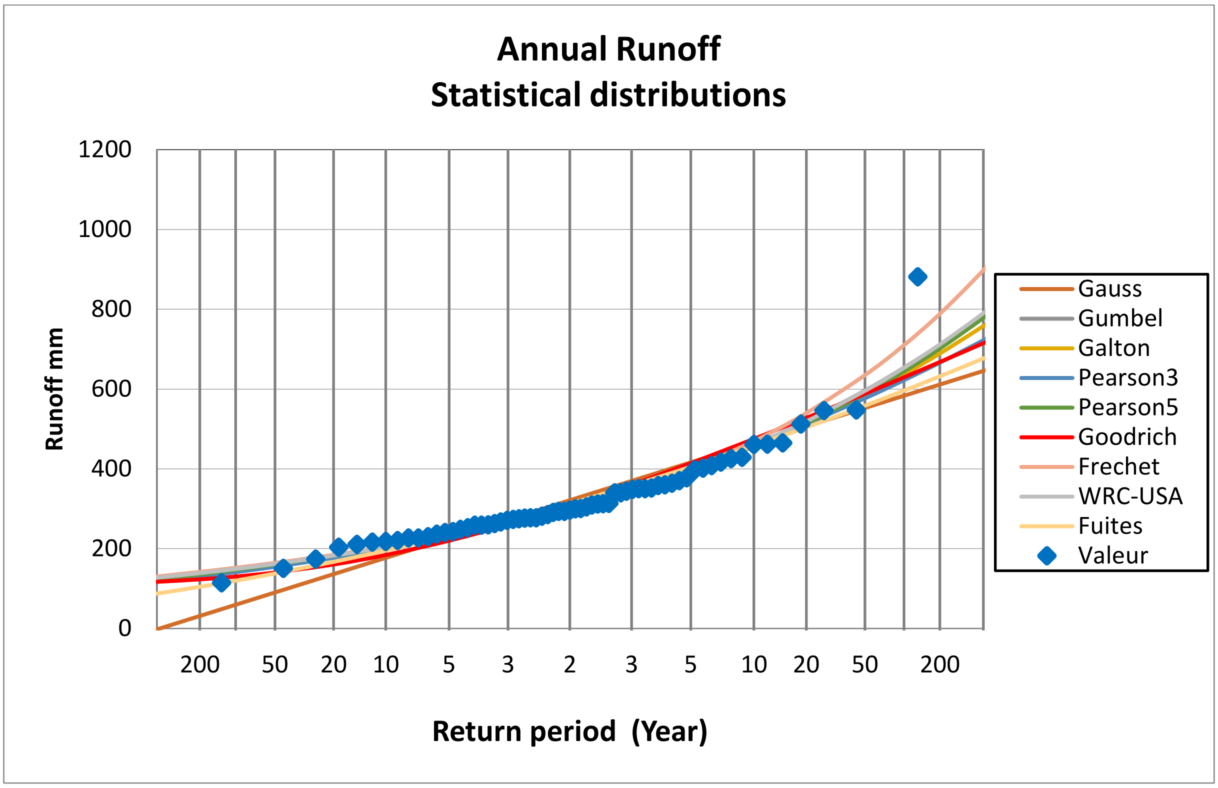

Figure 17: Statistical distributions annual runoff in Malawi

	Dry years			Median				Wet years		
Frequency	0.002	0.01	0.1	0.2	0.5	0.8	0.9	0.99	0.998	0.999
Return period	500	100	10	5	2	5	10	100	500	1000
Value (mm)	116.9	130.2	184.3	220.1	304.7	414.3	475.3	626.9	715.0	748.4

Table 3: Statistical distributions annual runoff in Malawi

The following conclusions can be drawn about the flood risk at the national level in the context of climate change scenarios:

1. Analysis of recent floods in Malawi shows an increase in tropical storms causing catastrophic flooding. Tropical storms cause a lot of damage to infrastructure and agriculture, which have a significant impact on the economy and people's livelihoods. It is important to understand the underlying causes of the increase in tropical storms. Climate change is a major factor that has been linked to the increase in extreme weather events, including tropical storms. Warmer sea surface temperatures provide more energy to fuel tropical storms, and changes in atmospheric circulation

patterns can affect the frequency and intensity of storms. There are measures that can be taken to prepare for and mitigate the impact of tropical storms. This includes investing in early warning systems, improving infrastructure to make it more resilient to storms, and promoting sustainable land use practices to reduce the risk of flooding and erosion.

2. The analysis of land use changes shows a stabilization of the surface covered by forests since 2005 and even a recovery of some forests with the reforestation programs. However, deforestation is still taking place, albeit at a slower rate, due to continuing demand for charcoal and firewood and this is off a much lower base compared to the 1980s and 1990s when the rate of deforestation was at its highest.[15] The area of agricultural land is not increasing, we are even seeing more attention to crop systems to limit runoff and soil degradation. The surfaces described as "bush," that one can assimilate into the 'degraded lands' strongly contributing to the floods, also seem stabilized.
   On the other hand, there has been an almost exponential increase in urbanized areas, even though the country remains essentially rural. The flood risk factor related to "Land cover" is not expected to grow in the future in rural areas, but much more so in cities, which host an increasingly large share of the population and house industrial infrastructures. We will note mainly the towns and cities on the lakeshore and those in the proximity of substantial rivers. More details will be given below in the watershed study.
3. Regarding floods by overflow of the lake, the Digital Elevation Model associated with the heights of the lake (data provided by the ESA) has permitted identification of the most sensitive towns and cities to floods. An inventory of the infrastructures around the lake and the knowledge of their elevation should allow better qualification of this risk (commercial and fishing ports, landing docks, fish markets and processing facilities, power plants, roads, etc.).
4. In order to identify the risk of flooding by river overflow and landslides, it was possible to define a flood risk index that corresponds well to the floods already identified. This index is based on topography and rainfall. It will be used in the study at the basin scale.

The analysis of rainfall and runoff displays an increasing tendency over the period 1957 - 2001 without this tendency being significant in the statistical term. It would be interesting to repeat this work on rainfall records actually observed in several locations in the country. A statistical distribution adjustment allowed us to quantify the rainfall and the runoff in dry and wet years.

[15] https://www.globalforestwatch.org/dashboards/country/MWI/?category=forest-change

3. FLOOD RISK ASSESSMENT AT CATCHMENT SCALE

The map in Figure 18 shows the districts considered in the study as well as the catchments and sub-catchments the consultancy was requested to consider.

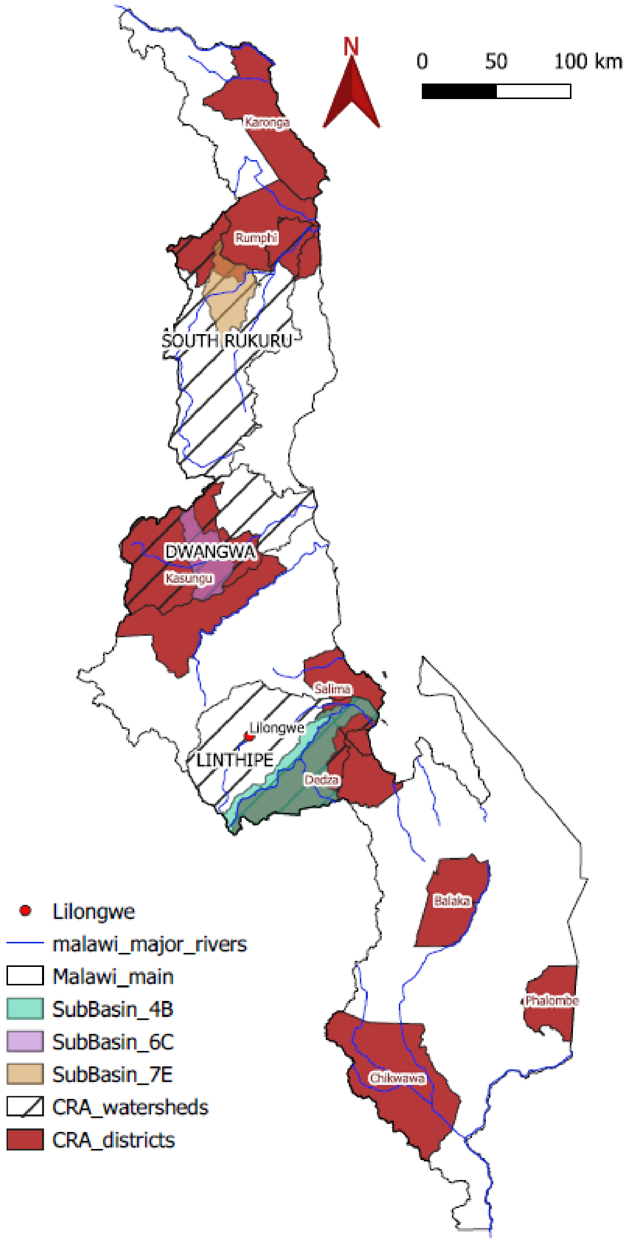

Figure 18: Study Districts, Catchments, and Sub-Catchments Considered by the Consultancy

3.1 South Rukuru Catchment and Sub Catchment 7E

The South Rukuru River is located in northern Malawi. It rises in southern Mzimba District, and flows roughly north-northeast to empty into Lake Malawi. Its watershed mostly lies in the Mzimba Plain. Its tributaries drain the western slopes of the Viphya Mountains. To the east, a low divide which forms the Malawi-Zambia border separates the South Rukuru's watershed from that of the Luangwa River in Zambia. The lower valley of the river separates the northern end of the Viphya Range from the Nyika Plateau to the north.

The South Rukuru River is the second largest tributary flowing into Lake Malawi. It is the significant stream in the Water Resource Area (WRA) 7 that includes the smaller North Rumphi River. It is an important water resource in the region, used for irrigation, domestic use, and fishing, and it also supports a diverse range of aquatic and terrestrial species.

The Department of Irrigation is currently developing a large irrigation scheme which will cover an area of 4,000 hectares in the Rumphi district on the left bank of the South Rukuru River. The project is supported by the European Union and will benefit almost 2,300 farmers in the region. However, as with many rivers in Malawi, the South Rukuru River is facing environmental challenges such as deforestation, soil erosion, and pollution, which can negatively impact the health of the river ecosystem and the communities that depend on it.

The exact size of the South Rukuru catchment can vary depending on the source (12,110 km^2 according to Shela (2000) and 12,719 km^2 according to JICA (2014).[16] The catchment includes the South Rukuru River and its tributaries, as well as the surrounding land area that drains into the river. According to the shape file provided by the Water Department, its surface is 10,596 km^2 and its perimeter is 794 km, which gives it a Gravelius compactness index of 2.183. The two sources mentioned above include the North Rumphi catchment area. The Malawi Water Resources Master Plan indicates a surface area of 12,719 km^2 for WRA 7, which includes the South Rukuru and North Rumphi catchments. The ratio of the length of the watercourses to the surface of the catchment area gives the density of drainage, for South Rukuru, it is 1.142e-4 m/m^2. Floods observed at the outlet of the catchment area are more sudden and acute as the compactness index of the catchment area is close to 1 and the density of drainage is important. In the same climate, these morphological parameters are good indices of comparison of the "flood hazard" violence.

For an analysis of the factors favouring flooding, we extracted the annual land occupations from the Climate Data Store LCCS within the boundaries of the South Rukuru basin given by the shape file transmitted by the Department of Water Resources (Appendix 3). We note substantial deforestation in the 1990s and early 2010s in favour of cultivation or degraded land (shrubs). From 2010 onwards, there is a reforestation of the watershed (Figure 19).

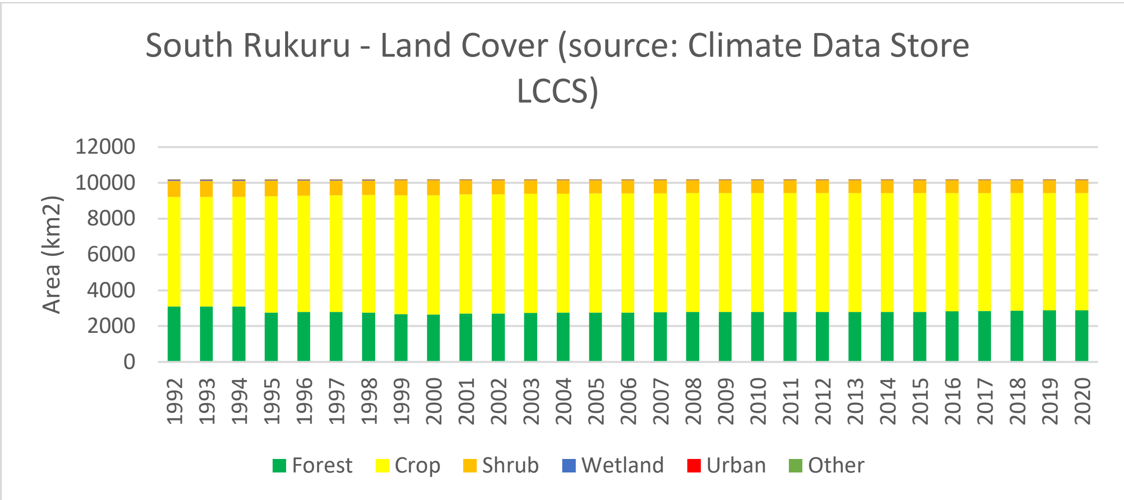

Figure 19: Land cover and land Use change in South Rukuru Catchment between 1993 – 2020

The South Rukuru River catchment in Malawi is a predominantly rural area, with one major city located within the catchment itself. Towns and smaller urban centres located in or near the catchment, include:

[16] Project for National Water Resources Master Plan in the Republic of Malawi – Final Report Volume II: Main Report 2014, JICA (Japanese International Cooperation Agency.)

- Mzuzu - the capital of the Northern Region, Mzuzu is the third-largest city in Malawi (population 221,272 {NSO 2018]), with an annual growth rate of 5.4%,[17] and is an important commercial and transportation nodal hub for the region.
- Ekwendeni - situated approximately 45 kilometers north of the city of Mzuzu, is known for its market, which is one of the largest in the region, as well as for its hospital and a teacher training college.
- Rumphi - Located to the northwest of the catchment, Rumphi is a town that serves as a centre for commerce and transportation in the surrounding area.

However, these small urban centres have experienced strong growth in the 2010s and 2020s (Figure 20) together with soil sealing that makes them vulnerable to flood hazards.

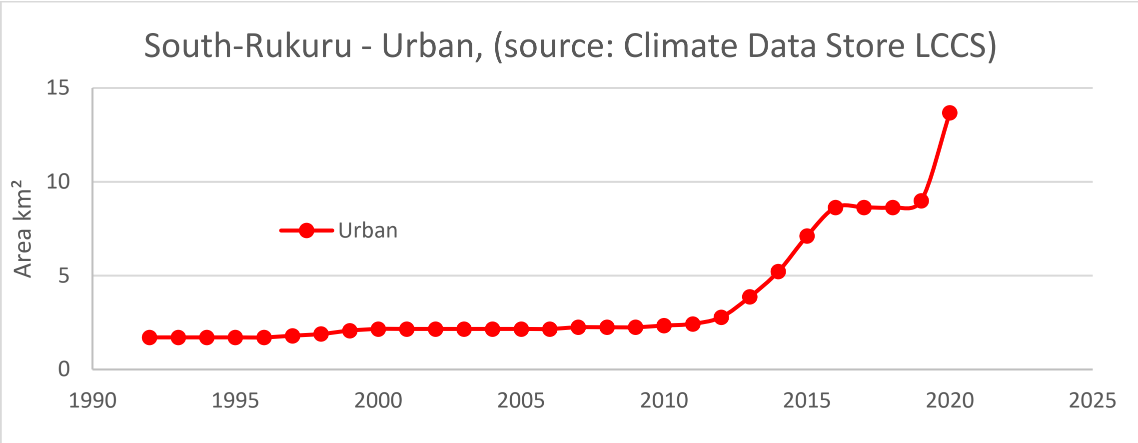

Figure 20: Urban Areas growth on South Rukuru (1992 – 2020)

The application of the flood hazard index to this basin manifests 4 risk zones: i) low, moderate, elevated and high. On this map, it was possible to plot the main cities and note those with a high risk (Figure 21). The area in dark blue at the top of the map is a high flood risk combining high precipitation and high ground. Most of them are villages or small towns. The small towns in this region are known for fertile soils, which support the cultivation of a wide range of crops, including tobacco, maize, beans, and groundnuts. In addition to their agricultural activities, these towns are also home to several schools, health facilities, and small businesses:

- Bandawe is a small town located on the northern shores of Lake Malawi, in the Nkhata Bay District. The town is situated in a hilly area that overlooks the lake and is surrounded by natural beauty, including scenic hills and forests.
- Bwengu in the Mzimba District, is located about 110 km northwest of Mzuzu. Bwengu is primarily an agricultural town, with most of the local population engaged in farming activities.
- Enukweni in the Mzimba District, situated about 65 km northeast of Mzuzu is a small but bustling town that is an important hub for the surrounding rural areas. The town, is primarily an agricultural area, with most of the local population engaged in farming activities.
- Mlowe is a small town located in the Rumphi District, about 56 kilometers northwest of Mzuzu. Mlowe has a population of approximately 6,000 people and it is primarily an agricultural area, with most of the local population engaged in farming activities.
- Nkombezi is a small town located in the Chitipa District, about 14 kilometers north of the district capital, Chitipa, and close to the border with Tanzania. Nkombezi has a population of approximately 2,500 people.

[17] https://foodfoundation.org.uk/sites/default/files/2022-04/FOOD%20CITIES%202022_Mzuzu.pdf

- Rukuru Point is a small peninsula that juts out into Lake Malawi. It is situated just north of the town of Nkhata Bay. It is a popular destination for tourists and locals alike due to its beautiful scenery, crystal-clear waters, and stunning sunsets. It is home to several lodges, guesthouses, and campsites where visitors can stay and enjoy the natural surroundings.

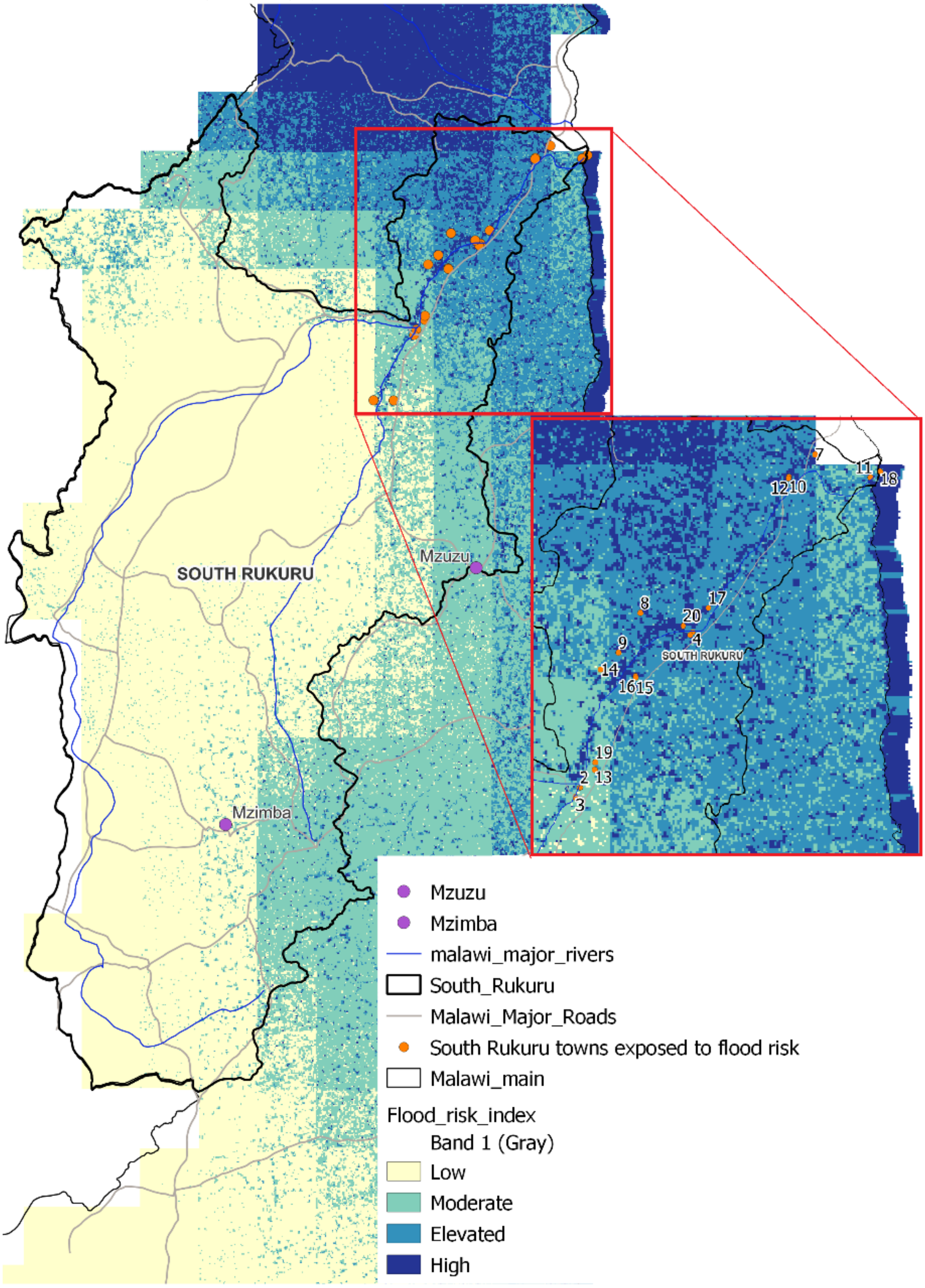

Figure 21: South Rukuru flood index, towns and roads exposed to a flood risk

South Rukuru towns exposed to flood hazard					
ID	Name	ID	Name	ID	Name
1	Bandawe	8	Luwagha	15	Nkombezi

2	Bwengu	9	Mlangali	16	Nkombezi TC
3	Chandiwira Moyo	10	Mlondoma	17	Phwedzi
4	Chisokowo	11	Mlowe	18	Rukuru Point
5	Chiwato Jere	12	Mojowa	19	Thumbi
6	Enukweni	13	Msowoya	20	Walowoka
7	Jalawe	14	N'gonga		

*Table 4: **South Rukuru towns exposed to flood hazard***

Mzuzu, the capital of the Northern Region, was originally situated on the watershed divide of the South Rukuru River basin, and therefore, outside the risk of flooding. Figure 22 overlays the growth map of Mzuzu with the flood risk map for the years 1992, 2000, and 2020. It is evident how the city (grey pixels) has expanded towards the lower parts of the watershed in areas where the risk of flooding is high (blue pixels) or even severe (dark blue pixels).

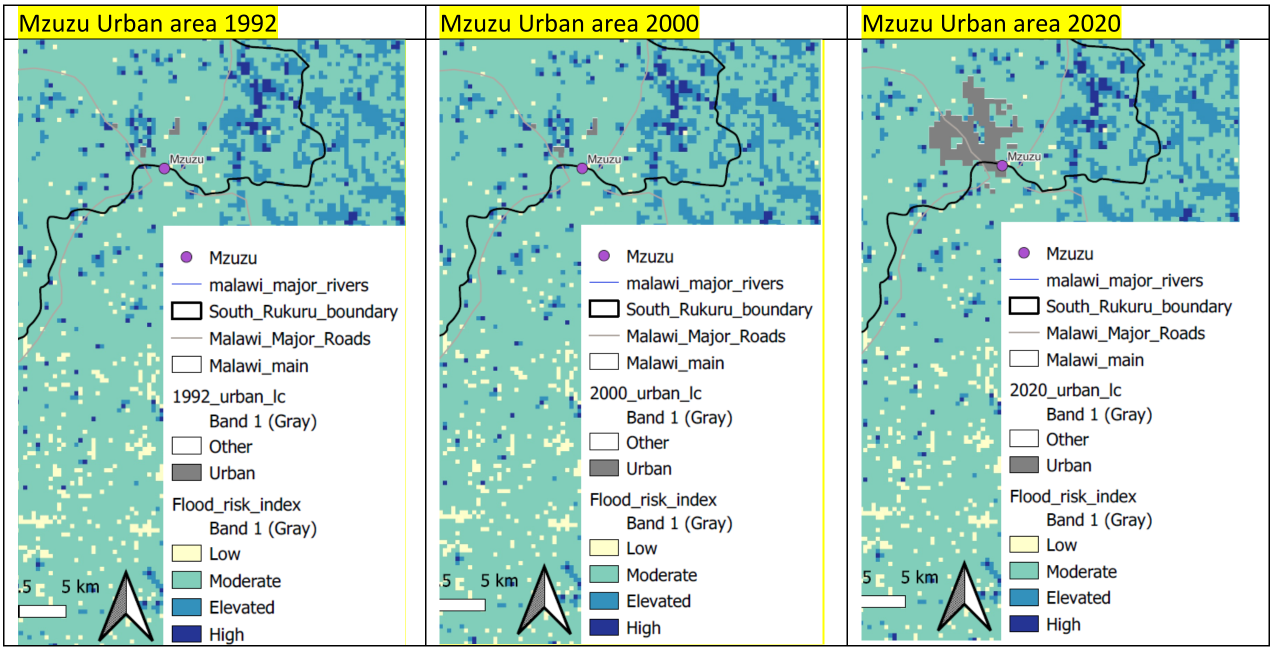

Figure 22: Growing urbanization of Mzuzu and risk of infrastructure loss through flooding

Mzuzu, as the capital of Malawi's Northern Region, has seen rapid urban expansion. The city has expanded beyond its original boundaries, encroaching into surrounding rural areas. This expansion often lacks adequate urban planning, leading to informal settlements and increased pressure on the environment and resources. Mzuzu is susceptible to seasonal floods, which are common in Malawi. The city's rapid expansion, often into low-lying areas and floodplains, exacerbates this vulnerability.

The effects of climate change, including more intense and frequent rainfall, increase the risk of severe flooding in the region. This poses a threat to infrastructure, especially in poorly planned or informal settlements. Inadequate drainage systems in rapidly urbanizing areas contribute to the risk. During heavy rains, these areas can experience significant flooding, damaging roads, buildings, and other infrastructure. Deforestation and land degradation in and around Mzuzu also contribute to the increased risk of flooding. The loss of vegetation reduces the land's ability to absorb rainwater, leading to greater runoff and potential floods (see figure 7).

To characterize the flood hazard, we extracted from the ERA5 database the average rainfall over the basin on the day with the highest precipitation of the year for statistical analysis. The ERA5 database also gives the total Runoff and the sub-surface Runoff (Appendix 4). Figure 23 shows the variation of these two variables and the trend lines over the ERA5 reconstruction period. The trend lines indicate an increase in these values over time. But these increases are not statistically validated.

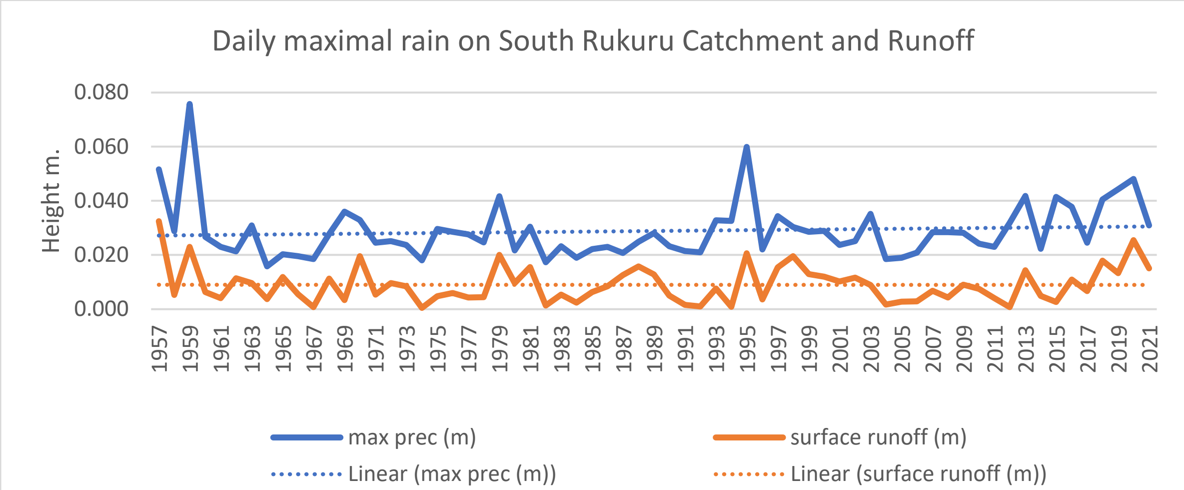

Figure 23: South Rukuru maximum daily rainfall and associated runoff (source CDS - ECMWF)

The following figure (Figure 24) shows the relationship between maximum daily rainfall for the year and runoff.

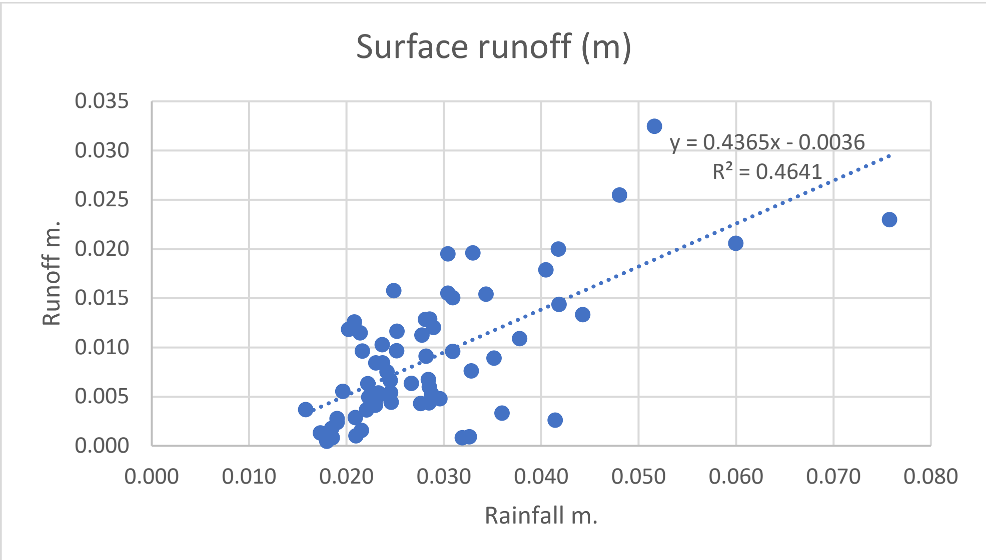

Figure 24: Correlation between daily max rain and runoff – South Rukuru

We performed a statistical analysis of the higher daily rainfalls in the year and runoff induced over the South Rukuru Catchment. Figure 25 shows the fit of the statistical distributions not rejected by the software DIXLOIS (χ^2 test =0) on the max daily rain in a logarithmic scale and figure 24 on the daily runoff.

For daily rainfalls the best distribution fitting to the data is the Pearson Type III distribution with a threshold of 21mm. The Pearson Type III distribution is a continuous probability distribution that is commonly used in statistical analysis. It is a three-parameter distribution that is defined by its skewness, mean, and standard deviation. The probability density function (PDF) of the Pearson Type III distribution is given by:

$$f(x; a, b, c) = \frac{c}{b} * \left(\frac{x-a}{b}\right)^{c-1} * e^{-\left(\frac{x-a}{b}\right)^c}$$

where:

- a: location parameter (shifts the distribution along the x-axis)
- b: scale parameter (controls the spread of the distribution)
- c: shape parameter (controls the skewness of the distribution)

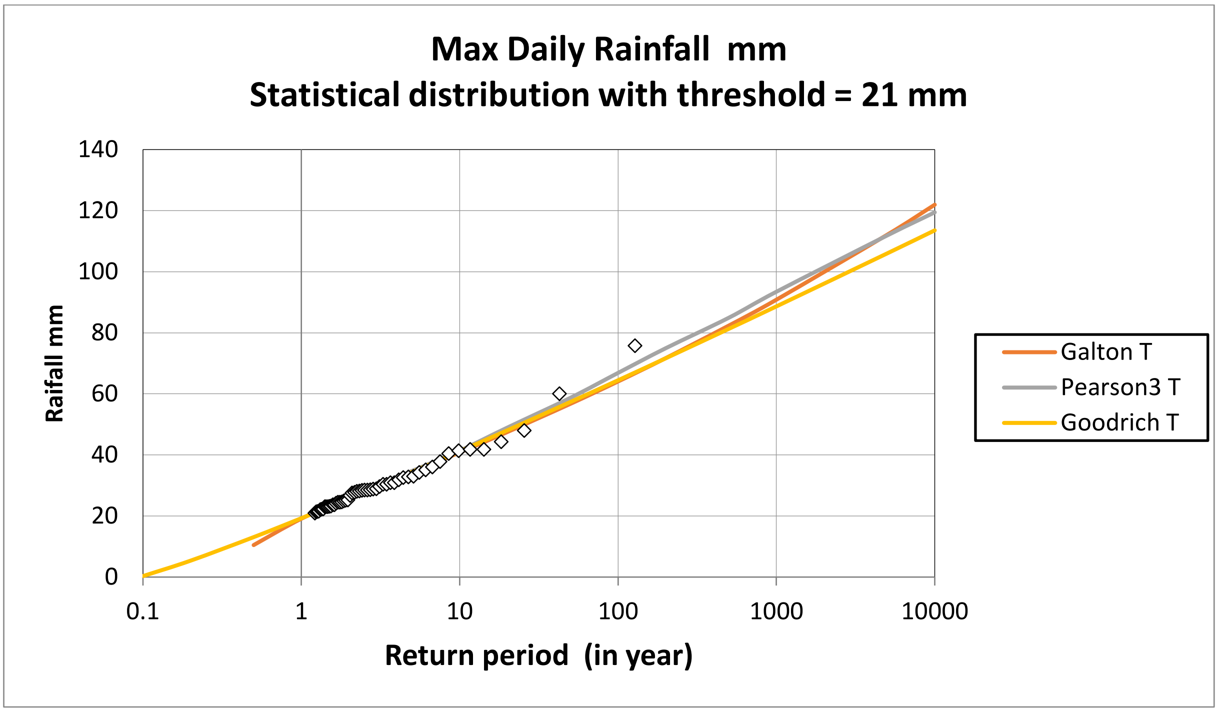

Figure 25: South Rukuru - Statistical distributions, max daily rainfall in mm

Frequency	0,5	0.2	0.1	0.05	0.02	0.01	0.005	0.002	0.001
Return period	2	5	10	20	50	100	200	500	1000
Value (mm)	26.1	36.8	41.4	49.0	58.7	66.9	75.0	84.9	93.5

Table 5: South Rukuru - Statistical distributions, max daily rainfall in mm

The statistical analysis of runoff, the best distribution that fits the daily runoff resulting in the highest daily rainfall in the year (Figure 26).

The South Rukuru sub-catchment (7E on Figure 17) is one of the eight sub-catchments that make up the South Rukuru River catchment in Malawi. The South Rukuru sub-catchment is located in the central part of the South Rukuru River catchment and covers an area of approximately 14634 km², and its perimeter is 215 km, which gives it a Gravelius compactness index of 1.403. The combined length of the major watercourses is 188 km and drainage density of 1.3 e-4 m/m².

The South Rukurusub-catchment is an important source of water for both domestic and agricultural use, with many communities relying on the South Rukuru River for their daily water needs. However, the sub-catchment is also facing several challenges related to water resource management, including soil erosion, deforestation, and water pollution from agricultural activities and mining.

To address these challenges, various organizations and stakeholders (GEF UNDP projects) [18] are working to promote sustainable water resource management in the South Rukuru sub-catchment. These efforts

[18] https://sgp.undp.org/component/sgpprojects/?view=allprojects&country=MLW&start=20

include promoting conservation agriculture practices, reforestation, and the establishment of water user committees to help manage and protect water resources in the sub-catchment.

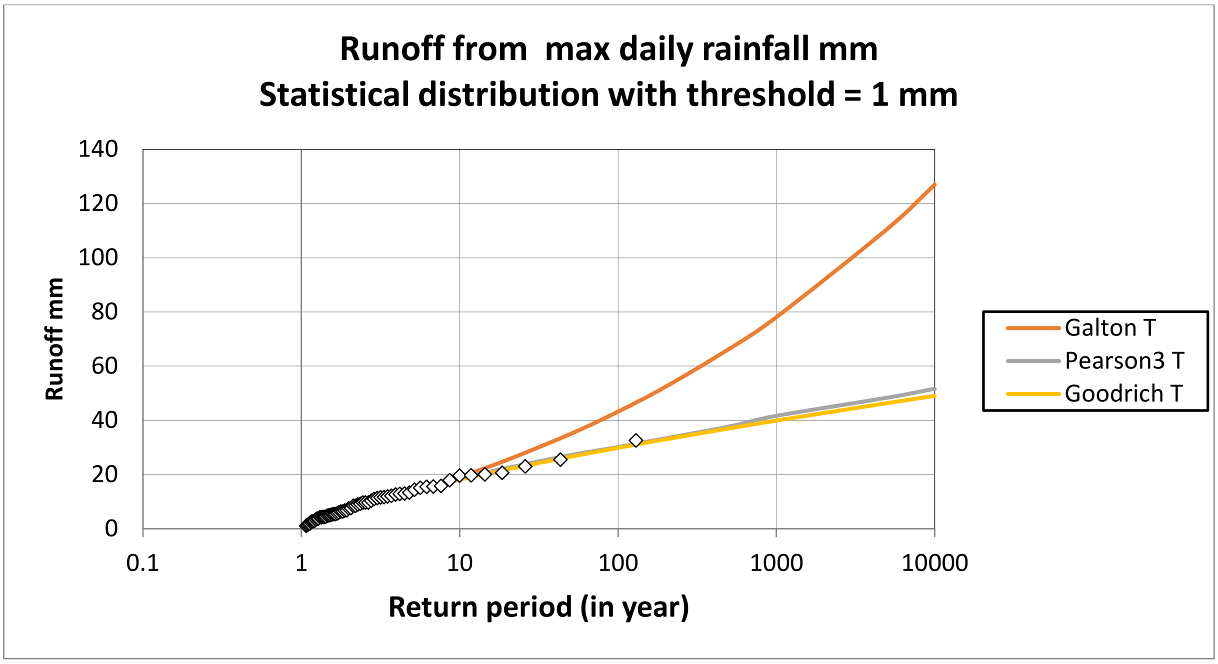

Figure 26: South Rukuru - statistical distributions, runoff from max daily rainfall in mm

Frequency	0,5	0.2	0.1	0.05	0.02	0.01	0.005	0.002	0.001
Return period	2	5	10	20	50	100	200	500	1000
Value (mm)	8.56	14.1	18.5	22.4	27.2	30.1	33.4	37.7	41.7

Table 6: South Rukuru - statistical distributions, runoff from max daily rainfall in mm

3.2 Linthipe Catchment and Sub-catchment 4B: Lifidzi River

The Linthipe Catchment encompasses the upper reaches of the Linthipe River and its tributaries. The Linthipe River is a tributary of the Lilongwe River, which is a major river in the Central Region of Malawi. The Linthipe Catchment is home to over 300,000 people who rely on the river for their livelihoods. A mix of urban and rural landscapes, with smallholder farms, forests, and wetlands dominating the landscape characterize the catchment. According to the shape file provided by the Water Department its surface is 8,885 km² and its perimeter is 468 km, which gives it a Gravelius compactness index of 1.391. The density of drainage is 1.102e-4 m/m².

The Linthipe River catchment can be categorized into five geographic regions: the Dzalanyama Range, Lilongwe Plain, Dowa/Dedza hills, Rift Valley Scarp, and Lakeshore Plain. Elevation ranges from 500 m above mean sea level at the lakeshore to 1500 m. The eastern and central parts of the catchment comprise the Lilongwe Plain, which is undulating with broad marshy valleys. South-west of the Lilongwe Plain is the Dzalanyama Range with high ridges covered by forest reserves. On the east of the Lilongwe Plain are the Dowa/Dedza Hills, with moderate to high relief extending north to south of the catchment. East of this region lie the Rift Valley Scarp and Lakeshore Plain consecutively. Slope gradient is gentle (1–6%) in the Lilongwe and Lakeshore Plains, moderate to steep (6.1–50%) in the Scarp and Dowa regions[19].

[19] Mkanda FX, Contribution by farmers' survival strategies to soil erosion in the Linthipe River Catchment: implications for biodiversity conservation in Lake Malawi/Nyasa. Biodiversity and Conservation 11: 1327–1359, 2002. Kluwer Academic Publishers. Netherlands

The Linthipe River flows from the south-western corner of the region on the Malawi Mozambique frontier and is joined by the Diamphwe, Lilongwe and many other rivers and streams before emptying its waters into Lake Malawi at Salima. It is one of the major tributaries to Lake Malawi. In its mature stage, the river enters a flat and swampy area where the gradient and aquatic vegetation inhibit flow velocities. In its upper and middle reaches, its tributaries consist of dambos, i.e. wet flat valleys that act as a sponge and gradually release water to the river channel. The Linthipe River and its tributaries are an important source of water for irrigation, and other uses.

The availability and quality of water from the river has a strong bearing on the survival of aquatic life in Lake Malawi. The river also serves as a breeding ground for endemic endangered species of *Opsaridium microlepsis* (Mpasa) and *Labeo mesops* (Ntchila). These fish species have high economic value because they fetch better prices on the market. *Opsaridium microlepsisis* are principally caught during seasonal breeding migration from Lake Malawi into the Linthipe River[20].

Water resources are facing several environmental challenges, including deforestation, soil erosion, water pollution, and overfishing. These challenges are exacerbated by climate change, which is causing more frequent and severe floods and droughts.

To address these challenges, the Malawi government, in collaboration with development partners and local communities, has implemented several initiatives aimed at promoting sustainable land use, conserving forests and wetlands, and improving water quality. These initiatives include afforestation and reforestation programs, sustainable land management practices, and the establishment of community-based water management committees.

The land cover in the catchment (Figure 27) is predominantly agricultural, with subsistence farming being the main economic activity in the area. The most commonly grown crops include maize, cassava, groundnuts, beans, and vegetables.

Apart from agriculture, the catchment area also includes some forest reserves and grasslands. The forest reserves are mostly located in the upper catchment and include the Dedza-Salima Forest Reserve and the Dowa Forest Reserve. These forests provide important ecosystem services, including water regulation and biodiversity conservation. Drastic deforestation appears to have taken place at the end of the 1990s and especially in 1999. This deforestation seems to have halted. The region experienced significant population growth in the 1990s, which could have strained the available land and resources, leading to increased deforestation as people sought to meet their basic needs. Early in the 2000s, the Malawian government, recognizing the importance of forests for ecosystem services and sustainable development, have implemented measures to address deforestation. These include the establishment of protected areas, implementation of forestry regulations, and the promotion of sustainable land-use practices.

In the Linthipe Catchment as in much of Central Malawi, Urbanization has been increase rapidly in recent years, particularly in and around the city of Lilongwe, which is the capital of Malawi. According to the World Bank, the urban population in Malawi has been increasing at an average annual rate of 4.4% between 2010 and 2020,[21] and is projected to continue to increase in the coming years.

Lilongwe has experienced rapid urbanization due to factors such as rural-urban migration, increased economic opportunities, and the expansion of infrastructure and services. The city has a growing population of approximately one million people, and is expected to continue to grow in the coming years. As a result,

[20] Chigamba, G.; Limuwa, M.; Kaunda, E. Does Paying for Aquatic Resources Matter? A Case of an African Riverine Ecosystem. Sustainability 2021, 13, 4177. https://doi.org/10.3390/su13084177
[21] https://data.worldbank.org/indicator/SP.URB.TOTL.IN.ZS?locations=MW

there has been a corresponding increase in the demand for housing, employment opportunities, and basic services such as water, sanitation, and electricity.

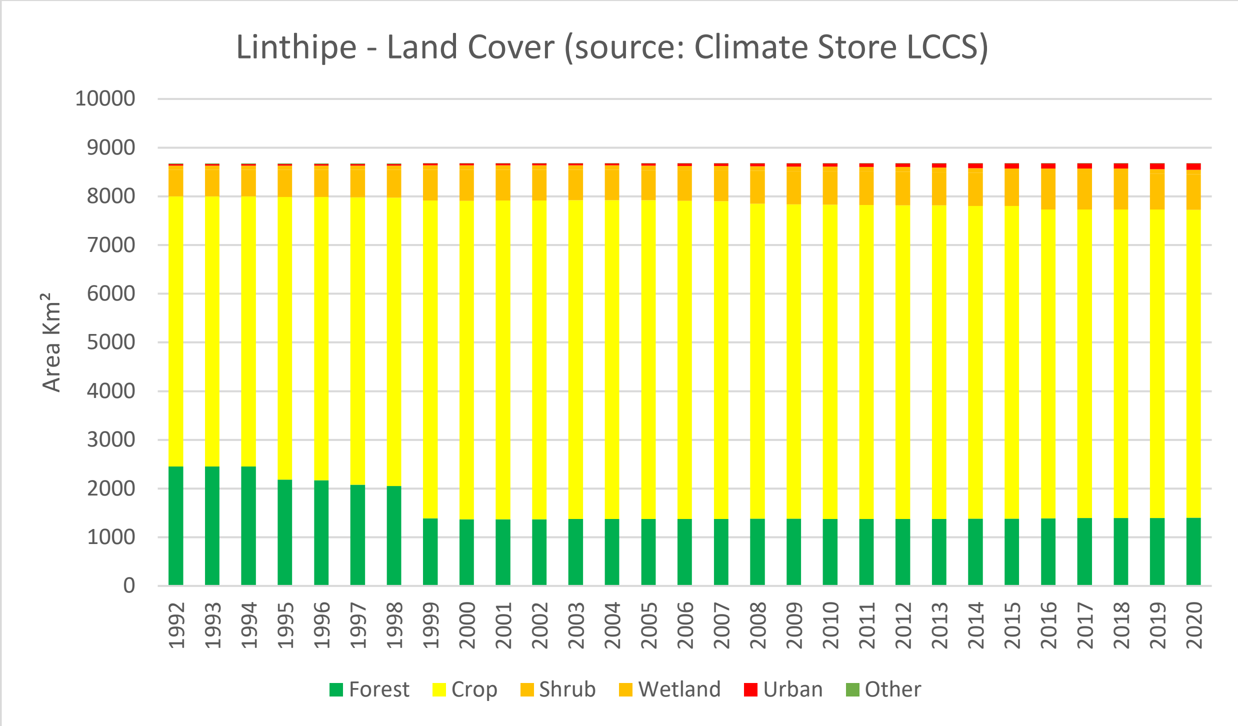

Figure 27: Land cover and land Use change in Linthipe Catchment between 1993 – 2020

Other towns in Linthipe catchment, such as Dedza (a town located approximately 70 kilometres southeast of Lilongwe), or Salima Town (located on the shores of Lake Malawi, approximately 80 kilometres east of Lilongwe) have also experienced some level of urbanization, although to a lesser extent than Lilongwe. These towns have growing populations, and there is a need for investment in infrastructure and services to support their development.

However, rapid urbanization in Linthipe catchment (Figure 28) has also brought challenges such as urban sprawl, informal settlements, traffic congestion, environmental degradation and an increase in the local risk of flooding, firstly through an increase in the hazard (soil sealing) and concentration of infrastructures. There is a need for effective urban planning and management to ensure that urbanization in Central Malawi is sustainable and inclusive, and that it contributes to the overall development of the country.

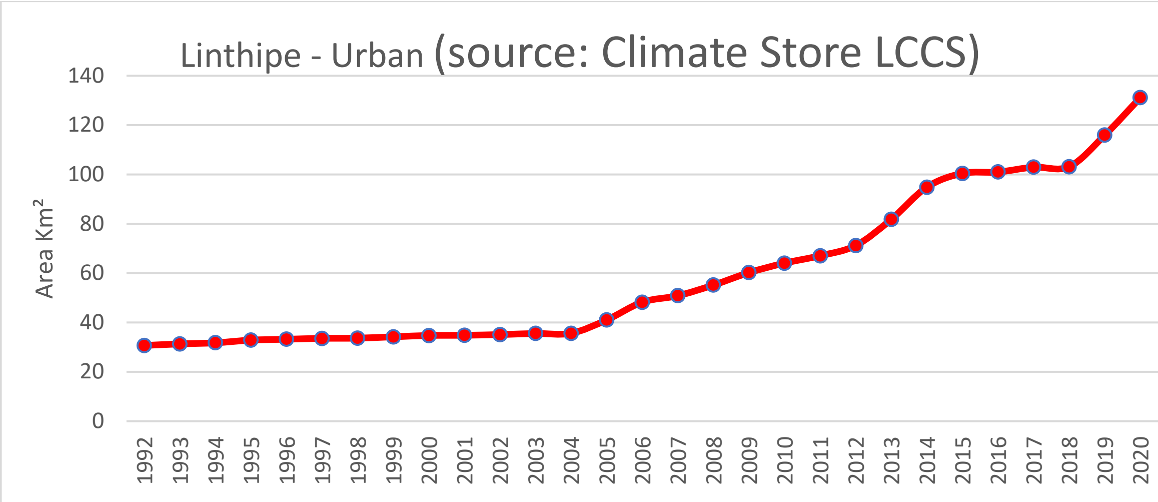

Figure 28: Urban Areas growth on Linthipe catchment (1992 – 2020)

The map of the flood hazard index according to the 4 classes: low, moderate, elevated and high (Figure 29) exhibits two zones with important risks of flooding of infrastructure in the towns, cities and roads. All these small towns or villages are mainly agricultural with populations ranging from 1000 to 5000 inhabitants. Some of them have infrastructures such as a school, a clinic and shops. Salima Town is the most important town on the list.

Salima Town is the capital of Salima District and has a population of approximately 37,000 people while the district population was recorded at a little under 480,000 in the 2018 census. The district lies to the east of Lilongwe District, which it adjoins, while the town lies approximately 100 km from the national capital, Lilongwe, by road. The economy of Salima is largely based on agriculture, with maize, cassava, rice, and tobacco being the main crops grown in the area. Fishing is also an important economic activity, as the district is situated on the shores of Lake Malawi, which is known for its diverse fish species. Salima is also home to several tourist attractions, including the Senga Bay beach resort, the Salima Cultural Museum, and the Kuti Wildlife Reserve. It is prone to flooding, particularly during the rainy season. Located on the western shore of Lake Malawi, heavy rains and run-off that enters the lake from feeder tributaries, most though not all in Malawi can cause the lake to overflow and flood nearby communities.

Flooding in Salima can cause significant damage to homes, crops, and infrastructure. It can also lead to the displacement of people and loss of life. In recent years, flooding in Salima has been exacerbated by climate change, which has led to more intense rainfall and more frequent extreme weather events. These floods are also due to siltation of those reaches of the river close to its outflow into the Lake causing overbanking and inundation of the lowest lying lands of Salima District.

The Malawi government, with the support of various international organizations, is working to mitigate the impact of flooding in Salima. This includes measures such as building floodwalls and embankments, improving drainage systems, and relocating people from high-risk areas. However, serious urban flooding still occurs as evidenced in 2022 in the wake of Tropical Storm Ana.[22]

[22] https://www.unicef.org/malawi/reports/malawi-floods-humanitarian-situation-report-2-february-2022#:~:text=In%20Salima%20district%20in%20central,temporary%20shelter%20in%20displacement%20sites.

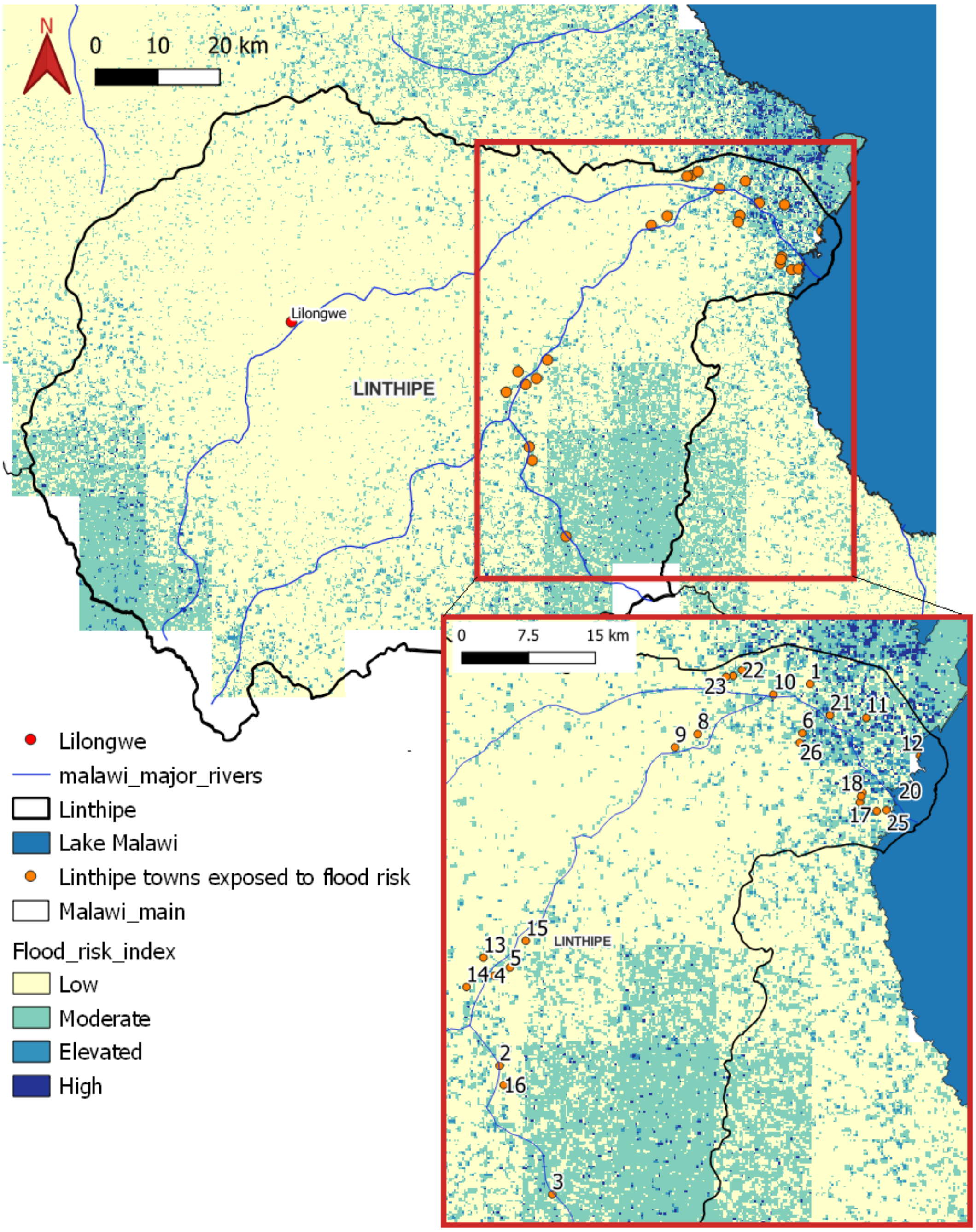

Figure 29: Linthipe - flood index, towns exposed to a flood hazard

Linthipe - towns exposed to a flood hazard							
ID	Name	ID	Name	ID	Name	ID	Name
1	Salima	8	Kalibe	15	Chiowa	22	Chipalapata village
2	Linthipe	9	Mphinzi	16	Linthipe	23	Mtonga Village
3	Mnyanga	10	Kambwiri	17	Kabumbu	24	GVH Kandulu
4	Mchokela	11	Pemba	18	Kapanda	25	GVH Mphunga
5	Mikundi	12	Maganga	19	Naliwomba	26	Katelera
6	Ngolomi	13	Gwenembe	20	mkwaila village		Lilongwe
7	Mwankundi	14	Mkhalala	21	CHIKUNI		

Table 7: Linthipe - flood index, towns exposed to a flood hazard

Lilongwe, the capital of Malawi is in a moderate index area. However, in recent years, Lilongwe has experienced several instances of flooding, resulting in loss of property and displacement of people. The city is not located in a very flood-prone area, but straddles the Lilongwe River and experiences heavy rainfall during the rainy season (December to March), whichcan result in flooding of the Lilongwe River and its tributaries. Low-lying areas and informal settlements are typically at greater risk of flooding, as they are located in areas with poor drainage systems or close to rivers and streams. Lilongwe has a population of approximately 1 million people, making it the largest city in Malawi.

The main economic activities in Lilongwe include agriculture, trade, and services. The city is a major centre for tobacco processing and distribution, and is a nodal point for international and national institutions. Additionally, the city has a growing tourism industry, with several hotels, restaurants, and cultural attractions such as the Lilongwe Wildlife Centre and the Lilongwe Nature Sanctuary.

Lilongwe, as the capital city of Malawi, has experienced rapid urbanization and population growth over the three decades. This expansion is partly due to rural-urban migration and the city's role as an administrative and economic hub. The physical footprint of the city has significantly increased, with new residential, commercial, and industrial areas developing, often sprawling into what were once rural or undeveloped lands.

The city, which was around 9 km² in 1992, will be over 150 km² in 2021 (Figure 30), absorbing several satellite towns that can be considered now as part of the wider conurbation. The growth includes a rise in informal settlements or peri-urban areas, which often lack proper urban planning and infrastructure. The rapid and often unplanned expansion has increased Lilongwe’s vulnerability to flooding. This is particularly evident in areas where development has occurred without adequate consideration of natural water flow patterns and drainage.

Deforestation and land degradation in and around the city, due to urban expansion, have exacerbated the risk of flooding. The reduction in natural vegetation affects the ground’s ability to absorb rainwater, leading to higher runoff during heavy rains. In many newly urbanized areas, especially informal settlements, the infrastructure for flood management (like stormwater drainage systems) is often inadequate or non-existent.

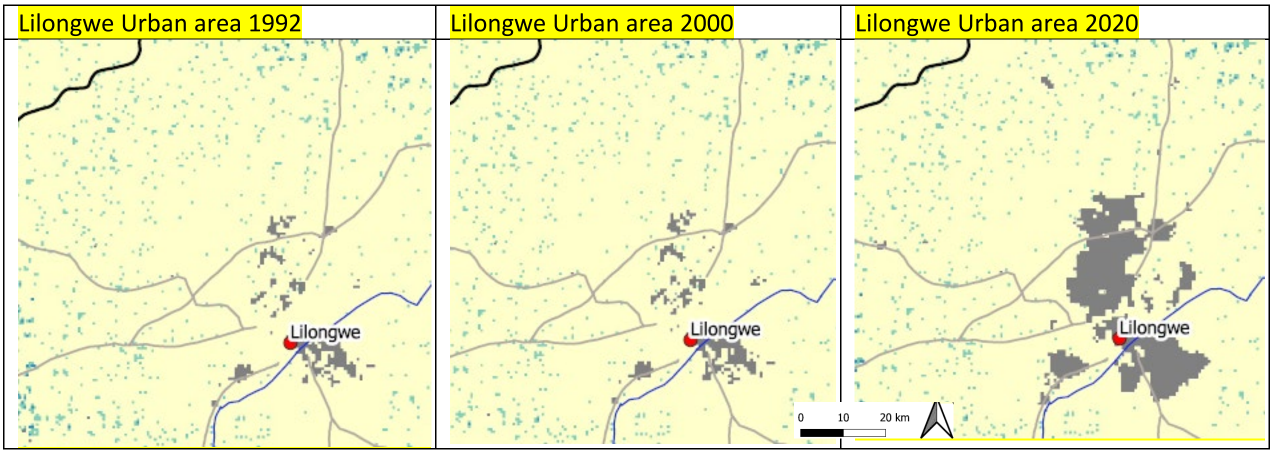

Figure 30: Growing urbanization of Lilongwe and risk of infrastructure loss through flooding

To characterize the flood hazard, we extracted from the ERA5 database, the average rainfall over the basin on the day with the highest precipitation of the year for statistical analysis. The ERA5 database also gives the total Runoff and the sub-surface Runoff (Appendix 4). Figure 31 shows the variation of these two variables and the trend lines over the ERA5 reconstruction period. The trend lines indicate an increase in these values over time. However, these increases are not statistically validated. However, this figure shows that the proportion of rainfall classed as run-off is increasing and indicate loss of land absorption.

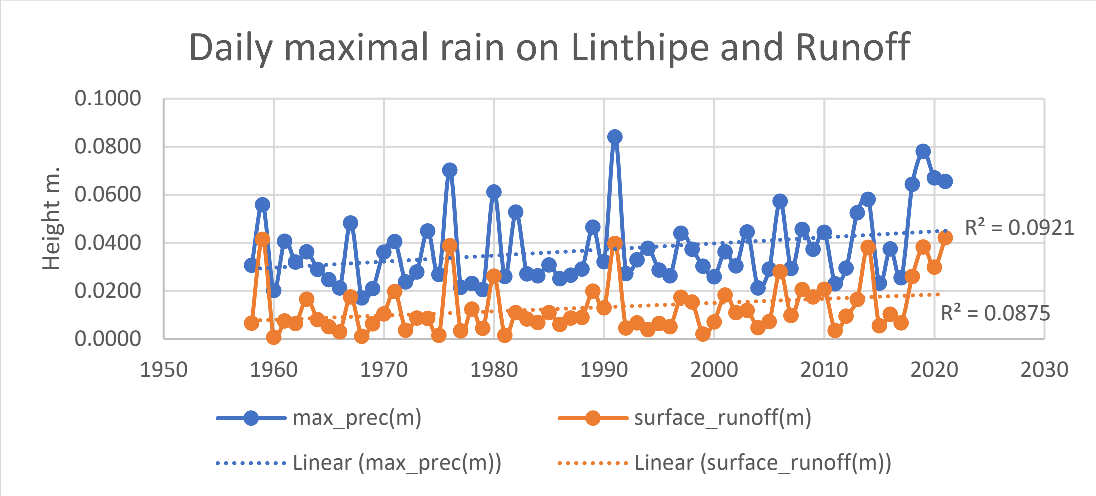

Figure 31: Linthipe maximum daily rainfall and associated runoff (source CDS - ECMW)

Figure 32 shows the relationship between maximum daily rainfall for the year and runoff. We see a correlation. This correlation is significant enough to be used for hydraulic engineering. The watershed being smaller than the South Rukuru, the flow of each day is better characterized by the daily rainfall.

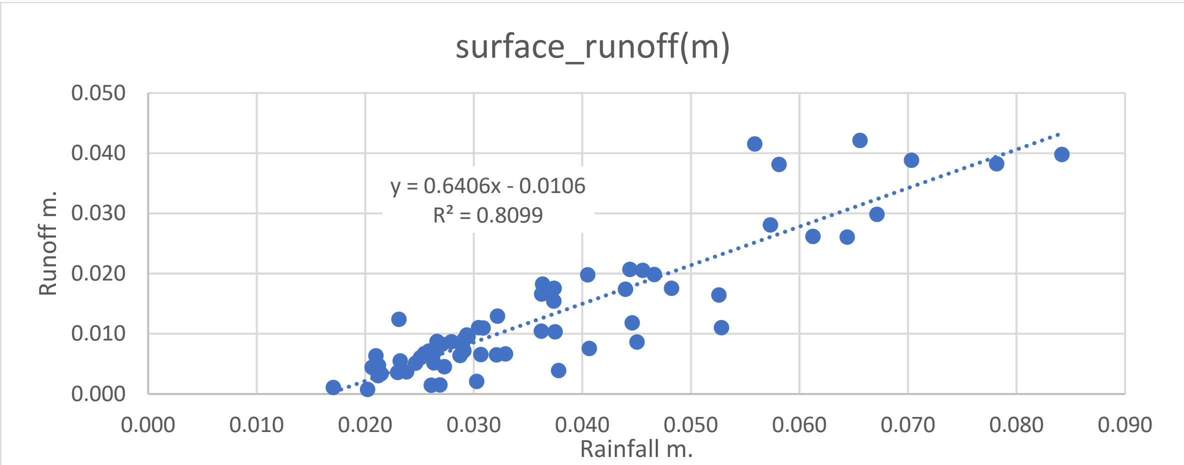

Figure 32: Correlation between daily max rain and runoff – Linthipe

We performed a statistical analysis of the higher daily rainfalls in the year and runoff induced over the Linthipe Catchment. Figure 33 shows the fit of the statistical distributions not rejected by the software DIXLOIS (χ^2 test =0) on the max daily rain in a logarithmic scale and Figure 34 on the daily runoff.
For maximum daily rainfalls the best distribution fitting to the data is the Pearson Type III distribution with a threshold of 10 mm.

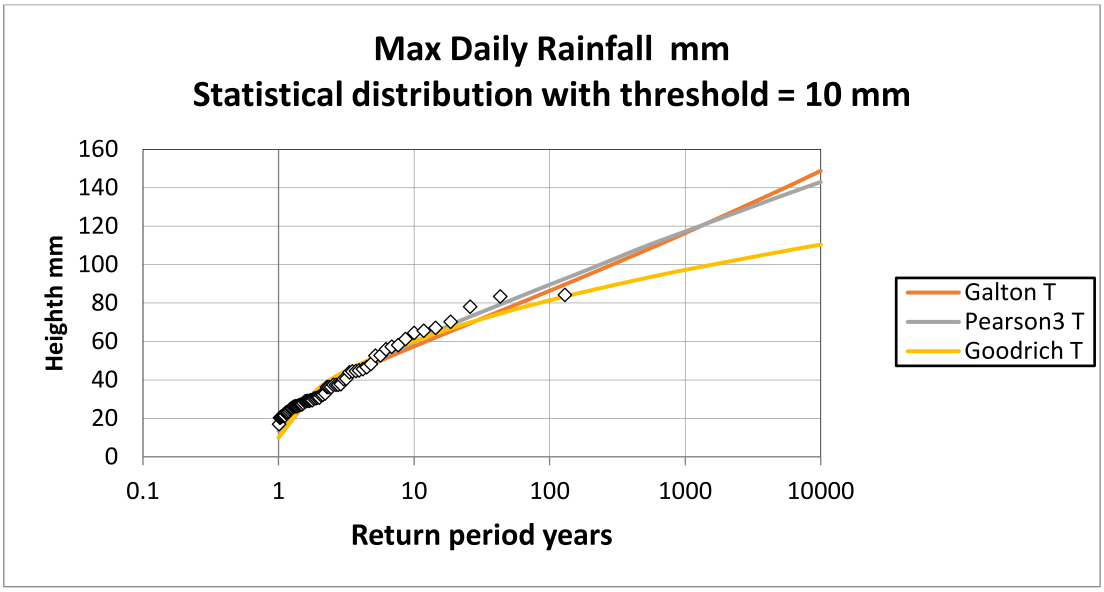

Figure 33: Linthipe - statistical distributions, max daily rainfall in mm

Frequency	0,5	0.2	0.1	0.05	0.02	0.01	0.005	0.002	0.001
Return period (years)	2	5	10	20	50	100	200	500	1000
Value (mm)	35.3	50.0	59.8	69.6	81.1	89.6	97.9	109.4	117.3

Table 8: Linthipe - statistical distributions, max daily rainfall in mm

For runoff from maximum daily rainfall the best distribution fitting to the data is the Pearson Type III distribution with a threshold of 1 mm.

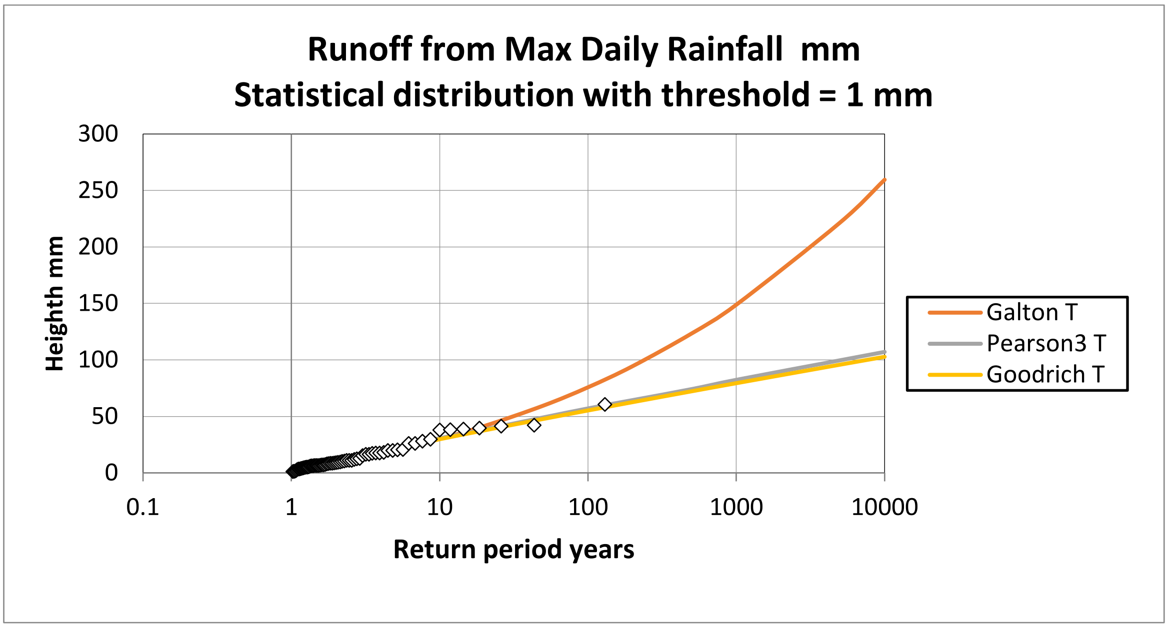

Figure 34: Linthipe - statistical distributions, runoff from max daily rainfall in mm

Frequency	0,5	0.2	0.1	0.05	0.02	0.01	0.005	0.002	0.001
Return per.	2	5	10	20	50	100	200	500	1000
Value (mm)	11.4	23.0	30.7	38.4	49.1	57.1	64.4	74.2	82.4

Table 9: Linthipe - statistical distributions, runoff from max daily rainfall in mm

In his MSc thesis,[23] Laisi notes 9 hydrometric stations that have been operating in the Linthipe basin and we were able to retrieve in the appendices the annual maximum flow data from the following stations (Annexe 5):

- Linthipe at Salima Rail Bridge, the most downstream station.
- Lilongwe at Old Town, the capital city station.

Linthipe at Salima Rail Bridge, 4.B.1 (From Laisi 2016)
The station was opened on February 1st, 1953 (Malawi Government, 1986)[24] and is a primary station. It is located at the rail bridge between Salima and Chipoka in a very flat area within the lakeshore plain. Examination of flows from 1971 to 2009 indicates that good effort was taken in the collection of water levels. However, within this period, data for 5 years is regarded as unsatisfactory as much of it was missing. Meanwhile, from 1987 to 2009 there is no break in record from which the absolute maximum flows were isolated for this study.

Lilongwe at Old Town, 4.D.4 (From Laisi 2016)
Regular Gauging Station No. 4.D.4 was opened on October 21, 1955 (Malawi Government, 1986) and is located upstream of the road bridge in Old Town. The station has a compound weir with staff gauges and an automatic water level recorder has been here for some time indicating its primary status. Above this station, the catchment area is 1,870km² and the station gauges all the flow originating from the other rivers above it such as Katete and Likuni. River flow record at this station is satisfactory and it is almost continuous from 1971 to 2003 even though no data was available for the period from 1996 to 1998. Some notable high flows occurred in 1978 and 1982 with discharges of about 400m3/s and 375m3/s respectively. From 2003 to 2009, no record is available or is of poor quality

A statistical adjustment of 11 distributions to these two maximum flow records by Software 10LOIS retained 3 statistical laws and in each case the truncated Pearson 3 law appeared to be the best in the sense of the Brunet Moret test. Figure 35/ Salima Bridge & Figure 36/ Old Town.

.

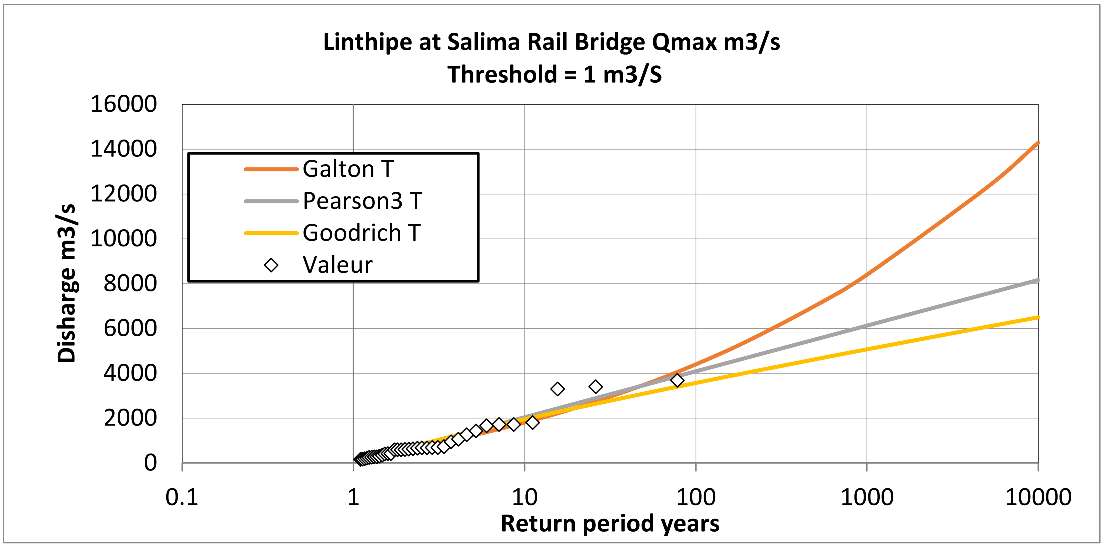

Figure 35: Characteristic floods for different return periods – Linthipe at Salima Rail Bridge, 4.B.1

[23] Laisi, E. (2016) 'Development of a flood frequency model for the river basins of the central region of Malawi as a tool for engineering design and disaster preparedness in flood prone areas,' Unpublished MSc thesis, University of South Africa

[24] Malawi Government (1986b). National Water Resources Master Plan, Annex 4, Hydrological Data Part II, WRA 4 to 8, Department of Water, Ministry of Works and Supplies, Lilongwe

Frequency	0,5	0.2	0.1	0.05	0.02	0.01	0.005	0.002	0.001
Return period	2	5	10	20	50	100	200	500	1000
Value (m3/s)	582	1415	2037	2656	3471	4087	4701	5513	6126

Table 10: Characteristic floods for different return periods – Linthipe at Salima Rail Bridge, 4.B.1

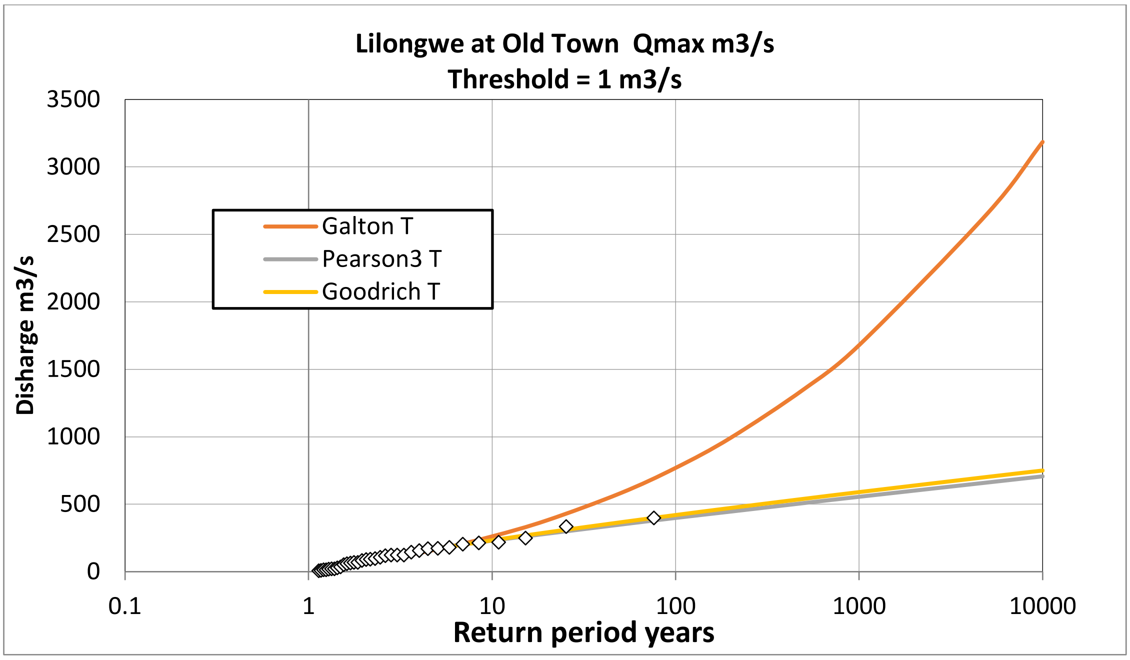

Figure 36: Characteristic floods for different return periods – Lilongwe at Old Town, 4.D.4

Frequency	0,5	0.2	0.1	0.05	0.02	0.01	0.005	0.002	0.001
Return per.(year)	2	5	10	20	50	100	200	500	1000
Value (m^3/s)	86,4	174	230	282	349	399	446	509	555

Table 11: Characteristic floods for different return periods – Lilongwe at Old Town, 4.D.4

Note that for the 100-year return period project flood, this statistical study based on observations proposes a Q100years flow = 4090 m^3/s for Linthipe at Salima Rail Bridge and a Q100years flow = 399 m^3/s for its tributary the Lilongwe at Old Town.

These estimates of the 100 years return flood are lower than proposed by the model used by Laisi in his thesis but are of the same order of magnitude. Q100years flow = 4636 m^3/s for Linthipe at Salima Rail Bridge and a Q100years flow = 509 m^3/s for its tributary the Lilongwe at Old Town. This is more realistic than the value proposed SOGREAH study,[25] Q100years flow = 1301 m^3/s at Old Town (President's Bridge).

3.3 Lifidzi River (4 B)

Lifidzi River is a stream in Central Malawi and has an elevation of 1,175 metres. Lifidzi River is situated nearby to the localities Kanyezi and Simeon. The Lifidzi Catchment covers an area of approximately 3274 km^2, its perimeter is 397 km, which gives it a Gravelius compactness index of 1.699. The density of drainage

[25] Sogreah (2010). Feasibility Studies and Preliminary Design for Lilongwe's New Water Source, Contract Number LWB/C/01, Lilongwe Water Board, Lilongwe

is 1.1 e-4 m/m². Lifidzi River is an important source of water for irrigation and domestic use in the surrounding areas.

The river is also important for fishing and supports a variety of fish species, including bream, catfish, and tilapia. However, like many rivers in Malawi, the Lifidzi River is facing environmental challenges such as pollution, deforestation, and climate change, which threaten its health and the well-being of the people and wildlife that depend on it.

The catchment is characterized by a mix of woodland, grassland, and cropland, with agriculture being the main economic activity. However, deforestation, soil erosion, and land degradation are significant challenges that threaten the sustainability of the catchment and the well-being of its inhabitants. The Lifidzi catchment is prone to flooding, especially during the rainy season, which typically occurs between November and April. Floods in the catchment are usually caused by heavy rainfall, which can lead to the Lifidzi River and its tributaries overflowing their banks and inundating nearby communities. Floods in the Lifidzi catchment can have significant social and economic impacts, including damage to crops, infrastructure, and homes, displacement of people, and loss of lives.

Efforts are being made to improve flood management in the Lifidzi catchment, including the construction of flood protection structures such as dykes and embankments, the establishment of early warning systems, and the promotion of community-based disaster risk reduction strategies. These efforts are aimed at reducing the impacts of floods and improving the resilience of local communities to the effects of extreme weather events (FAO, UNEP, and UNDP in 2017)[26].

In addition to these flood management projects, efforts are being made to promote sustainable water management practices in all Linthipe catchment and sub-catchments. These include the establishment of water user committees to oversee water allocation and management, the promotion of rainwater harvesting and conservation practices, and the implementation of integrated water resources management strategies to ensure the long-term sustainability of water resources in the catchments.

3.4 Dwangwa catchment and Sub-catchment 6C: Dwangwa, Livulezi and Rupashe Rivers, Mpasadzi.

The Dwangwa River rises in the west of Malawi's central plateau and flows in a northeasterly direction for about 160 km until it enters Lake Malawi. The river's upper reaches exhibit ancient broad valleys and meanders, while the gorge cut for the river's descent to the lake is narrow and recent. The Dwangwa River's drainage into Lake Malawi occupies a flat swampy area 40 km north of Nkhotakota.

The Dwangwa River catchment shares its southern border with the Bua River catchment. To the west is the Kasungu National Park, which forms part of the Dwangwa catchment basin, a well-vegetated flat plain consisting mainly of indigenous woodlands and white sandy soils. The northern frontier of the basin is marked by the headwaters of the numerous streams that drain the southern foothills of the Viphya Plateau. As the main river, the Dwangwa flows eastwards, it passes through a terrain of gentle slopes before abruptly falling over the Escarpment Zone on its way to the lake. Much of the middle and lower parts of this basin are well vegetated with indigenous forests.

The major rivers in this basin are the Liziwazi, Mpangala, Lingadzi, Chitete, Livwezi, Liwala, Kangwa, Lilavwa, Mlozi, Mpasadzi, Milenje, Livulesi, Phazi and the Rupashe. Many of these rivers flow during the wet season only even though during years of high precipitation, they are able to trickle throughout the year (Laisi 2016).

---

26 https://www.unccd.int/sites/default/files/documents/2017-09/GLO_Full_Report_low_res.pdf

Much of the upper basin of the Dwangwa lies in the aforementioned Kasungu National Park where the mean annual rainfall is less than 700mm. Its major tributaries such as Liziwazi, Mpangala, Lingadzi and Mpasadzi have their sources in this part of the basin. However, despite being dry in the upper reaches, the Dwangwa River Basin still enjoys adequate rainfall as it flows towards the lake where the mean annual rainfall increases sharply from 700 mm to over 1,300 mm per annum, recorded at Dwangwa Trading Centre on the Nkhotakota – Nkhata Bay Lakeshore Road.

The Dwangwa basin covers an area of 7750 km² according to the shape file provided by the Water Department, its perimeter is 486 km, which gives it a Gravelius compactness index of 1.557. The density of drainage is 1.117e-4 m/m². The land cover and land use (Figure 37) in the Dwangwa Catchment can be broadly categorized into five major classes:

1. Forest and woodland cover: This class includes natural and planted forests and woodlands. Forest and woodland cover accounts for about 44 % of the catchment's total land area.
2. Agricultural land use, this class includes various forms of crop cultivation and livestock farming, including maize, cassava, rice, sugarcane, and tobacco. Agricultural land use accounts for about 53% of the catchment's total land area. Over the observed period, deforestation is in favour of cultivation took place from 1992 to 2001. Reforestation is visible from 2006 and land cover and land use stabilize from this date.
3. In the dryer parts, shrubs are an important component of the catchment's ecosystem, providing habitat for wildlife, preventing soil erosion, and contributing to the overall biodiversity of the area. Some common shrubs found in the Dwangwa Catchment include Croton spp., Erythrococca spp., and Brachystegia spp. Shrubs cover about 4% of the total catchment area.
4. Water bodies and wetlands: This class includes rivers, lakes, and wetlands such as swamps and marshes. Water bodies and wetlands account for about 0.7% of the catchment's total land area.
5. Built-up areas, urban and peri-urban settlements, infrastructure such as roads, schools, and hospitals, and industrial facilities such as sugar factories account for 0.4% of the catchment's total land area. Despite a large increase in the area built on or occupied by roads in 2020, it remains modest (3.33 km²).

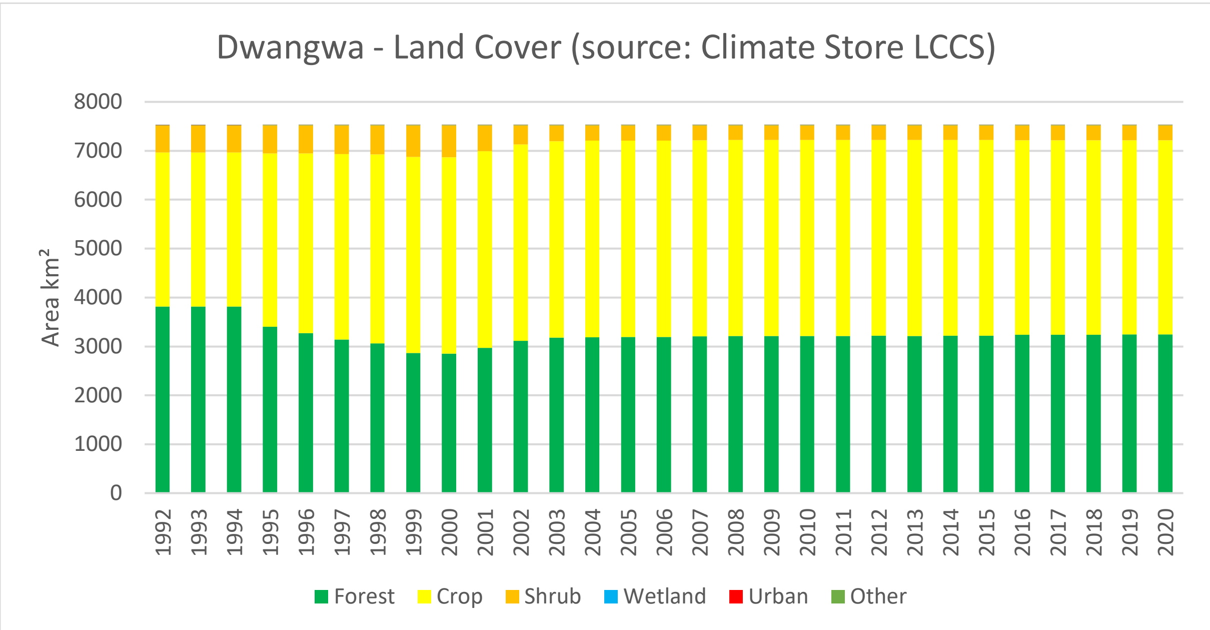

Figure 37: Land cover and land Use change in Dwangwa Catchment between 1993 – 2020

The map of the flood hazard index according to the 4 classes: low, moderate, elevated and high (Figure 38) exhibits one zone with important risks on the flooding of the infrastructures in the towns and on the roads.

Only two towns are potentially at elevated risk of flooding: Dwangwa and Nkhunga. Dwangwa and Nkhunga are two neighbouring towns located near the Lake Malawi shoreline. Dwangwa is known for its sugar industry, as there is a sugar factory located in the town. Nkhunga is known for its natural beauty and is a popular destination for tourists. Both towns are located in an area that is susceptible to flooding, especially during the rainy season, which runs from November to April.

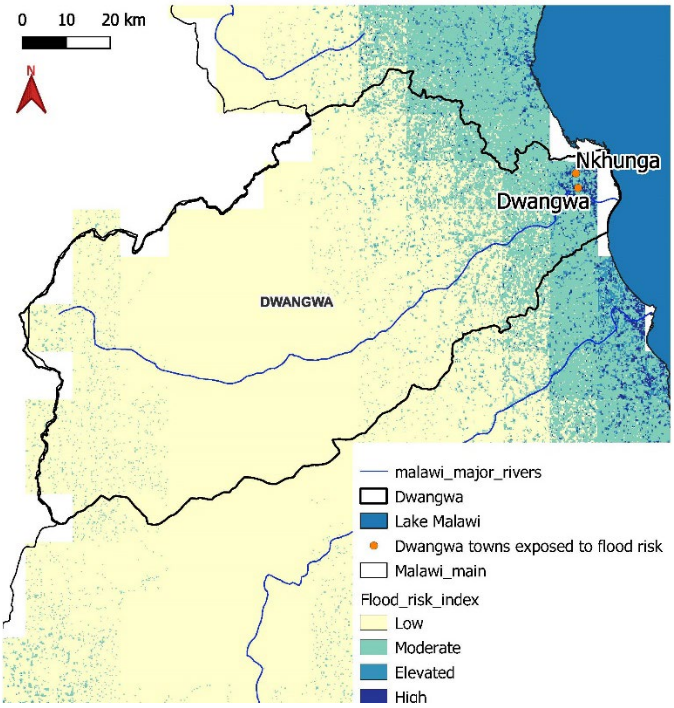

Figure 38: Dwangwa - flood index, towns and roads exposed to a flood hazard

To characterize the flood hazard, we extracted from the ERA5 database the average rainfall over the basin on the day with the highest precipitation of the year for statistical analysis. The ERA5 database also gives the total Runoff and the sub-surface Runoff (Appendix 4).

Figure 39 shows the variation of these two variables and the trend lines over the ERA5 reconstruction period. The trend lines indicate an increase in these values over time. But these increases are not statistically validated. Less pronounced than in the Linthipe basin, the figure also shows an increase in rainwater runoff.

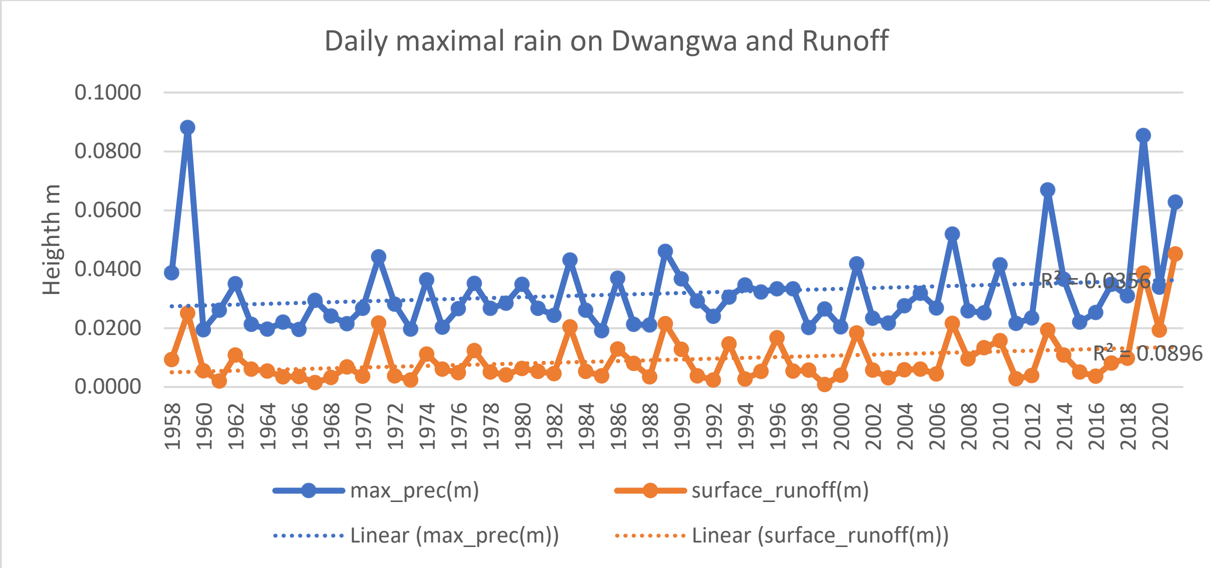

Figure 39: Dwangwa maximum daily rainfall and associated runoff (source CDS - ECMWF)

Figure 40 shows the relationship between maximum daily rainfall for the year and runoff. We see a correlation. This correlation is significant enough to be used for hydraulic engineering.

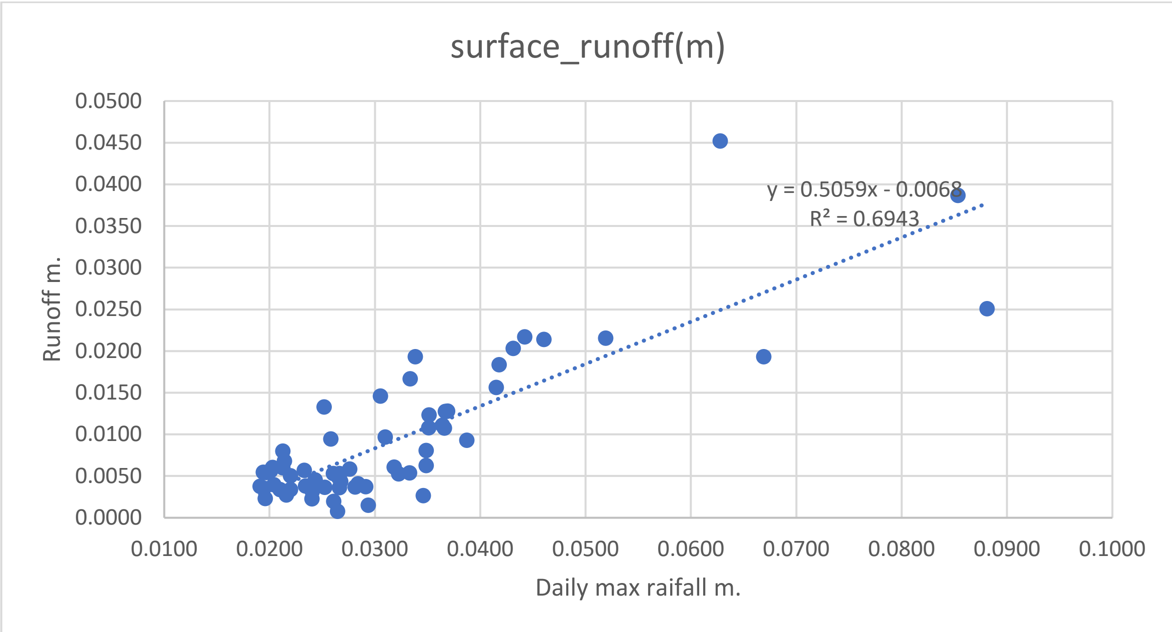

Figure 40: Correlation between daily max rain and runoff – Dwangwa

We performed a statistical analysis of the higher daily rainfall and runoff induced over the Dwangwa Catchment. Figure 41 shows the fit of the statistical distributions not rejected by the software DIXLOIS (χ^2 test =0) on the max daily rain in a logarithmic scale and Figure 42 on the daily runoff. For maximum daily rainfalls the best distribution fitting to the data is the Pearson Type III distribution with a threshold of 10 mm.

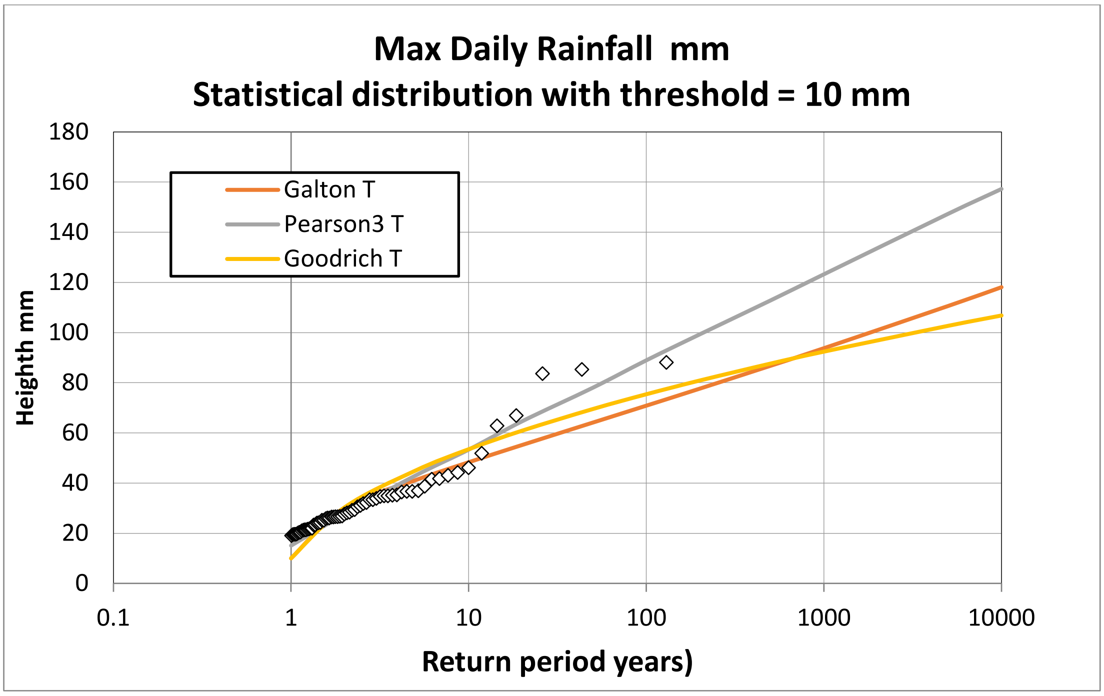

Figure 41: Dwangwa - statistical distributions, max daily rainfall in mm

Frequency	0,5	0.2	0.1	0.05	0.02	0.01	0.005	0.002	0.001
Return period	2	5	10	20	50	100	200	500	1000
Value (mm)	27.9	42.9	53.3	64.7	78.0	88.9	99.3	112.8	123.3

Table 12: Dwangwa - statistical distributions, max daily rainfall in mm

For runoff from maximum daily rainfall the best distribution fitting to the data is the Pearson Type III distribution with a threshold of 1 mm.

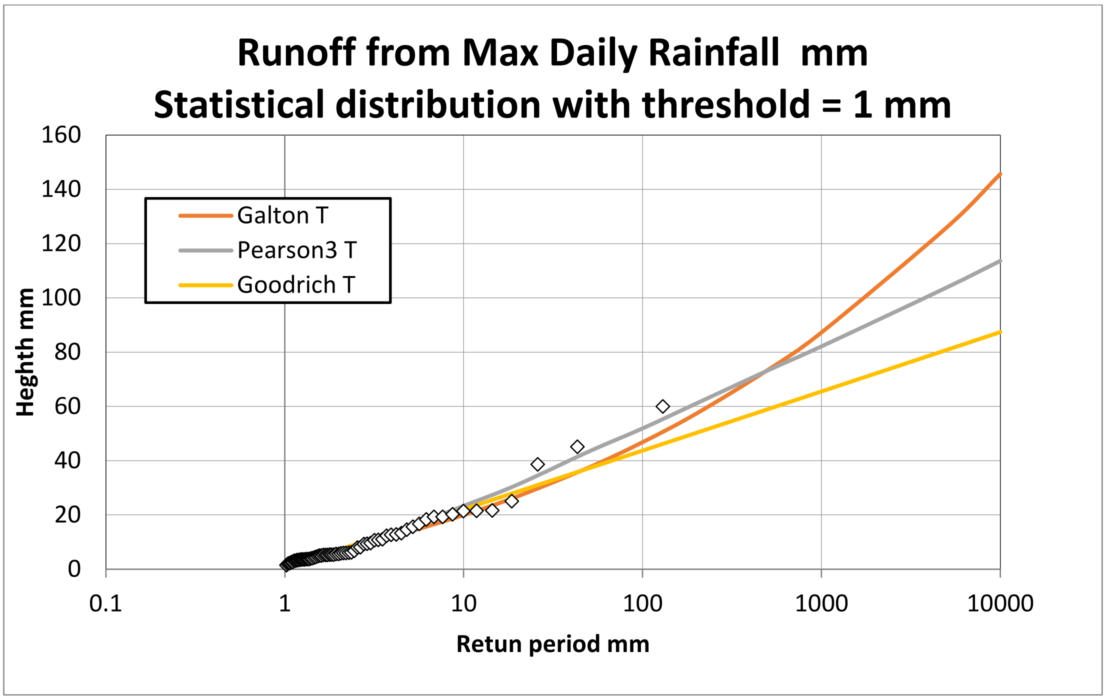

Figure 42: Dwangwa - statistical distributions, runoff from max daily rainfall in mm

Frequency	0,5	0.2	0.1	0.05	0.02	0.01	0.005	0.002	0.001

Return period	2	5	10	20	50	100	200	500	1000
Value (mm)	6.70	15.9	23.4	31.2	43.4	51.9	61.1	73.3	82.1

Table 13: Dwangwa - statistical distributions, runoff from max daily rainfall in mm

Laisi (2016) notes 2 hydrometric stations that have been operating in the Dwangwa catchment and we were able to retrieve in the appendices the annual maximum flow data from the following stations (Annexe 5):

- Dwangwa at Dwangwa, RGS 6.C.1; and
- Mpasadzi at M1 Road Bridge, 6.C.5.

Dwangwa at Dwangwa, RGS 6.C.1 (from Laisi, 2016)
The station is situated a few metres upstream of the M1 road bridge on the Lilongwe–Mzimba Road and was opened in February, 1953 (Malawi Government, 1986) with a compound rectangular weir as the control. For a long time, the station has had a cable car for measuring discharges at high water levels and an automatic water level recorder to assist in measuring gauge heights. From 1971 to 2009 the station has provided high quality data. Throughout this period, flood flows have been ably captured mainly through the presence of the water level recorder and the cable car. However, data is missing between1996 and 1998 and between 2003 and 2007. Observed highest flows of the absolute maxima with discharges of more than 150m^3/s occurred in 1980, 1989, 1996, 2003 and 2007 with flows of 172m^3/s, 232m^3/s, 174m^3/s, 216m^3/s and 156m^3/s respectively.

Mpasadzi at M1 Road Bridge, 6.C.5 (from Laisi, 2016)
This station drains an area of 309 km^2 and was opened on November 12, 1965 (Malawi Government, 1986). The channel itself has acted as the control at the station and data is of good quality for low and medium levels. Due to the absence of a cable car, it has not been possible to measure exceptionally high stages during flood periods. Save for the period 1977 to 1980, the record of high flows is continuous. The highest flows were recorded in 1981 and 1989 with magnitudes in excess of 140m^3/s.

A statistical adjustment of 11 distributions to these two maximum flow records by Software 10LOIS retained 3 statistical laws. For Dwangwa at Dwangwa the truncated Pearson 3 law appeared to be best in the sense of the Brunet Moret test and for Mpasadzi at Road Bridge, the truncated Galton low fits better to data. Figure 43 / Dwangwa at Dwangwa, RGS 6.C.1 and Figure 44 / Mpasadzi at M1 Road Bridge, 6.C.5 show the statistical distributions, Absolute maximum flows (m3/s). Discharge

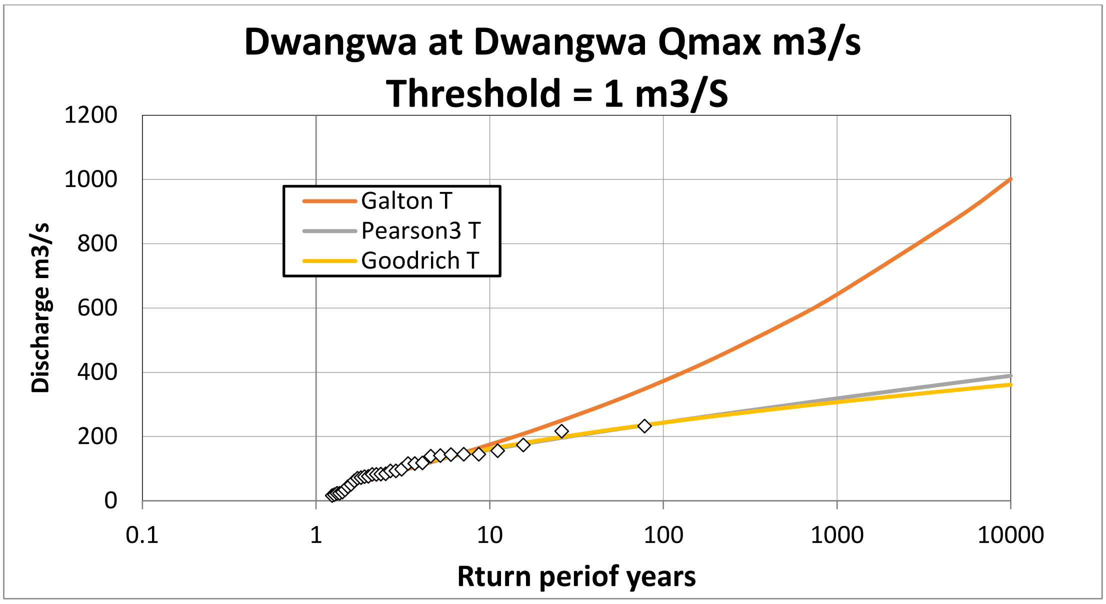

Figure 43: Characteristic floods for different return periods - Dwangwa at Dwangwa, RGS 6.C.1,

Frequency	0,5	0.2	0.1	0.05	0.02	0.01	0.005	0.002	0.001
Return period	2	5	10	20	50	100	200	500	1000
Value (m3/s)	77.1	129	159	186	220	243	267	296	319

Table 14: Characteristic floods for different return periods - Dwangwa at Dwangwa, RGS 6.C.1,

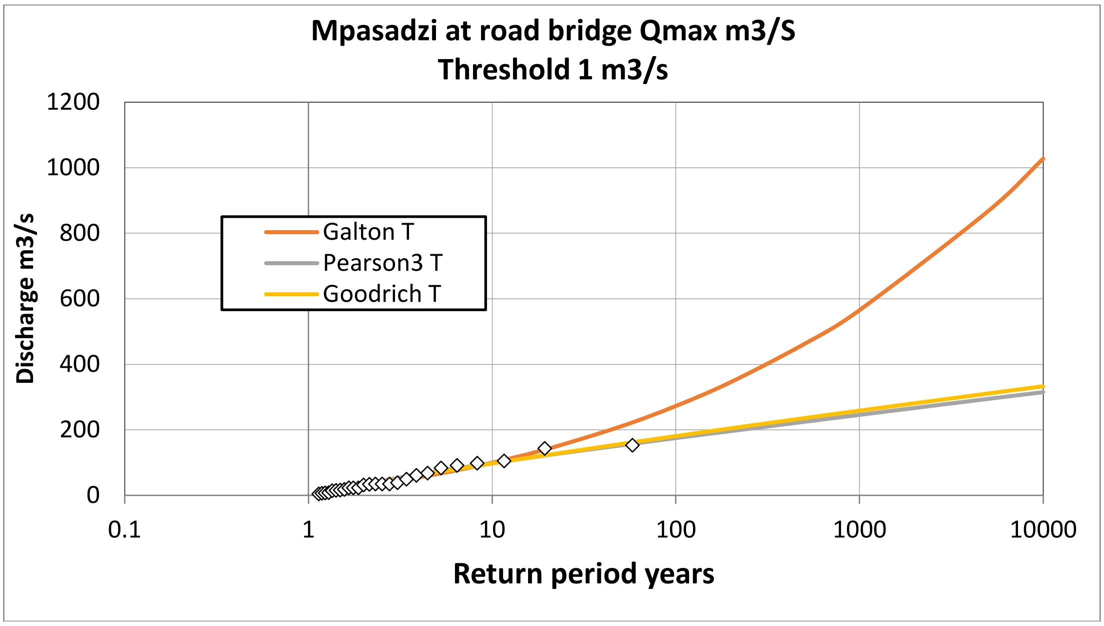

Figure 44: Characteristic floods for different return periods Mpasadzi at M1 Road Bridge, 6.C.5

Frequency	0,5	0.2	0.1	0.05	0.02	0.01	0.005	0.002	0.001
Return period	2	5	10	20	50	100	200	500	1000
Value (m3/s)	27.6	64.9	99.7	142	210	273	346	462	565

Table 15: Characteristic floods for different return periods Mpasadzi at M1 Road Bridge, 6.C.5

Sub-catchment 6C: Dwangwa, Livulezi and Rupashe Rivers, Mpasadzi.
The Livulezi and Rupashe rivers are both tributaries located in the Dwangwa catchment area of Malawi. The Mpasadzi River is a tributary of the Dwangwa River, approximately 160 km long and flows through the central region of Malawi.
6C sub-catchment covers an area of approximately 1321 km², its perimeter is 209 km, which gives it a Gravelius compactness index of 1.407. The density of drainage is 0.9 e-4 m/m².

3.5 Conclusion of the study on catchments and sub-catchments

At the catchments scale we were able to analyse the variation in land cover and land use. The three catchments have substantial deforestation in common until the beginning of the 2000s, followed by a noticeable reduction (tho deforestation continues) and even some reforestation in recent years. The extent of built-up areas or areas with roads and infrastructure is increasing, in the Linthipe basin, in particular.

The mapping of the flood risk index on catchments allowed for the definition of areas where risk seems to be higher and the provision of a list of places where this risk is significant. From what we found in the literature at our disposal, we showed those places under threat. We noted that this index did not take into account the sealing of the soil in the cities and did not allow classifying Lilongwe in a region where the hazard is strong, especially in low-lying areas and informal settlements.

The analysis of the catchment average maximum rainfall observed each year and the runoff it causes on the catchment (ERA5 - ECMWF) shows in the three cases studied an upward trend even if this trend is not significant in the sense of a statistical test. In each of the three catchments, we established a significant correlation between the maximum daily rainfall and the induced runoff. The establishment of new annual maximum rainfall in the climate scenarios should allow for measuring the increase of the flood hazard.
For the Linthipe and Dwangwa catchments, we had access to a database of measured flows. From this database, we extracted the annual maximum flows and calculated project (heaviest likely) floods for characteristic return times.

For the sub-catchments proposed in the study, we have given the details found in the literature. The size of these sub-catchments does not allow for the use of satellite databases, we did not find any observed data except for the Mpazadzi, and it was possible to estimate the design (hypothetical) flood for different return periods at the road bridge.

4. UTILISATION OF RAINFALL CLIMATIC PROJECTIONS

4.1 Projection Scenarios and Employed Climatic Models

Following the submission of: "Flood Assessment in Malawi" document Report ARIA / 2023.050,[27] we were asked to carry out a further analysis and to use the DCCMS's projections made at the country's climatological stations to specify the risk of flooding in the climate change scenarios used for these projections.
The Malawi Climate Risk Assessment chose two scenarios:

1. The Shared Socioeconomic Pathway 2 (SSP2) with the radiative forcing level of 4.5 watts per square meter (W/m²) in the year 2100. It is one of the scenarios used in climate modelling by the Intergovernmental Panel on Climate Change (IPCC). This scenario represents a particular

27 Jean Albergel, Lawrence Flint and Céline Déandréis (2023), MALAWI-Climate Change Adaptation – Flood Assessment in Malawi 66 p Hydroscience, Acterra and Aria - Paris

combination of socio-economic and climate development pathways. Here's a brief overview of SSP2-4.5:

a. SSP2 (Shared Socioeconomic Pathway 2): represents a middle-of-the-road or moderate development pathway. It assumes a world with relatively balanced and sustainable economic growth, moderate population growth, and a mix of challenges and opportunities for mitigation and adaptation.

b. 4.5 W/m² Radiative Forcing: Radiative forcing measures the change in the Earth's energy balance due to factors like greenhouse gas emissions and other climate-related factors. 4.5 W/m² represents the level of radiative forcing by the year 2100 in this scenario. A radiative forcing of 4.5 W/m² corresponds to a pathway where global warming is limited but still exceeds the targets of the Paris Agreement. It implies a global temperature increase above pre-industrial levels.

2. The SSP5-8.5 scenario, or Shared Socioeconomic Pathway 5 with a radiative forcing of 8.5 watts per square meter (W/m²), is one of the scenarios used in climate modelling by the Intergovernmental Panel on Climate Change (IPCC). Here's an overview of SSP5-8.5:

   a. SSP5 (Shared Socioeconomic Pathway 5) represents a scenario characterized by high population growth, high-energy demand, and a fossil-fuel-intensive energy system. It assumes that there is limited global cooperation in addressing environmental and climate challenges, leading to higher emissions of greenhouse gases.

   b. A radiative forcing of 8.5 W/m² corresponds to a pathway where greenhouse gas emissions and other climate drivers lead to a significant increase in global temperatures. SSP5-8.5 is often referred to as a high emissions scenario and is associated with a worst-case scenario for climate change, resulting in substantial global warming.

In summary, SSP2-4.5 is a scenario that envisions a world with moderate socioeconomic development and a radiative forcing level of 4.5 W/m² by 2100. It represents a future where efforts to mitigate climate change are not as aggressive as in some other scenarios, resulting in a level of global warming that exceeds the more ambitious climate goals.

SSP5-8.5 is a scenario that envisions a future with high population growth, high energy demand, and limited global cooperation to mitigate climate change. It is characterized by a radiative forcing level of 8.5 W/m², which implies a significant increase in global temperatures and is often used to study the potential impacts of high greenhouse gas emissions on the climate system.

DCCMS uses 9 atmospheric circulation models to generate climate data.
These models are part of the ongoing efforts in climate science to develop and improve Earth system models for simulating climate processes and understanding future climate scenarios.

1. CNRM-ESM2.1, also known as the Centre National de Recherches Météorologiques Earth System Model version 2.1, is a climate model developed by the Centre National de Recherches Météorologiques (CNRM) in France.

2. MIROC6, which stands for the "Model for Interdisciplinary Research on Climate version 6," is a climate model developed by a collaboration of Japanese research institutions, including the University of Tokyo, the National Institute for Environmental Studies (NIES), the Japan Agency for Marine-Earth Science and Technology (JAMSTEC), and the Meteorological Research Institute (MRI).

MIROC6 is part of the MIROC family of climate models and is used for a wide range of climate research purposes.

3. ACCESS.CM2 refers to the Australian Community Climate and Earth System Simulator Climate Model, version 2. It is a climate model developed by the Australian scientific community for research and simulations related to climate and Earth system science. ACCESS.CM2 is an advanced and comprehensive Earth system model that simulates various components of the Earth's climate system, including the atmosphere, oceans, land surface, and sea ice.

4. EC-Earth3.Veg.LR is a specific configuration or version of the EC-Earth model developed for climate research. The "EC" in EC-Earth stands for "European Consortium for High-Resolution Climate Modeling," and it represents a collaborative effort among European research institutions to develop and use climate models for simulating the Earth's climate system.

5. The MPI-ESM1.2.LR, developed by the Max Planck Institute for Meteorology (MPI-M) in Germany, is a climate model that belongs to the MPI-ESM (Max Planck Institute Earth System Model) family of models. It is designed to simulate various components of the Earth's climate system and is used for climate research and simulations. The "LR" in the model name indicates that it operates at a relatively low spatial resolution.

6. MRI-ESM2.0 (Meteorological Research Institute Earth System Model version 2) is a climate model developed by the Japan Meteorological Research Institute (MRI). It is part of the ongoing efforts in climate science to develop and improve Earth system models for simulating climate processes and understanding future climate scenarios.

7. CMCC-ESM2 is a climate model developed by the Centro Euro-Mediterraneo sui Cambiamenti Climatici (CMCC), which is the Euro-Mediterranean Center on Climate Change. It's part of the CMCC's efforts in climate science to understand and project the Earth's climate system under various scenarios. CMCC-ESM2 is used for climate research and simulations and is a part of the broader community of Earth system models.

8. The INM.CM5.0, also known as the "Institute for Numerical Mathematics Earth System Model version 5.0," is a climate model developed by the Institute for Numerical Mathematics (INM) in Russia.

9. EC-Earth3.CC, also known as EC-Earth3 Community Configuration, is a specific configuration of the EC-Earth (European Consortium for High-Resolution Climate Modeling Earth System Model) developed for climate research. EC-Earth is a collaborative project among European research institutions that focuses on developing and using climate models to simulate various aspects of the Earth's climate system.

4.2 Data prepared by DCCMS

W Daily rainfall data observed at 8 meteorological stations used for the CRA, located in each Agricultural Development Division (ADD) (Table 16) distributed throughout the country. Figure 45 shows the location of these 8 stations in relation to the catchment areas and administrative districts targeted by this work.

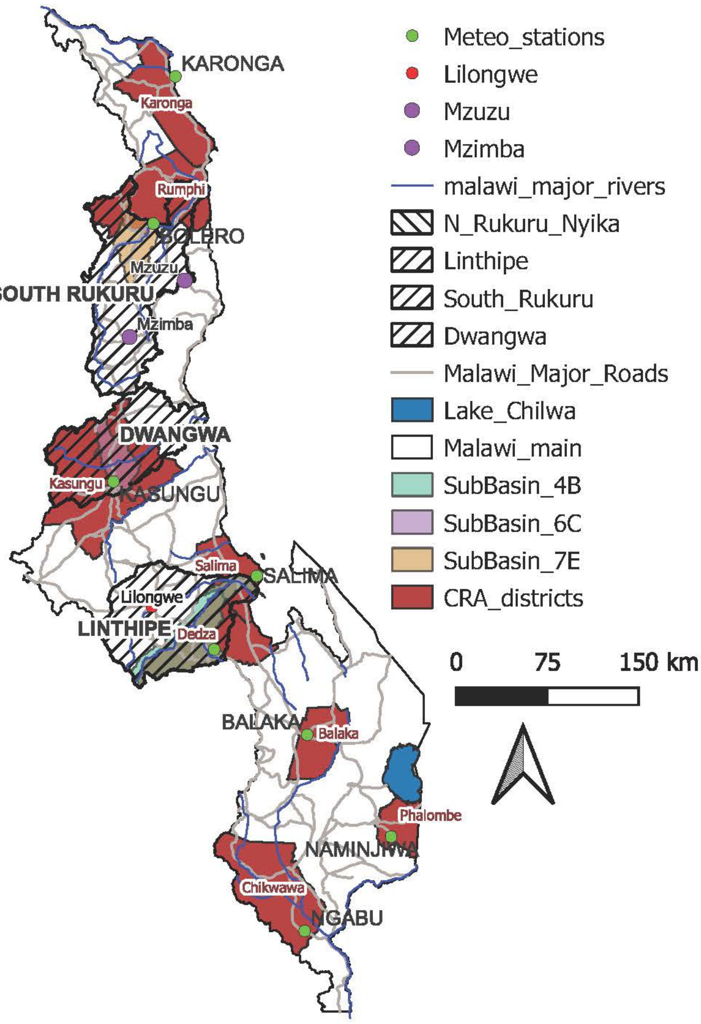

Figure 45: DCCMS Meteorological station

Table 16: Data forwarded by DCCMS

Station	Lat -long	Elevation (m)	Observed Precip	Precip SSP2-4.5	Precip SSP5-8.5
Balaka	-14.98 - 34.97	482	1976 - 1981	1981 - 2100	1981 - 2100
Bolero	-13,75 - 34,58	1100	2013 - 2021	1981 - 2100	1981 - 2100
Dedza	-14.32 - 34.25	1632	1961 - 2021	1981 - 2100	1981 - 2100
Karanga	-9.88 - 33.95	529	1961 - 2020	1981 - 2100	1981 - 2100
Kasungu	-13.02 - 33.47	1028	1961 - 2021	1981 - 2100	1981 - 2100
Naminjiwa	-15.77 - 35.62	1029	1969 - 2019	1981 - 2100	1981 - 2100
Ngabu	-16.5 - 34.95	102	1961 - 2021	1981 - 2100	1981 - 2100
Salima	-13.75 - 34.58	512	1961 - 2021	1981 - 2100	1981 - 2100

For these 8 stations, we received the 1981 - 2100 projections of daily temperature and daily rainfall data for two climate scenarios, SSP2-4.5 and SSP5-8.5, using 9 atmospheric circulation models. We did not get any data on flow rates or observed or projected runoff.

In the daily data simulated with the climate models, several files show gaps, either the entire series for a model, or the years 2990 to 2100. Some climate models do not consider leap years. The absence of April 29 eliminates data for the whole year in the climate software (i.e. one year in four for the periods 1981 - 2100). We have taken the decision to set a 0 mm on 29 April for these years and to recover 30 years of data for each simulation. For all the stations, DCCMS files give the minimum and maximum daily rainfall values for the simulated models, as well as the median value.

The geographical position of the available stations represents the latitudinal gradient, but not the orography of the country. Our attempts to spatialise rainfall using the observations or the projections have been unsuccessful; at least 50 points would be needed to represent the spatial variability of rainfall. We have decided to analyse the point data for each station and say that they represent trends in the catchment areas or districts where they are located (see Table 17). We began by reconstructing the observed and projected monthly and annual rainfall for the SSP 2-4.5 scenario and the SSP5-8.5 scenario.

Table 17: Areas represented by the 8 climatological stations

Meteorological Station	Catchment in the consultancy	CRA in the consultancy
Balaka	N/A	Balaka
Bolero	South Rukuru	Rumphi
Dedza	Linthipe	Dedza
Karanga	N/A	Karanga
Kasungu	Dwangwa	Kasungu
Naminjiwa	N/A	Phalombe
Ngabu	N/A	Chikawa
Salima	Lake Malawi	Salima

4.3 Data analyses

4.3.1 Yearly rainfall

On an annual scale, given the linearity of the average operation, the average of the daily data obtained by the various models and aggregated over the year, appears to be a reasonable solution and is aa recommended practice. We began with a quick review of the observed rainfall data and deleted data from years that seemed too incomplete. We plotted the observed values and the projected values (using the median values of the models used) on the same graph for each station (see Figure 46) for SSP 2-4.5.

These graphs show a good representation of the inter-model averages for annual rainfall for all stations except Balaka, although the inter-annual variability is much less compared to observations. The Balaka station appears to have major observation problems. We have eliminated it in the work that follows.

Figure 46: Observed and projected rainfall (mm) at DCCMS' stations

4.3.2 Monthly rainfall

On a monthly scale, a comparison between the mean of the simulated data and the observed data shows that in the simulated data, the months with no rainfall virtually disappear. This has led us to consider each model separately.

As Malawi's territorial extent is relatively small, we have looked for the climate model that best reconstructs monthly precipitation for all the stations, eliminating Balaka (which greatly diminishes comparisons). Appendix 1 compares the average observed monthly values for the selected stations with those simulated by the different climate models on the present period. Figure 47 shows the correlation between observed and simulated average monthly rainfall on the same periods for each climatic model.

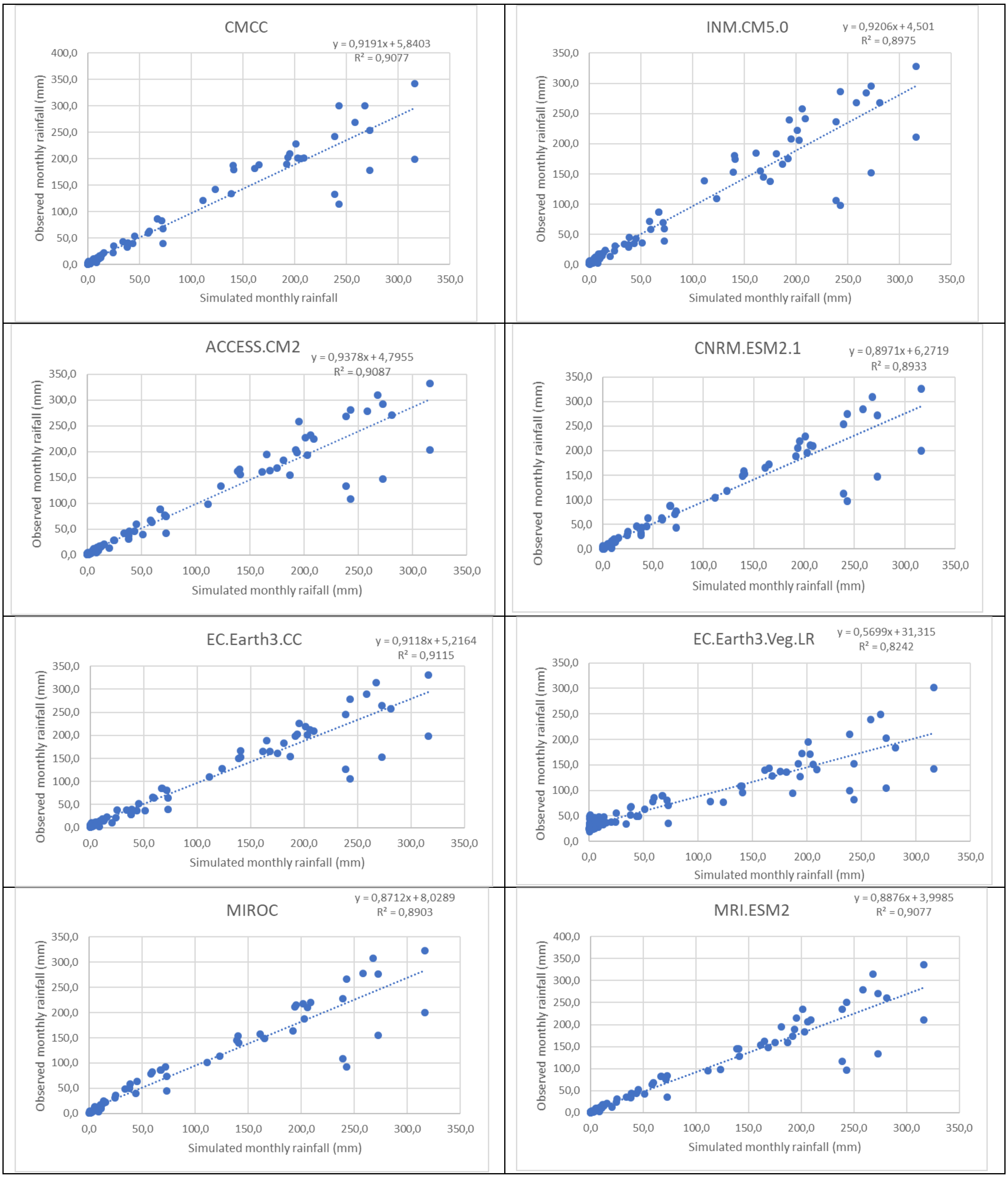

Figure 47: Observed and simulated average monthly rainfall.

The 8 climate models reproduce monthly and annual rainfall quantities well. The best model is the one that shows the strongest correlation coefficient over all the stations and a slope of the correlation line that is closest to 1. Table 18 gives the following parameters:

- The correlation coefficient (often denoted as "R") measures the strength and direction of a linear relationship between two variables. It quantifies how closely the data points in a scatterplot cluster around a straight line. The correlation coefficient can range from -1 to 1. A positive value of "R" (closer to 1) indicates a positive linear relationship, meaning that as one variable increases, the other tends to increase as well. A negative value of "R" (closer to -1) indicates a negative linear relationship, meaning that as one variable increases, the other tends to decrease. In our case the value needs to be positive and best model is one where r is the closest to 1.
- The coefficient of determination, denoted as "r-squared" or "R^2," is a measure of the proportion of the variance in one variable that can be predicted or explained by another variable in a linear regression model. In simple terms, it tells you how well one variable can predict or account for the variation in another variable. An R^2 value can range from 0 to 1. An R^2 of 0 means that the independent variable does not explain any of the variance in the dependent variable. An R^2 of 1 means that the independent variable can perfectly explain all the variance in the dependent variable. In practical terms, an R^2 value closer to 1 indicates a stronger relationship between the variables, while an R^2 value closer to 0 suggests a weaker relationship.
- 1-Slope of correlation line (1-s). When the correlation line has a slope close to 1, the model reconstructs the data without drift.

Table 18: Coefficients of correlation (R), regression line slope (S)

	CMCC	INM.CM5.0	ACCESS.CM2	CNRM.ESM2.1	**EC.Earth3.CC**	EC.Earth3.Veg.LR	MIROC	MRI.ESM2
R	0.953	0.948	0.954	0.946	**0.955**	0.909	0.944	0.953
R^2	0.909	0.899	0.910	0.895	**0.913**	0.827	0.892	0.909
1-S	0.012	0.025	0.031	0.004	**1.6 E-05**	0.449	0.023	0.023

The model EC.Earth3.CC is developed as a collaborative effort by various European research institutions. It is part of the Earth System Model (ESM) family and is used to simulate the Earth's climate system. The "CC" in the model's name typically refers to "Coupled Climate," which means that it includes multiple components of the Earth's system, including the atmosphere, ocean, land surface, and sea ice, all interacting with each other.
The competence of this model also shows that the downscaling from the 80 km^2 grid to the station was carried out with a satisfactory simulation of precipitation volumes.

4.3.3 Daily Rainfall

To compare daily model data with observations, we compared the distribution of daily rainfall over the current period with the aim of choosing the model that is best suited to our stations. We considered five categories of rainy days: 1) days with no rain or rain of less than 1 mm; 2) days with rain of more than 25 mm; 3) days with rain of more than 50 mm; 4) days with rain of more than 90 mm; 5) days with rain of more than 100 mm. The following tables give the number of rain days per year for each station, for the seven stations selected and for each model.

Table 19: Number of rains per year corresponding to thresholds – Current period

a- Bolero station

Model	Days/year_ no_rain	Days/year>25 mm	Days/year>50 mm	Days/year>90 mm	Days/year>120 mm
OBS	301.44	16.18	5.80	2.03	1.19
CMCC	53.93	1.14	0.41	0.00	0.00
INM.CM5.0	54.62	1.20	0.24	0.00	0.00
ACCESS.CM2	53.91	1.20	0.22	0.00	0.00
CNRM.ESM2.1	54.51	1.14	0.20	0.00	0.00
EC.Earth3.CC	53.80	1.11	0.19	0.00	0.00
EC.Earth3.Veg.LR	54.59	1.16	0.25	0.00	0.00

MIROC	53.40	1.06	0.23	0.01	0.00
MRI.ESM2	54.48	1.08	0.20	0.00	0.00

b- Dedza station

Model	Days/year_ no_rain	Days/year>25 mm	Days/year>50 mm	Days/year>90 mm	Days/year>120 mm
OBS	288.13	9.97	2.08	2.00	1.00
CMCC	52.28	1.79	0.42	0.12	0.03
INM.CM5.0	51.70	1.89	0.52	0.06	0.02
ACCESS.CM2	51.79	1.99	0.39	0.08	0.02
CNRM.ESM2.1	52.01	1.93	0.39	0.07	0.02
EC.Earth3.CC	51.47	1.83	0.44	0.06	0.02
EC.Earth3.Veg.LR	52.09	1.92	0.38	0.05	0.02
MIROC	51.34	1.74	0.38	0.07	0.02
MRI.ESM2	52.26	1.74	0.38	0.05	0.02

c- Karanga station

Model	Days/year_ no_rain	Days/year>25 mm	Days/year>50 mm	Days/year>90 mm	Days/year>120 mm
OBS	288.79	12.74	3.64	1.36	1.00
INM.CM5.0	52.73	1.94	0.56	0.08	0.03
ACCESS.CM2	52.14	2.07	0.52	0.08	0.05
EC.Earth3.CC	52.09	1.99	0.47	0.08	0.05
EC.Earth3.Veg.LR	52.56	1.99	0.45	0.09	0.05
MRI.ESM2	52.51	2.06	0.54	0.08	0.06

d- Kasungu station

Model	Days/year_ no_rain	Days/year>25 mm	Days/year>50 mm	Days/year>90 mm	Days/year>120 mm
OBS	304.84	8.57	2.15	1.10	0.00
CMCC	54.67	1.75	0.58	0.06	0.00
INM.CM5.0	54.51	1.56	0.47	0.09	0.00
ACCESS.CM2	54.31	1.55	0.49	0.11	0.02
CNRM.ESM2.1	54.58	1.58	0.41	0.05	0.00
EC.Earth3.CC	54.23	1.54	0.37	0.08	0.00
EC.Earth3.Veg.LR	54.58	1.65	0.38	0.04	0.00
MIROC	54.27	1.51	0.41	0.08	0.00
MRI.ESM2	54.61	1.49	0.37	0.06	0.00

e- Naminjiwa station

Model	Days/year_ no_rain	Days/year>25 mm	Days/year>50 mm	Days/year>90 mm	Days/year>120 mm
OBS	276.14	10.10	2.86	1.29	1.25
CMCC	46.50	1.69	0.47	0.19	0.07
INM.CM5.0	46.18	1.91	0.57	0.13	0.04
ACCESS.CM2	46.28	1.84	0.47	0.13	0.05
CNRM.ESM2.1	46.13	1.80	0.45	0.10	0.04
EC.Earth3.CC	45.91	1.86	0.45	0.10	0.04
EC.Earth3.Veg.LR	46.56	1.69	0.44	0.10	0.04
MIROC	46.09	1.76	0.43	0.15	0.06
MRI.ESM2	46.42	1.68	0.47	0.09	0.03

f- Ngabu station

Model	Days/year_ no_rain	Days/year>25 mm	Days/year>50 mm	Days/year>90 mm	Days/year>120 mm
OBS	306.93	9.16	2.59	1.16	1.00
CMCC	54.71	1.70	0.52	0.17	0.09
INM.CM5.0	54.03	1.85	0.63	0.12	0.04
ACCESS.CM2	54.37	1.81	0.53	0.14	0.06
CNRM.ESM2.1	54.46	1.82	0.52	0.09	0.03
EC.Earth3.CC	54.12	1.83	0.54	0.07	0.03
EC.Earth3.Veg.LR	54.67	1.76	0.51	0.07	0.02
MIROC	54.02	1.72	0.52	0.12	0.04
MRI.ESM2	54.59	1.64	0.45	0.08	0.03

g- Selima station

Model	Days/year_ no_rain	Days/year>25 mm	Days/year>50 mm	Days/year>90 mm	Days/year>120 mm
OBS	301.44	16.18	5.80	2.03	1.19
CMCC	53.93	2.82	1.08	0.37	0.13
INM.CM5.0	53.95	2.82	1.25	0.33	0.11
ACCESS.CM2	53.97	2.93	1.14	0.44	0.17
CNRM.ESM2.1	53.84	2.89	1.11	0.30	0.11
EC.Earth3.CC	53.94	2.81	1.14	0.33	0.08
EC.Earth3.Veg.LR	53.92	2.91	1.20	0.34	0.11
MIROC	53.39	2.80	1.14	0.31	0.10
MRI.ESM2	53.88	2.73	1.19	0.35	0.11

We note a very different distribution of rainy days between observations and simulations, whatever the atmospheric circulation model. All the models give fairly similar results, but they are very far from the observations. For example, at Salima, 301.44 days without rain (less than 1 mm) per year are observed, compared with 53.85 for the average of the models. Similarly, there are 1.19 days of rainfall greater than 120 mm, compared with 0.11 for the average model.

While downscaling was able to reconstitute rainfall totals, it did not group them well by rainy day. It spread the total rainfall over the large mesh of 80 km² over a large number of rainy days without any grouping criteria for moving from the mesh to the station point.

This increase in the number of rainy days and the disappearance of the heaviest rains is contradictory to the trends noted in the earlier report, where the rainfall reanalyses ERA 5 showed, on the contrary, a greater occurrence of days of heavy rain and an increase in the number of rain-free periods. The increase in heavy rainfall is also borne out by previous work which, based on NOAA (National Oceanic and Atmospheric Administration) data, shows an increasing number of cyclones from the Indian Ocean reaching Malawi.

To give future trends in flood risk for each region represented by one of the 7 stations, we analyse rainfall on three-time scales: annual, monthly and daily.

1. On an annual scale, we use the averages between the different models to see the evolution of quantitative rainfall distributions.
2. On a monthly scale, we will compare the evolution of the hyetographs using the results of the EC.Earth3.CC model on three reference periods.
3. At the daily scale we cannot use projections. We give a statistic of the daily rainfall values based on the observations and we indicate the threshold for which the rainfall can be considered at risk of flooding.

4.4 Trend in flood risk by region

4.4.1 Bolero -South Rukuru catchment and Rumphi CRA

Figure 48 shows the evolution of interannual rainfall over the observed period, and over three thirty-year periods (present, 2050 and 2100) according to the two scenarios SSP2-4.5 and SSP5-8.5.

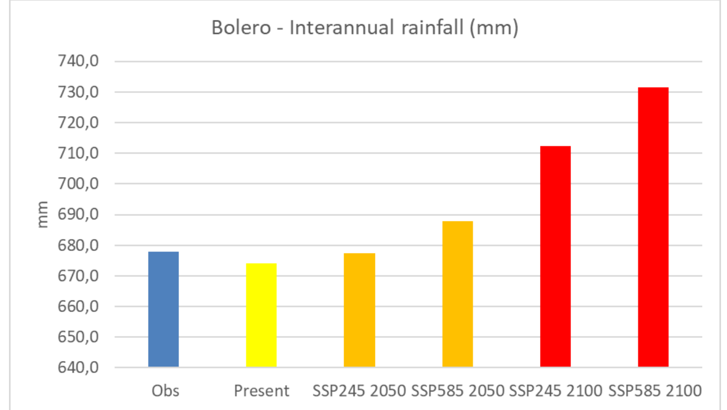

	Bolero - Interannual rainfall (mm)
Obs	677.9
Present	674.1
SSP245 2050	677.4
SSP585 2050	687.9
SSP245 2100	712.4
SSP585 2100	731.4

Figure 48: Bolero - Interannual Rainfall projections.

For this region, there is a clear increase in interannual rainfall. The interannual averages for the observed period and those simulated by the models are very close, which reinforces the downscaling carried out on annual rainfall volumes.

The quantile distribution of annual rainfall for three periods of 30 successive years after fitting a Goodrich distribution (Figure 49) in the SSP2.4-5 scenario shows that it is mainly the occurrence of very wet years that propels an increase in rainfall in average years. In median years (probability 0.5), interannual rainfall does not vary, while in wet decadal years (probability 0.9), rainfall increases by 2.7% compared with the current period for the 2050 period and by 3.8% for the 2010 period.

This increase in annual rainfall translates into an increase in river runoff and therefore an increase in the risk of flooding.

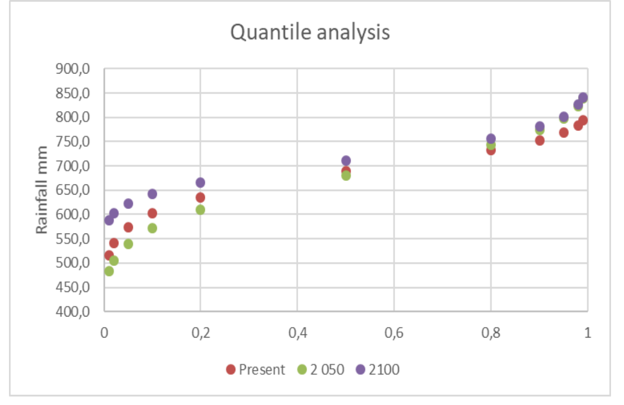

Ex Proba	Present	2 050	2100
0.01	483.7	588.5	516.8
0.02	505.6	602.3	540.4
0.05	540.2	623.2	574.6
0.1	571.7	642.0	603.3
0.2	609.9	665.1	635.6
0.5	679.7	710.3	689.1
0.8	743.1	756.7	733.1
0.9	773.5	781.5	753.0
0.95	797.3	802.2	768.0
0.98	822.8	825.9	783.7
0.99	839.0	841.8	793.5

Figure 49: Quantile distribution of annual rainfall (Goodrich law)

To analyse the risk of flooding according to the season, we computed the monthly rainfall hietograms simulated by the EC.Earth3.CC model, which we have found to be the best. Figure 50 shows the distribution of monthly rainfall for the two scenarios over the present, 2050 and 2100 periods.

The wettest months are December, January and February. The increase in rainfall occurs with the greatest effect in February and March, which become the months with the highest risk of overflow flooding.

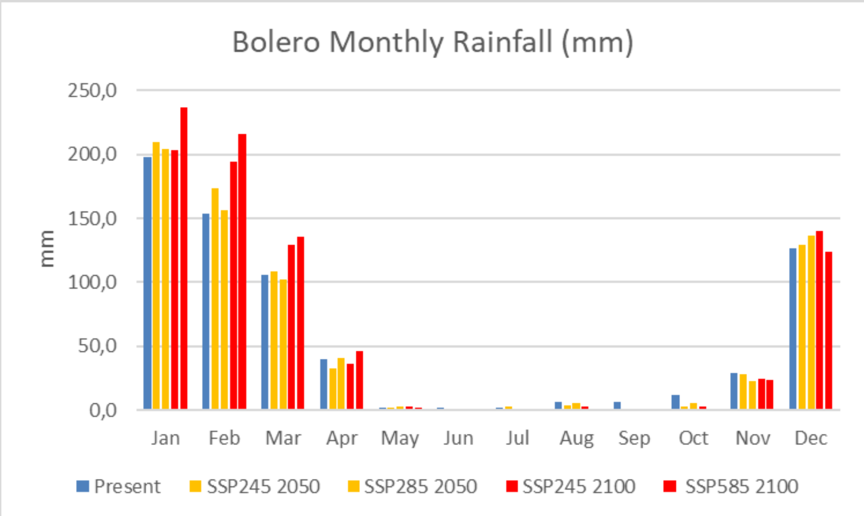

Rainfall (mm)	Jan	Feb	Mar	Apr	May	Jun	Jul	Aug	Sep	Oct	Nov	Dec
Present	198.3	153.3	106.1	39.8	2.3	1.9	2.0	6.1	6.0	12.2	28.7	126.6
SSP245 2050	210.1	173.9	108.8	32.4	2.2	1.3	2.8	3.3	1.2	3.0	28.1	129.2
SSP285 2050	203.9	156.7	102.6	40.5	2.6	1.0	0.8	5.2	0.8	5.3	22.5	136.8
SSP245 2100	203.1	194.5	129.6	36.3	2.5	1.0	1.0	2.4	0.9	2.8	24.9	140.4
SSP585 2100	236.4	216.3	135.4	45.8	1.7	1.1	0.7	0.8	0.8	1.4	23.2	123.5

Figure 50: Bolero – Observed and simulated monthly rainfall (mm)

To have a trend in the risk of flooding by runoff or flash-flood, we would need to have daily rainfall projections, but we saw above that the projections obtained by atmospheric circulation models and downscaling of the model grid at the station did not represent reality. Compared with the observed values, these models exhibit a very large number of rainy days but a lot of small amounts of rainfall each day. For quantile distribution, Goodrich's law fitting on the sample of observed rainfall greater than 5 mm over 62 years meets the acceptance conditions (Figure 51).

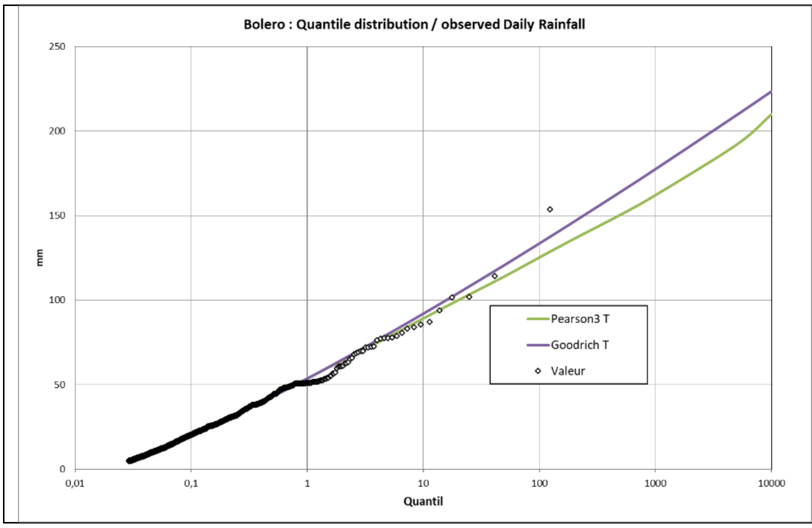

		Goodrich (mm)
5.000	0.2	29.5
2.000	0.5	43.0
1.000	1.0	53.8
0.500	2.0	64.9
0.200	5.0	80.2
0.100	10.0	92.1
0.050	20.0	104.3
0.020	50.0	120.8
0.010	100.0	133.6
0.005	200.0	146.6

Figure 51: Bolero – Quantile distribution daily rainfall (mm)

We can consider that from a probability of 0.1, the risks of flash flood become significant, a daily rainfall of over 90 mm.

In conclusion, for this region of the Bolero CRA and for the South Rukuru catchment area, both represented by the Bolero rainfall station, we can say:

1. Interannual rainfall tends to increase by the time, more in the SSP5-8.5 scenario than in the SSP2-4.5 scenario. This increase is due to a significant increase in the number of high to very high rainfall years. There is therefore an increased risk of flooding from overflowing rivers.
2. The months in which this increase in the risk of flooding from overflowing rivers is most likely to occur are February and March.
3. The rainfall projection data did not allow us to analyse the trend for runoff and flash flooding. However, rainfall in excess of 90 mm is the cause of this type of flooding. Revisiting the downscaling model to improve the reproduction of daily point data would make it possible to identify this risk.

4.4.2 Dedza - Linthipe catchment and Dedza CRA

Interannual rainfall tends to increase in both scenarios (Figure 52).

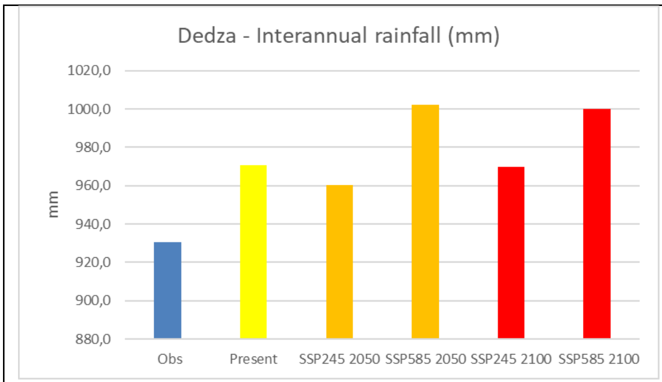

Dedza – Interannual rainfall (mm)

Obs	930.6
Present	970.6
SSP245 2050	960.5
SSP585 2050	1002.3
SSP245 2100	969.7
SSP585 2100	1000.0

Figure 52: Dedza - Observed and simulated interannual rainfall (mm)

The quantile distribution of annual rainfall for three periods of 30 successive years after fitting a Goodrich distribution (Figure 53) in the SSP2.4-5 scenario shows that it is mainly the occurrence of very wet years that increases that an increase in rainfall in average years. In median years (probability 0.5), interannual rainfall does not vary, while in wet decadal years (probability 0.9), rainfall increases by 1.6% compared with the current period for the 2050 period and by 1.9% for the 2010 period.

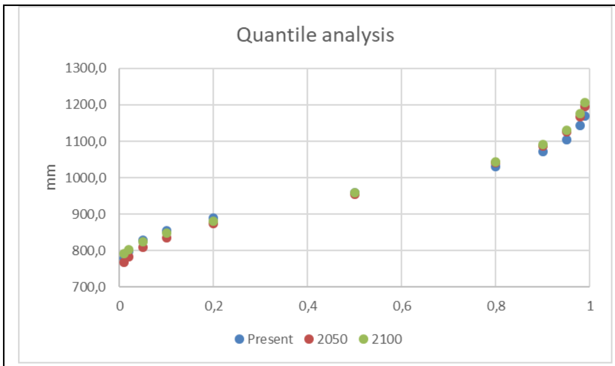

	Present	2050	2100
0.01	778.1	767.7	791.8
0.02	797.9	782.4	803.1
0.05	828.2	808.9	824.6
0.1	855.9	836.5	848.2
0.2	890.3	874.4	881.8
0.5	959.0	955.6	958.1
0.8	1031.6	1042.1	1044.1
0.9	1071.2	1087.8	1091.2
0.95	1104.8	1125.5	1130.6
0.98	1143.7	1167.6	1175.5

Figure 53: Quantile distribution of annual rainfall (Goodrich law)

To analyse the risk of flooding according to the season, we computed the monthly rainfall hietograms simulated by the EC.Earth3.CC model, which we have found to be the best. Figure 54 shows the distribution of monthly rainfall for the two scenarios over the present, 2050 and 2100 periods.
The wettest months are December, January and February. The increase in rainfall occurs with the greatest effect in January, which becomes the month with the highest risk of overflow flooding.

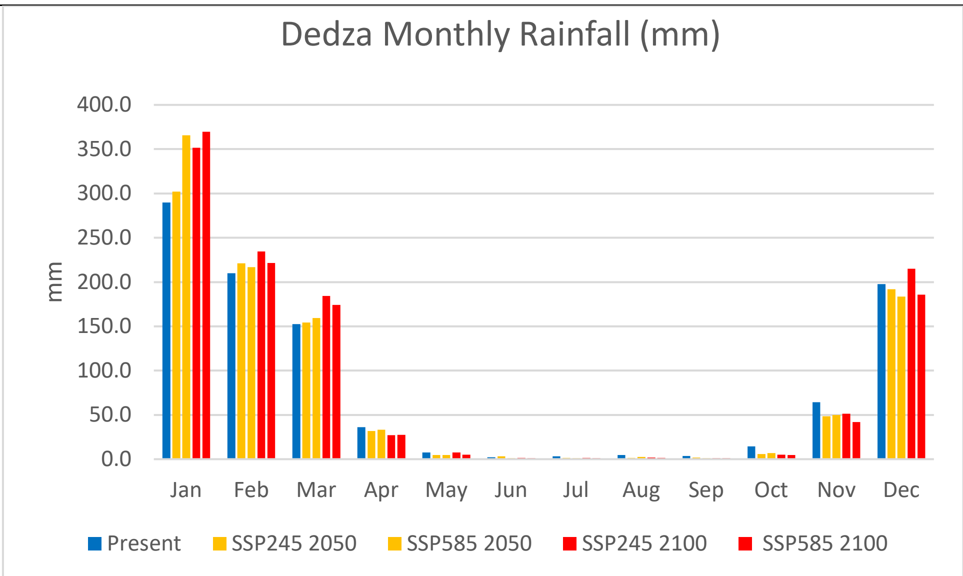

Rainfall (mm)	Jan	Feb	Mar	Apr	May	Jun	Jul	Aug	Sep	Oct	Nov	Dec
Present	289.9	210.0	152.7	36.3	7.6	2.1	3.3	4.6	3.8	14.5	64.4	197.8
SSP245 2050	302.0	221.2	154.3	31.7	4.6	3.3	1.4	1.4	1.9	5.8	48.5	192.0
SSP585 2050	365.7	216.6	159.2	33.2	4.6	1.2	1.2	2.6	1.0	6.9	49.8	183.5
SSP245 2100	351.6	234.4	184.4	27.3	7.6	1.4	1.5	1.6	0.9	4.9	51.2	214.9
SSP585 2100	369.6	221.6	174.1	27.5	5.1	1.2	1.0	1.6	1.1	4.8	41.9	185.7

Figure 54: Dedza – Observed and simulated monthly rainfall (mm)

For quantile distribution, Goodrich's law fitting on the sample of observed daily rainfall greater than 5 mm over 62 years meets the acceptance conditions (Figure 55). We can consider that from a probability of 0.1, the risks of flash flood become significant, a daily rainfall of over 99 mm.

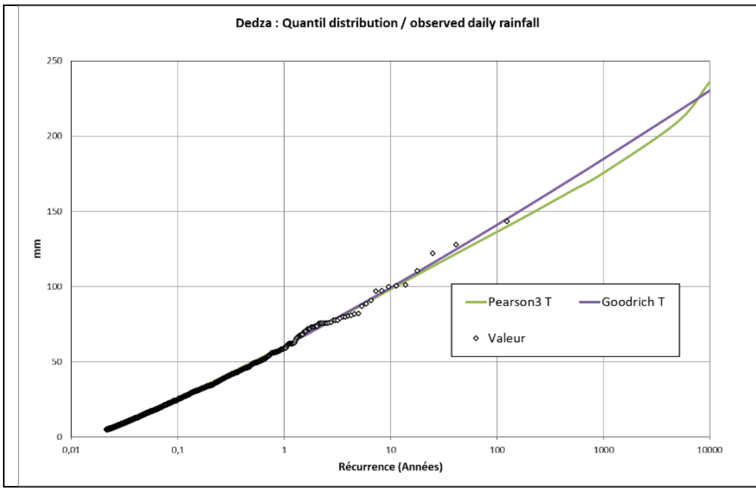

		Goodrich T
0.500	2.0	71.6
0.200	5.0	87.1
0.100	10.0	99.2
0.050	20.0	111.5
0.020	50.0	128.1
0.010	100.0	140.9
0.005	200.0	153.9
0.002	500.0	171.4
0.001	1000.0	184.7

Figure 55: Dedza – Quantile distribution daily rainfall (mm)

In conclusion, for this region of the Dedza CRA and for the Linthipe catchment area, both represented by the Dedza rainfall station, we can say:

Interannual rainfall tends to increase by the time, more in the SSP5-8.5 scenario than in the SSP2-4.5 scenario. This increase is due to a significant increase in the number of high to very high rainfall years. There is therefore an increased risk of flooding from overflowing rivers.

The months in which this increase in the risk of flooding from overflowing rivers is most likely to occur are January and February.

Rainfall in excess of 99 mm in the same day is the cause of runoff flooding.

4.4.3 Karonga - Karonga CRA

This representative station in the north of the country and the Karonga CRA does not enter into the study of the three requested catchment areas. It is treated here for the purposes of analysis of the CRAs. It is, however, representative of the supply to the lake in its northern part. Interannual rainfall tends to increase in both scenarios (Figure 56).

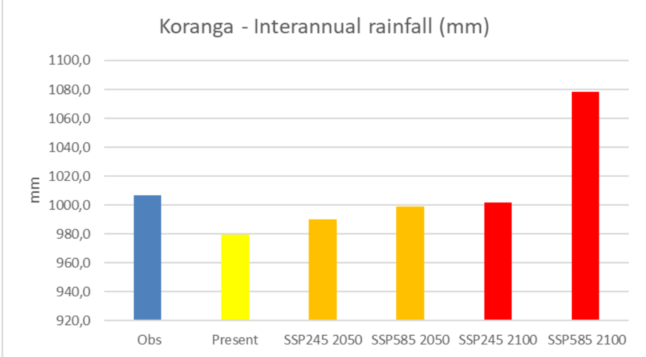

	Karonga - Interannual rainfall (mm)
Obs	1006.7
Present	979.6
SSP245 2050	990.1
SSP585 2050	999.2
SSP245 2100	1001.9
SSP585 2100	1078.5

Figure 56: Karonga - Observed and simulated interannual rainfall (mm)

The quantile distribution of annual rainfall for three periods of 30 successive years after fitting a Pearson 3 distribution (Figure 57) in the SSP2.4-5 scenario shows that it is mainly the occurrence of very wet years that increases that an increase in rainfall in average years. In median years (probability 0.5), interannual rainfall does not vary, while in wet decadal years (probability 0.9), rainfall increases by 1.0% compared with the current period for the 2050 period and by 4.8% for the 2010 period.

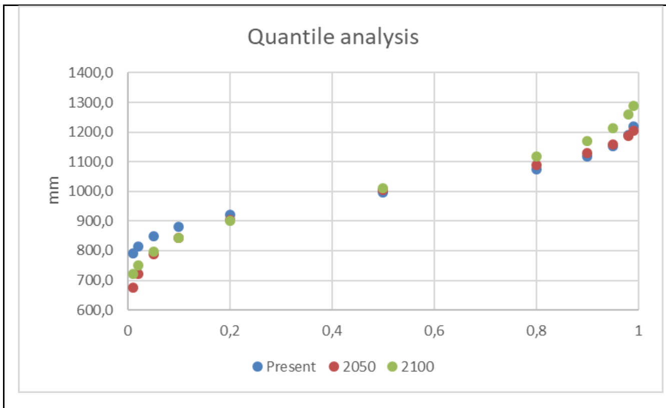

	Present	2050	2100	
0.01	791.9	676.1	722.1	0.01
0.02	815.1	721.5	750.5	0.02
0.05	850.2	787.1	797.5	0.05
0.1	881.9	842.1	842.6	0.1
0.2	920.8	903.8	899.8	0.2
0.5	996.8	1006.3	1010.7	0.5
0.8	1075.0	1090.3	1117.6	0.8
0.9	1116.7	1128.2	1170.8	0.9
0.95	1151.6	1156.9	1213.2	0.95
0.98	1191.4	1186.8	1259.3	0.98
0.99	1218.2	1205.5	1289.2	0.99

Figure 57: Quantile distribution of annual rainfall (Pearson 3 law)

To analyse the risk of flooding according to the season, we computed the monthly rainfall hietograms simulated by the EC.Earth3.CC model, which we have found to be the best. Figure 58 shows the distribution of monthly rainfall for the two scenarios over the present, 2050 and 2100 periods. The wettest months are December, January and February. The increase in rainfall occurs with the greatest effect in January and February, which become the months with the highest risk of overflow flooding.

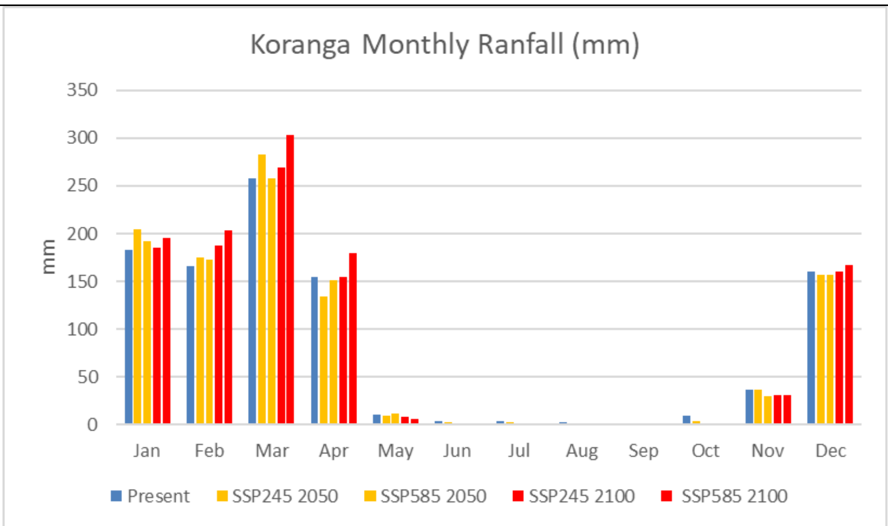

Rainfall (mm)	Jan	Feb	Mar	Apr	May	Jun	Jul	Aug	Sep	Oct	Nov	Dec
Present	183.4	165.4	258.1	154.8	10.2	3.3	3.5	2.5	1.3	10.0	36.4	160.6
SSP245 2050	204.9	174.7	283.0	134.0	9.6	2.3	2.6	1.2	0.0	3.4	36.4	157.4
SSP585 2050	192.4	172.6	258.1	151.8	11.3	1.1	0.7	1.3	0.4	1.7	29.4	157.3
SSP245 2100	185.3	187.4	269.1	154.8	8.2	1.1	1.6	0.6	0.2	1.0	31.3	160.6
SSP585 2100	195.9	203.9	303.0	180.2	6.6	1.3	1.6	0.3	0.1	1.1	30.4	167.7

Figure 58: Karonga – Observed and simulated monthly rainfall (mm)

For quantile distribution, Goodrich's law fitting on the sample of observed daily rainfall greater than 5 mm over 62 years meets the acceptance conditions (Figure 59). We can consider that from a probability of 0.1, the risks of flash flooding become significant,with a daily rainfall of over 136 mm.

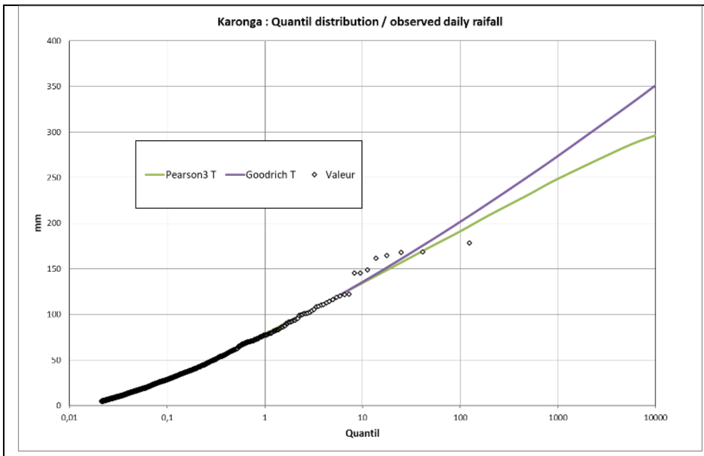

		Goodrich T
0.500	2.0	94.0
0.200	5.0	117.3
0.100	10.0	135.7
0.050	20.0	154.9
0.020	50.0	181.1
0.010	100.0	201.7
0.005	200.0	222.8
0.002	500.0	251.5
0.001	1000.0	273.8

Figure 59: Karonga – Quantile distribution daily rainfall (mm)

In conclusion, for this region of the Karonga CRA represented by the Karonga rainfall station, we can say:

Interannual rainfall tends to increase by the time, more in the SSP5-8.5 scenario than in the SSP2-4.5 scenario. This increase is due to a significant increase in the number of high to very high rainfall years. There is therefore an increased risk of flooding from overflowing rivers.

The months in which this increase in the risk of flooding from overflowing rivers is most likely to occur are February, March and April.

Rainfall in excess of 136 mm in the same day is the cause of runoff flooding.

4.4.4 Kazungu – Dwangwa catchment and Kazungu CRA

Figure 60 shows the evolution of interannual rainfall over the observed period, and over three thirty-year periods (present, 2050 and 2100) according to the two scenarios SSP2-4.5 and SSP5-8.5. For this station, the interannual average rainfall over the observed period is significantly different from that simulated over the current period. This suggests that missing observed data may have been computed for days with no rain. It is likely that this lack of observation led to errors in the projections. Nevertheless, we are presenting the analysis for this station because the results are in line with those from previous stations.

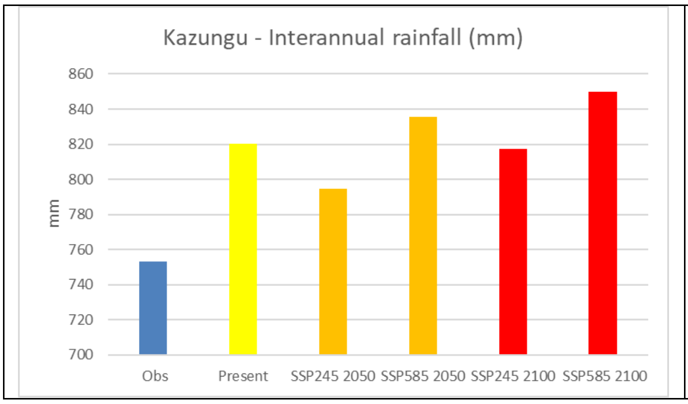

	Kazungu - Interannual rainfall (mm)
Obs	753.1
Present	820.4
SSP245 2050	794.8
SSP585 2050	835.4
SSP245 2100	817.3
SSP585 2100	849.6

Figure 60: Kazungu - Observed and simulated interannual rainfall (mm)

The quantile distribution of annual rainfall for three periods of 30 successive years after fitting a Pearson 3 distribution (Figure 61) in the SSP2.4-5 scenario shows that it is mainly the occurrence of very wet years that increases that an increase in rainfall in average years. In median years (probability 0.5), interannual rainfall does not vary, while in wet decadal years (probability 0.9), rainfall increases by 3.8% compared with the current period for the 2010 period.

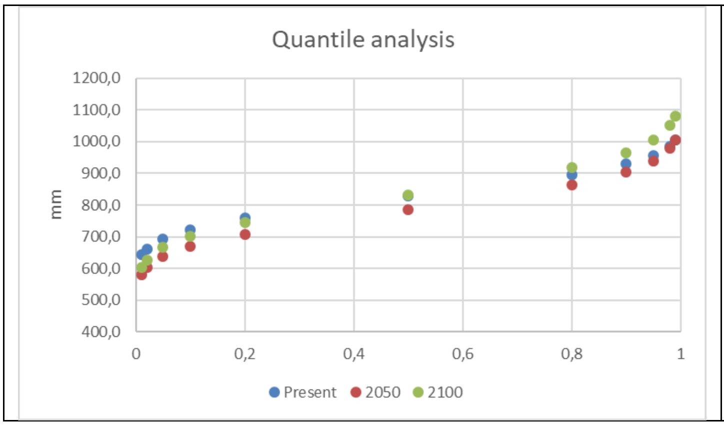

	Present	2050	2100
0.01	643.4	580.1	601.9
0.02	661.9	603.2	627.7
0.05	692.5	638.3	666.9
0.1	721.6	669.9	702.2
0.2	758.3	708.7	745.6
0.5	829.0	784.6	830.8
0.8	896.5	862.8	918.6
0.9	930.0	904.5	965.7
0.95	956.6	939.5	1005.1
0.98	985.5	979.3	1050.1
0.99	1004.2	1006.1	1080.4

Figure 61: Quantile distribution of annual rainfall (Pearson 3 law)

To analyse the risk of flooding according to the season, we computed the monthly rainfall hietograms simulated by the EC.Earth3.CC model, which we have found to be the best. Figure 62 shows the distribution of monthly rainfall for the two scenarios over the present, 2050 and 2100 periods.

The wettest months are December, January and February. The increase in rainfall occurs with the greatest effect in January and February, which become the months with the highest risk of overflow flooding.

.

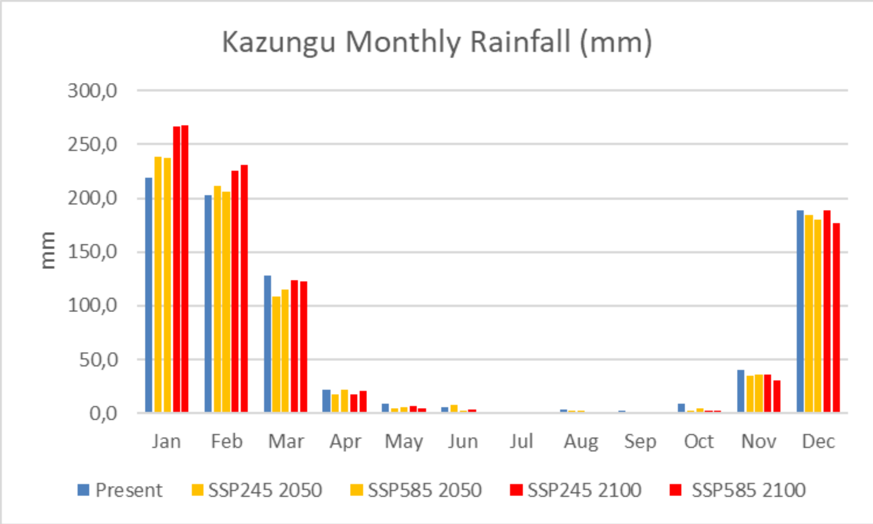

Rainfall (mm)	Jan	Feb	Mar	Apr	May	Jun	Jul	Aug	Sep	Oct	Nov	Dec
Present	218.8	202.8	127.9	21.5	8.3	5.4	0.9	3.7	2.5	8.3	39.9	188.8
SSP245 2050	238.7	211.6	108.3	17.8	4.8	7.5	0.8	2.3	0.2	2.2	34.5	184.2
SSP585 2050	237.0	205.7	114.5	21.5	5.1	2.4	0.2	2.6	0.3	4.8	35.5	180.1
SSP245 2100	267.0	225.7	123.7	17.3	6.4	3.7	0.8	0.8	0.3	2.1	35.9	188.7
SSP585 2100	267.4	231.4	122.2	20.5	4.2	1.6	0.3	0.4	0.1	2.3	30.3	176.6

Figure 62: Kazungu – Observed and simulated monthly rainfall (mm)

For quantile distribution, Pearson 3 's law fitting on the sample of observed daily rainfall greater than 5 mm over 62 years meets the acceptance conditions (Figure 63). We can consider that from a probability of 0.1, the risks of flash flood become significant, a daily rainfall of over 95 mm.

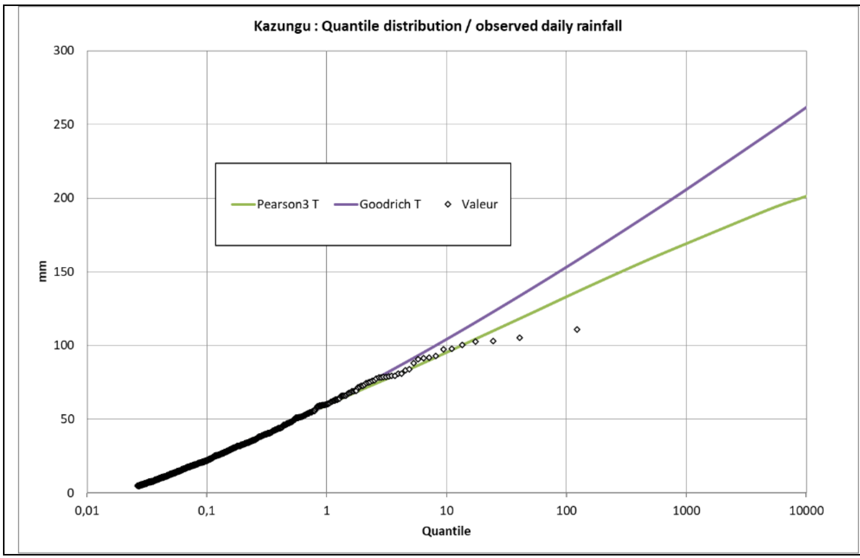

		Pears.
2.000	0.5	48.4
1.000	1.0	59.6
0.500	2.0	70.5
0.200	5.0	84.4
0.100	10.0	95.4
0.050	20.0	106.7
0.020	50.0	121.7
0.010	100.0	133.1
0.005	200.0	144.4
0.002	500.0	158.8
0.001	1000.0	169.1

Figure 63: Kazungu – Quantile distribution daily rainfall (mm)

In conclusion, for this region of Dwangwa catchment and Kazungu CRA represented by the Kazungu rainfall station, we can say:

Interannual rainfall tends to increase by the time, more in the SSP5-8.5 scenario than in the SSP2-4.5 scenario. This increase is due to a significant increase in the number of high to very high rainfall years. There is therefore an increased risk of flooding from overflowing rivers.

The months in which this increase in the risk of flooding from overflowing rivers is most likely to occur are January and February.

Rainfall in excess of 95 mm in the same day is the cause of runoff flooding.

4.4.5 Naminjiwa – Phalombe CRA

Over the three thirty-year periods selected and in the two scenarios, there is no significant change in interannual rainfall, which remains around 1100 mm. The simulated rainfall for the current period is greater than that calculated from observed data (Figure 64).

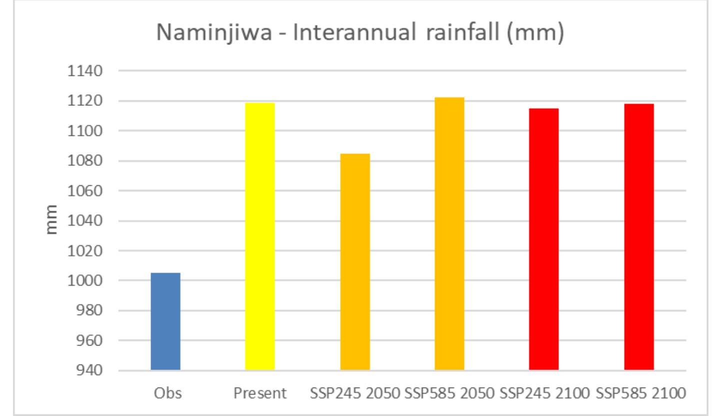

	Naminjiwa - Interannual rainfall (mm)
Obs	1005.1
Present	1118.6
SSP245 2050	1084.6
SSP585 2050	1122.3
SSP245 2100	1114.9
SSP585 2100	1118.3

Figure 64: Naminjiwa - Observed and simulated interannual rainfall (mm)

Similarly, there is no significate difference in the quantile distribution of mean interannual rainfall in the three reference periods (Figure 65). The distribution for the 2100 period even shows a lower occurrence of heavy rainy years than for the 2050 period or the current period!

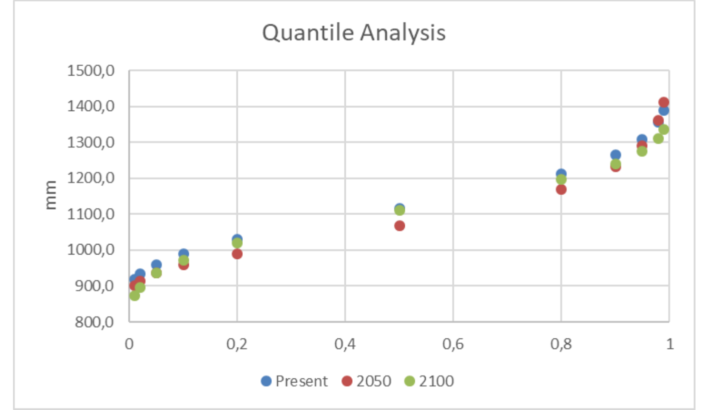

	Present	2050	2100
0.01	918.7	901.6	872.6
0.02	933.3	913.9	896.4
0.05	960.1	935.5	935.5
0.1	988.9	958.3	972.9
0.2	1028.9	990.7	1019.9
0.5	1116.9	1068.6	1110.7
0.8	1213.2	1169.8	1197.5
0.9	1264.9	1232.6	1240.5
0.95	1307.8	1289.9	1274.7
0.98	1356.1	1360.3	1311.8
0.99	1388.2	1410.9	1335.8

Figure 65: Quantile distribution of annual rainfall (Goodrich law)

To analyse the risk of flooding according to the season, we computed the monthly rainfall hietograms simulated by the EC.Earth3.CC model, which we have found to be the best. Figure 66 shows the distribution of monthly rainfall for the two scenarios over the present, 2050 and 2100 periods.

The wettest months are December, January, February and March. For scenario SSP5-8.5, the 2050 period shows strangely low rainfall in the wet season and very high rainfall in the dry season. We would suggest that this is a problem of rainfall distribution in the downscaling of the atmospheric circulation model.

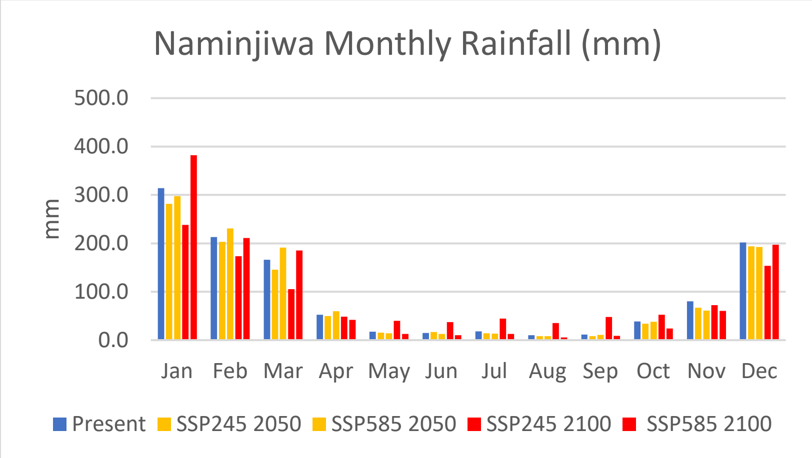

Rainfall (mm)	Jan	Feb	Mar	Apr	May	Jun	Jul	Aug	Sep	Oct	Nov	Dec
Present	313.8	212.7	166.4	52.5	17.7	15.0	18.2	10.3	11.2	38.3	80.3	201.8
SSP245 2050	281.9	203.2	145.8	49.9	15.2	16.6	14.2	8.4	8.2	33.7	67.1	193.8
SSP585 2050	297.8	230.5	190.9	60.0	14.0	12.8	13.4	8.4	10.7	37.8	61.1	192.3
SSP245 2100	238.4	173.5	105.5	48.4	39.7	37.1	44.4	35.1	47.5	52.2	72.6	153.4
SSP585 2100	382.0	211.3	185.3	41.7	12.7	10.5	13.0	5.6	8.8	24.2	60.5	197.0

Figure 66: Naminjiwa – Observed and simulated monthly rainfall (mm)

For quantile distribution, Goodrich law fitting on the sample of observed daily rainfall greater than 5 mm over 62 years meets the acceptance conditions (Figure 67). We can consider that from a probability of 0.1, the risks of flash flood become significant, a daily rainfall of over 132 mm.

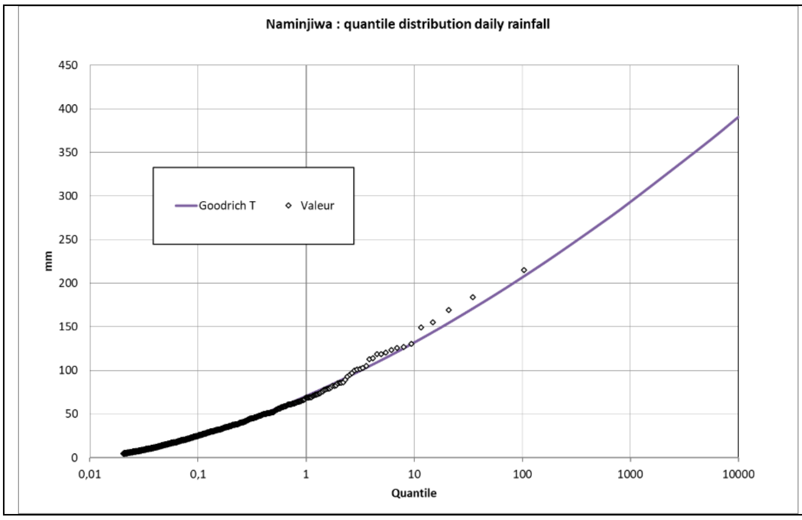

		Goodrich T
2.000	0.5	55.0
1.000	1.0	70.6
0.500	2.0	87.6
0.200	5.0	112.1
0.100	10.0	132.0
0.050	20.0	153.2
0.020	50.0	183.0
0.010	100.0	206.8
0.005	200.0	231.7
0.002	500.0	266.2
0.001	1000.0	293.4

Figure 67: Naminjiwa – Quantile distribution daily rainfall (mm)

In conclusion, for this region of Phalombe CRA represented by the Naminjiwa rainfall station, we can say:

There are no trends in the interannual mean values for either the SSP2-4.5 or SSP5-8.5 scenarios. This different behaviour compared to other stations in the country may be due to specific exposure of the station (sheltered location in relation to buildings or trees), or to poor observation or modelling of future weather. It calls into question the possibility of representing a region by a single station.

The monthly rainfall distribution for the SSP5-8.5 scenario raises questions.

Rainfall in excess of 132 mm in the same day will cause of runoff flooding.

4.4.6 Ngabu -Chikawa CRA

Figure 68 shows the evolution of interannual rainfall over the observed period, and over three thirty-year periods (present, 2050 and 2100) according to the two scenarios SSP2-4.5 and SSP5-8.5.

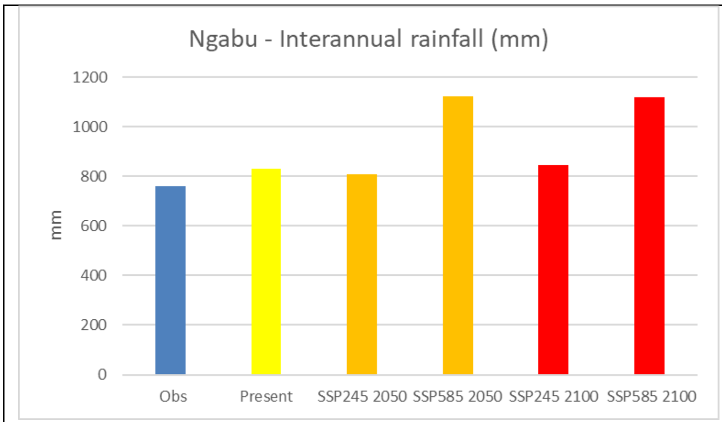

	Ngabu - Interannual rainfall (mm)
Obs	758.5
Present	830.9
SSP245 2050	807.2
SSP585 2050	1122.3
SSP245 2100	846.0
SSP585 2100	1118.3

Figure 68: Ngabu - Interannual Rainfall projections.

For this region, there is a clear increase in interannual rainfall. The interannual averages for the observed period and those simulated by the models are close. To analyse the risk of flooding according to the season, we computed the monthly rainfall hietograms simulated by the EC.Earth3.CC model, which we have found to be the best. Figure 69 shows the distribution of monthly rainfall for the two scenarios over the present, 2050 and 2100 periods.

The wettest months are December, January and February. The increase in rainfall occurs with the greatest effect in January, which becomes the month with the highest risk of overflow flooding.

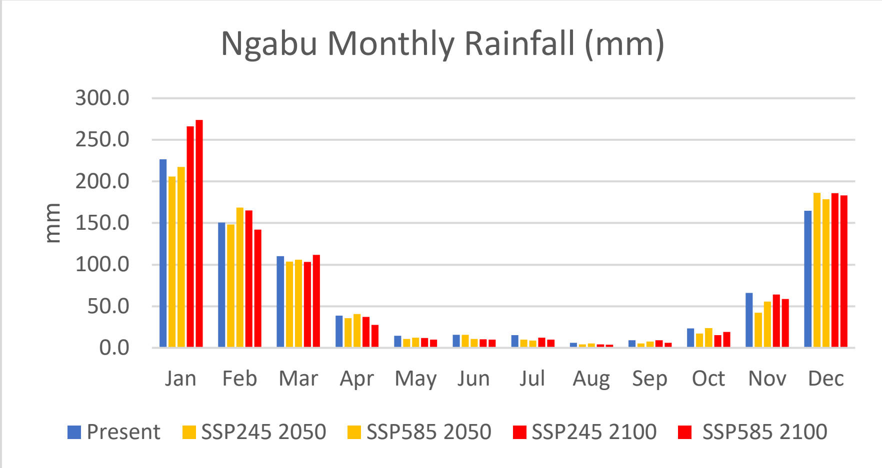

Rainfall (mm)	Jan	Feb	Mar	Apr	May	Jun	Jul	Aug	Sep	Oct	Nov	Dec
Present	226.6	150.6	110.4	38.6	14.5	15.6	15.2	6.0	9.2	23.3	66.2	164.9
SSP245 2050	206.0	148.4	103.8	35.6	10.7	15.8	9.8	4.0	5.5	17.1	42.2	186.4
SSP585 2050	217.5	168.6	106.0	40.7	12.3	10.6	8.7	5.4	7.5	23.8	55.5	178.6
SSP245 2100	266.2	165.1	103.3	37.1	11.9	10.4	12.2	4.0	9.2	15.1	64.1	185.7
SSP585 2100	273.9	141.9	111.6	27.6	9.8	10.1	10.0	3.9	6.3	19.0	58.6	183.4

Figure 69: Ngabu – Observed and simulated monthly rainfall (mm)

For quantile distribution, Goodrich's law fitting on the sample of observed rainfall greater than 5 mm over 62 years meets the acceptance conditions (Figure 70).

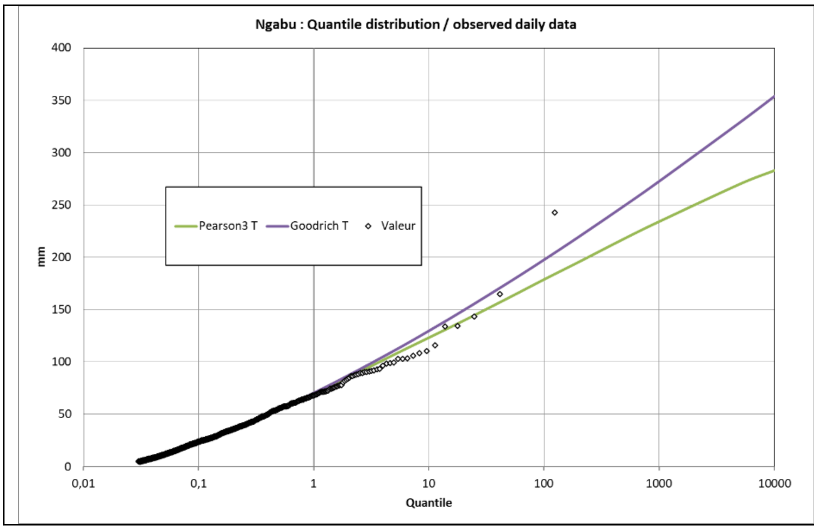

		Goodrich
2.000	0.5	110.8
1.000	1.0	129.7
0.500	2.0	149.3
0.200	5.0	176.4
0.100	10.0	197.6
0.050	20.0	219.5
0.020	50.0	249.4
0.010	100.0	272.6
0.005	200.0	110.8
0.002	500.0	129.7
0.001	1000.0	149.3

Figure 70: Ngabu – Quantile distribution daily rainfall (mm)

We can consider that from a probability of 0.1, the risks of flash flooding become significant, a daily rainfall of over 198 mm.

In conclusion, for this region of the Chikwawa CRA represented by the Ngabu rainfall station, we can say:
Interannual rainfall tends to increase over time, more in the SSP5-8.5 scenario than in the SSP2-4.5 scenario. This increase is due to a significant increase in the number of high to very high rainfall years. There is therefore an increased risk of flooding from overflowing rivers.
The month in which this increase in the risk of flooding from overflowing rivers is most likely to occur is January.

Rainfall in excess of 130 mm in the same day will cause of runoff flooding

4.4.7 Salima – Lake Malawi Shore and Salima CRA

Figure 71 shows the evolution of interannual rainfall over the observed period, and over three thirty-year periods (present, 2050 and 2100) according to the two scenarios SSP2-4.5 and SSP5-8.5.

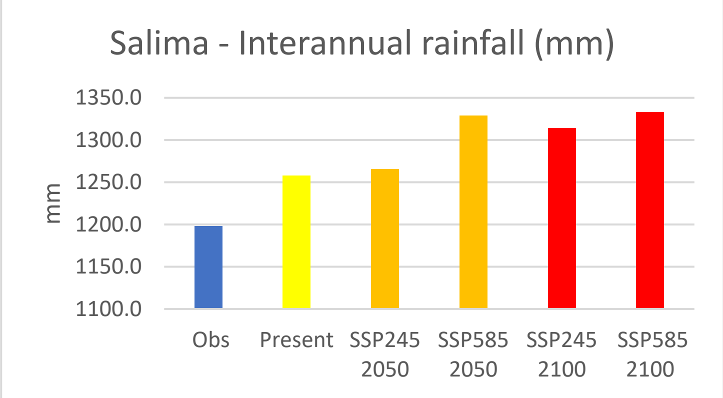

	Salima - Interannual rainfall (mm)
Obs	1198.1
Present	1257.8
SSP245 2050	1265.7
SSP585 2050	1328.6
SSP245 2100	1314.0
SSP585 2100	1332.8

Figure 71: Salima - Interannual Rainfall projections.

For this region, there is a clear increase in interannual rainfall. To analyse the risk of flooding according to the season, we computed the monthly rainfall hietograms simulated by the EC.Earth3.CC model, which we have found to be the best. Figure 72 shows the distribution of monthly rainfall for the two scenarios over the present, 2050 and 2100 periods.

The wettest months are December, January, February and March. The increase in rainfall occurs with the greatest effect in January and February, which become the months with the highest risk of overflow flooding.

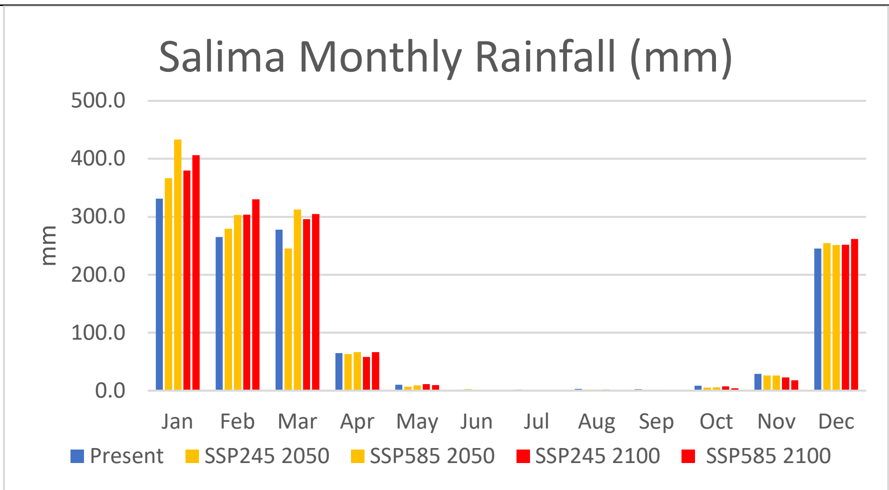

Rainfall (mm)	Jan	Feb	Mar	Apr	May	Jun	Jul	Aug	Sep	Oct	Nov	Dec
Present	331.3	265.0	278.0	64.8	10.4	1.6	1.7	2.9	2.3	8.4	28.7	245.4
SSP245 2050	366.6	279.2	245.3	63.3	7.0	2.6	0.9	1.9	0.6	5.3	26.3	254.6
SSP585 2050	433.1	303.2	312.5	66.4	9.3	0.8	0.5	1.8	1.5	6.0	26.4	251.1
SSP245 2100	380.0	303.8	295.8	58.0	11.3	0.7	0.8	1.7	0.6	7.6	23.1	251.9
SSP585 2100	406.5	330.3	304.5	66.5	9.7	0.7	0.3	1.0	0.3	4.0	18.1	261.7

Figure 72: Salima – Observed and simulated monthly rainfall (mm)

For quantile distribution, Goodrich's law fitting on the sample of observed rainfall greater than 5 mm over 62 years meets the acceptance conditions (Figure 73).

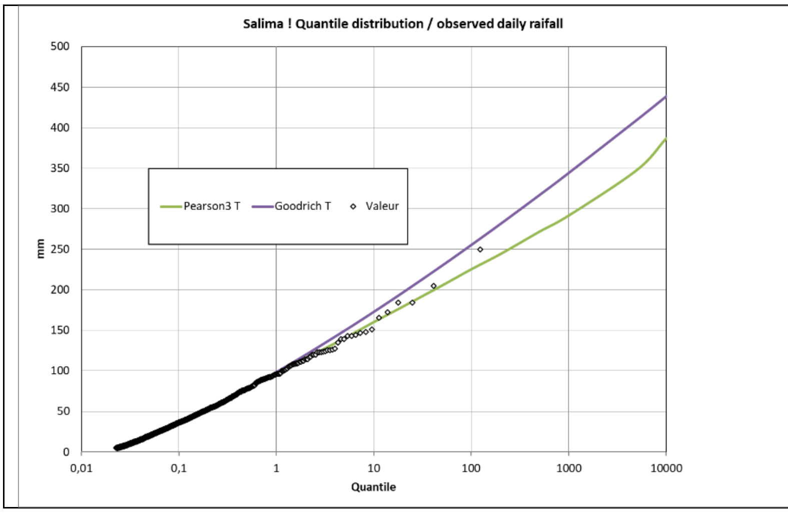

		Goodrich
2.000	0.5	78.0
1.000	1.0	98.4
0.500	2.0	119.8
0.200	5.0	149.5
0.100	10.0	172.8
0.050	20.0	196.9
0.020	50.0	229.8
0.010	100.0	255.3
0.005	200.0	281.5
0.002	500.0	316.9
0.001	1000.0	344.3

Figure 73: Salima – Quantile distribution daily rainfall (mm)

We can consider that from a probability of 0.1, the risks of flash flooding become significant, with a daily rainfall of over 173 mm.

In conclusion, for this region of Lake Malawi shoreline and the Salima CRA represented by the Salima rainfall station, we can say:
Interannual rainfall tends to increase over time, more in the SSP5-8.5 scenario than in the SSP2-4.5 scenario. There is therefore an increased risk of flooding from overflowing rivers.
The months in which this increase in the risk of flooding from overflowing rivers is most likely to occur is January and February.
Rainfall in excess of 173 mm in the same day will cause runoff flooding

4.5 Discussion

Malawi, like many other countries, is vulnerable to the impacts of climate change, including increased flood risk. Climate change exacerbates existing weather patterns and leads to more frequent and severe floods. Climate change also leads to changes in precipitation patterns. In Malawi, the projected data produced by DCCMS show increased inter annual and monthly rainfall. This can result in overflow flooding.
However, the trends examined in this work include that precipitation patterns manifest in increased rainfall intensity, equating to more rainfall over shorter periods. This results in flash flooding, which can be particularly dangerous and destructive. Earlier version of this work showed that the number of cyclones coming from the Indian Ocean was increasing. The data simulated by the DCCMS at the 8 stations we have analysed do not show this phenomenon; on the contrary, the number of heavy rainstorms decreases significantly in the two scenarios proposed.
Simulation of rainfall heights by atmospheric and downscale models at the scale of a single station shows good consistency in total rainfall volume on an annual or monthly scale, but a poor distribution of daily rainfall. Over the periods observed, there are sixty to eighty days of rain (greater than 1mm) per year, depending on the station, while in simulations over the same periods or in projected periods, there are 250 to 300 days of rain. Of course, the daily rainfall height is lower.
It also seems insufficient to use a single station to represent a region or catchment area. This station may have a particular situation in relation to the relief, the prevailing wind, or be in a sheltered position such as a rain shadow, or even have experienced a lack of observations at a given period.
Due to the small number of stations, it was not possible to spatialise the rainfall over the country and over the areas studied in particular. Without this spatialisation of precipitation, it is not possible to simulate

runoff data and thus characterise the risk of flooding. While runoff is a result of precipitation, it is also influenced by the state of the soil and its cover.
We therefore have an indicator based on a station to predict whether the risk of flooding by overflow is increasing and when in the season the risk is at its highest. Based on the daily data observed and taking the rainfall corresponding to probability 0.1 over the duration of the observations (ten-year risk rainfall), we have given the daily rainfall threshold for flooding by runoff and the appearance of flash floods for each region.

5. GENERAL CONCLUSION

In the context of evolving climate change scenarios, there's a discernible increase in tropical storms leading to catastrophic flooding in Malawi, with profound impacts on the nation's economy and the livelihoods of its inhabitants. One significant cause behind the upsurge of these storms is climate change, evidenced by warmer sea surface temperatures and altered atmospheric circulation patterns.

While recent land use analysis shows a promising trend towards stabilization and recovery of forested areas, primarily due to reforestation programs, the surge in urbanized zones, especially in proximity to substantial rivers and lakes, presents an imminent flood risk. Furthermore, the Digital Elevation Model and associated lake heights have enabled the identification of towns most vulnerable to lake or river overflow flooding.

Detailed analyses at the catchment scale highlight variations in land cover, including notable deforestation trends up to the early 2000s, followed by reforestation. Rapid increases in the areal extent of built-up areas, especially in regions like the Linthipe basin, signal a rising flood risk. Moreover, even though the flood risk index helps pinpoint higher-risk regions, it lacks comprehensiveness in accounting for factors like soil sealing in urban areas.

Climate change further intensifies existing weather challenges for Malawi. Notably, the projected data indicates amplified inter-annual and monthly rainfall, leading to potential overflow floods.

With regards to flash flooding risks in Malawi, the daily-scale rainfall data available did not enable a quantification of trends. To go forward, it is essential, in the initial phase, to have access to reliable climate projection for daily rainfall data. A key aspect of this reliability is ensuring a coherent distribution in terms of rainy days, accurately reflecting the precipitation regime of the studied region. Once this critical step is validated, a robust model that enables rainfall spatialization can be selected. This model will provide a detailed representation of precipitation on a regional scale. Simultaneously, predicting runoff volumes based on this spatial model will allow for the anticipation of flood-prone areas, thereby enabling proactive measures to safeguard territories and their inhabitants.

To effectively address and mitigate flooding challenges, it's crucial to invest in robust early warning systems, resilient infrastructure, sustainable land use, and further research employing diverse data points to ensure comprehensive risk assessment and timely interventions.

6. ANNEX 1: MALAWI'S LAND COVER (SOURCE: CLIMATE DATA STORE LCCS)

The total land area of Malawi is approximately 118,480 square kilometres (45,747 square miles). According to the World Bank. This makes Malawi one of the smaller countries in Africa and the world in terms of land area. The portion of Lake Nyasa that lies within the borders of Malawi has an area of approximately 29,600 square kilometres (11,400 square miles). This area includes both the main body of the lake and the various islands located within it.

Year	Area (km^2)						
Km²	Forest	Crop	Shrub	Wetland	Urban	Other	Total
1992	36326.88	44539.29	8166.96	2007.18	263.34	1988.91	93292.56
1993	36326.61	44539.11	8166.24	2007.09	264.69	1988.82	93292.56
1994	36325.98	44538.84	8165.25	2007.00	266.67	1988.82	93292.56
1995	33466.95	47287.89	8298.63	2025.45	270.45	1943.19	93292.56
1996	32889.96	47861.19	8295.75	2041.92	274.05	1929.69	93292.56
1997	31569.93	49118.76	8348.58	2064.06	278.55	1912.68	93292.56
1998	28708.74	51832.17	8478.27	2088.09	284.4	1900.89	93292.56
1999	22299.84	57465.18	9320.76	2157.39	289.08	1760.31	93292.56
2000	21660.93	57949.29	9443.07	2177.01	296.37	1765.89	93292.56
2001	21805.92	58127.94	9121.41	2167.56	296.64	1773.09	93292.56
2002	21939.57	58228.29	8915.49	2135.16	297.09	1776.96	93292.56
2003	22122.9	58257.81	8696.34	2134.71	298.26	1782.54	93292.56
2004	22132.17	58329.09	8606.88	2165.31	298.89	1760.22	93292.56
2005	22215.78	58289.94	8553.51	2180.88	308.43	1744.02	93292.56
2006	22246.92	58246.74	8548.83	2187.27	322.29	1740.51	93292.56
2007	22408.02	58175.01	8446.68	2191.59	332.01	1739.25	93292.56
2008	22481.73	58088.79	8446.14	2194.47	342.18	1739.25	93292.56
2009	22506.93	58004.46	8490.33	2198.70	354.42	1737.72	93292.56
2010	22458.42	58042.53	8486.73	2211.93	365.49	1727.46	93292.56
2011	22479.39	58022.64	8472.42	2227.41	375.39	1715.31	93292.56
2012	22474.98	58012.65	8463.06	2245.23	395.55	1701.09	93292.56
2013	22488.93	57982.14	8453.7	2264.76	422.91	1680.12	93292.56
2014	22525.47	57818.34	8552.61	2268.99	454.77	1672.38	93292.56
2015	22522.95	57811.5	8540.28	2268.99	476.46	1672.38	93292.56
2016	22796.37	57278.07	8809.29	2262.60	497.88	1648.35	93292.56
2017	22869.27	57211.83	8806.14	2271.33	502.56	1631.43	93292.56
2018	22989.96	57133.8	8775.09	2306.25	503.19	1584.27	93292.56
2019	23085.09	57044.7	8745.84	2307.33	525.69	1583.91	93292.56
2020	23084.64	57007.44	8740.17	2307.69	568.71	1583.91	93292.56

.

7. ANNEX 2: RAINFALL (SOURCE: ERA5 - ECMWF)

	Jan	Feb	March	April	May	June	Jul	Aug	Sept	Oct	Nov	Dec	
Av.	0.285	0.245	0.190	0.081	0.023	0.010	0.010	0.007	0.006	0.021	0.078	0.222	1.178
St.Dev	0.0754	0.061	0.056	0.033	0.02	0.004	0.005	0.004	0.004	0.016	0.04	0.067	0.186

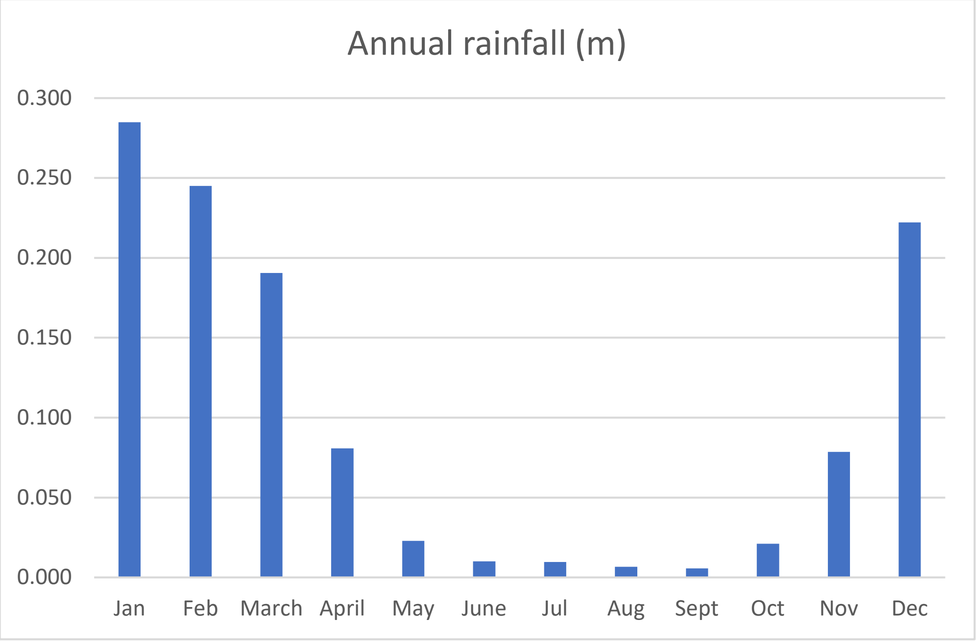

.

8. ANNEX 2B: ANNUAL EVAPOTRANSPIRATION (ENTIRE COUNTRY)

Year	Jan	Feb	Mar	Apr	May	Jun	Jul	Aug	Sep	Oct	Nov	Dec
1957	-0.111	-0.087	-0.106	-0.094	-0.087	-0.064	-0.048	-0.045	-0.044	-0.049	-0.046	-0.100
1958	-0.115	-0.099	-0.122	-0.105	-0.069	-0.049	-0.041	-0.041	-0.042	-0.046	-0.079	-0.101
1959	-0.122	-0.105	-0.123	-0.092	-0.077	-0.044	-0.041	-0.047	-0.047	-0.060	-0.069	-0.108
1960	-0.123	-0.110	-0.108	-0.081	-0.054	-0.038	-0.036	-0.032	-0.034	-0.034	-0.043	-0.092
1961	-0.117	-0.111	-0.116	-0.102	-0.068	-0.037	-0.034	-0.033	-0.029	-0.035	-0.088	-0.099
1962	-0.103	-0.109	-0.109	-0.106	-0.075	-0.047	-0.035	-0.033	-0.033	-0.037	-0.053	-0.107
1963	-0.118	-0.100	-0.116	-0.107	-0.074	-0.049	-0.040	-0.039	-0.036	-0.040	-0.088	-0.108
1964	-0.119	-0.120	-0.115	-0.094	-0.060	-0.041	-0.035	-0.033	-0.030	-0.033	-0.053	-0.103
1965	-0.106	-0.112	-0.117	-0.090	-0.055	-0.039	-0.030	-0.028	-0.031	-0.037	-0.044	-0.075
1966	-0.087	-0.097	-0.115	-0.098	-0.061	-0.036	-0.028	-0.025	-0.026	-0.028	-0.059	-0.087
1967	-0.120	-0.103	-0.108	-0.102	-0.066	-0.041	-0.035	-0.032	-0.032	-0.037	-0.079	-0.102
1968	-0.116	-0.109	-0.110	-0.085	-0.059	-0.035	-0.028	-0.026	-0.025	-0.035	-0.078	-0.101
1969	-0.115	-0.110	-0.122	-0.103	-0.068	-0.042	-0.032	-0.031	-0.031	-0.032	-0.049	-0.099
1970	-0.120	-0.108	-0.110	-0.089	-0.056	-0.034	-0.031	-0.028	-0.026	-0.044	-0.071	-0.109
1971	-0.111	-0.106	-0.123	-0.098	-0.065	-0.039	-0.034	-0.033	-0.034	-0.045	-0.079	-0.113
1972	-0.117	-0.112	-0.124	-0.102	-0.081	-0.052	-0.041	-0.038	-0.039	-0.064	-0.064	-0.113
1973	-0.118	-0.113	-0.113	-0.097	-0.070	-0.040	-0.034	-0.034	-0.032	-0.034	-0.062	-0.099
1974	-0.116	-0.097	-0.112	-0.100	-0.087	-0.062	-0.054	-0.048	-0.044	-0.047	-0.069	-0.104
1975	-0.123	-0.108	-0.118	-0.099	-0.068	-0.040	-0.036	-0.032	-0.031	-0.041	-0.060	-0.107
1976	-0.117	-0.108	-0.113	-0.100	-0.082	-0.054	-0.045	-0.039	-0.038	-0.056	-0.060	-0.095
1977	-0.113	-0.116	-0.116	-0.101	-0.071	-0.044	-0.039	-0.037	-0.038	-0.051	-0.088	-0.110
1978	-0.110	-0.105	-0.103	-0.107	-0.084	-0.055	-0.044	-0.041	-0.043	-0.053	-0.082	-0.101
1979	-0.128	-0.105	-0.116	-0.102	-0.076	-0.050	-0.044	-0.039	-0.042	-0.046	-0.077	-0.117
1980	-0.118	-0.116	-0.112	-0.097	-0.076	-0.044	-0.037	-0.036	-0.036	-0.062	-0.071	-0.101
1981	-0.130	-0.098	-0.122	-0.099	-0.075	-0.046	-0.037	-0.037	-0.039	-0.055	-0.063	-0.108
1982	-0.108	-0.104	-0.123	-0.098	-0.079	-0.047	-0.043	-0.040	-0.040	-0.063	-0.091	-0.117
1983	-0.117	-0.109	-0.129	-0.101	-0.071	-0.045	-0.040	-0.043	-0.035	-0.045	-0.053	-0.099
1984	-0.119	-0.104	-0.121	-0.106	-0.069	-0.044	-0.041	-0.037	-0.038	-0.042	-0.090	-0.103
1985	-0.123	-0.104	-0.116	-0.105	-0.077	-0.049	-0.042	-0.038	-0.041	-0.049	-0.083	-0.107
1986	-0.107	-0.108	-0.121	-0.108	-0.081	-0.052	-0.042	-0.040	-0.040	-0.064	-0.098	-0.108
1987	-0.113	-0.113	-0.122	-0.104	-0.068	-0.045	-0.035	-0.034	-0.035	-0.061	-0.050	-0.110
1988	-0.114	-0.111	-0.121	-0.107	-0.073	-0.049	-0.039	-0.036	-0.036	-0.054	-0.075	-0.105
1989	-0.097	-0.097	-0.109	-0.107	-0.080	-0.055	-0.044	-0.044	-0.044	-0.050	-0.081	-0.110
1990	-0.116	-0.107	-0.124	-0.096	-0.077	-0.049	-0.040	-0.039	-0.041	-0.045	-0.056	-0.100
1991	-0.115	-0.106	-0.118	-0.100	-0.072	-0.047	-0.039	-0.038	-0.035	-0.052	-0.072	-0.099
1992	-0.114	-0.111	-0.110	-0.090	-0.065	-0.040	-0.031	-0.030	-0.026	-0.029	-0.063	-0.096
1993	-0.119	-0.105	-0.117	-0.104	-0.078	-0.046	-0.037	-0.038	-0.039	-0.039	-0.088	-0.089
1994	-0.112	-0.108	-0.114	-0.097	-0.060	-0.036	-0.031	-0.031	-0.032	-0.046	-0.055	-0.108
1995	-0.112	-0.112	-0.119	-0.090	-0.058	-0.039	-0.031	-0.030	-0.028	-0.030	-0.044	-0.099
1996	-0.119	-0.108	-0.116	-0.100	-0.073	-0.052	-0.042	-0.039	-0.038	-0.042	-0.042	-0.092
1997	-0.115	-0.089	-0.126	-0.100	-0.077	-0.049	-0.045	-0.041	-0.046	-0.064	-0.083	-0.108
1998	-0.118	-0.114	-0.124	-0.107	-0.072	-0.042	-0.036	-0.039	-0.038	-0.047	-0.055	-0.097
1999	-0.108	-0.107	-0.117	-0.105	-0.078	-0.048	-0.040	-0.040	-0.041	-0.047	-0.065	-0.088

Year	Jan	Feb	Mar	Apr	May	Jun	Jul	Aug	Sep	Oct	Nov	Dec
2000	-0.108	-0.110	-0.114	-0.104	-0.076	-0.046	-0.041	-0.037	-0.036	-0.040	-0.100	-0.117
2001	-0.106	-0.102	-0.117	-0.106	-0.073	-0.046	-0.039	-0.044	-0.042	-0.044	-0.056	-0.090
2002	-0.114	-0.104	-0.118	-0.106	-0.069	-0.046	-0.037	-0.037	-0.041	-0.048	-0.067	-0.093
2003	-0.115	-0.101	-0.117	-0.109	-0.070	-0.046	-0.041	-0.041	-0.040	-0.044	-0.058	-0.106
2004	-0.118	-0.117	-0.121	-0.104	-0.068	-0.045	-0.040	-0.036	-0.039	-0.049	-0.083	-0.101
2005	-0.118	-0.119	-0.126	-0.088	-0.063	-0.039	-0.035	-0.030	-0.031	-0.039	-0.053	-0.094
2006	-0.120	-0.114	-0.113	-0.107	-0.072	-0.045	-0.036	-0.035	-0.032	-0.042	-0.068	-0.109
2007	-0.101	-0.108	-0.123	-0.101	-0.068	-0.045	-0.040	-0.037	-0.038	-0.053	-0.084	-0.099
2008	-0.108	-0.118	-0.121	-0.089	-0.059	-0.040	-0.036	-0.035	-0.037	-0.041	-0.067	-0.105
2009	-0.119	-0.112	-0.113	-0.101	-0.073	-0.045	-0.039	-0.036	-0.035	-0.042	-0.081	-0.103
2010	-0.117	-0.095	-0.115	-0.107	-0.075	-0.046	-0.040	-0.041	-0.038	-0.042	-0.055	-0.109
2011	-0.120	-0.109	-0.117	-0.104	-0.069	-0.045	-0.037	-0.034	-0.033	-0.060	-0.068	-0.109
2012	-0.107	-0.120	-0.117	-0.105	-0.072	-0.045	-0.036	-0.035	-0.035	-0.040	-0.074	-0.097
2013	-0.109	-0.102	-0.123	-0.101	-0.066	-0.045	-0.036	-0.038	-0.036	-0.062	-0.057	-0.099
2014	-0.107	-0.097	-0.127	-0.100	-0.074	-0.047	-0.039	-0.039	-0.040	-0.053	-0.060	-0.080
2015	-0.104	-0.105	-0.124	-0.103	-0.069	-0.041	-0.034	-0.034	-0.035	-0.040	-0.066	-0.102
2016	-0.115	-0.120	-0.119	-0.104	-0.068	-0.043	-0.037	-0.035	-0.032	-0.036	-0.057	-0.114
2017	-0.110	-0.107	-0.116	-0.104	-0.076	-0.047	-0.038	-0.038	-0.035	-0.044	-0.076	-0.108
2018	-0.122	-0.111	-0.119	-0.102	-0.079	-0.046	-0.043	-0.039	-0.036	-0.048	-0.061	-0.099
2019	-0.107	-0.108	-0.119	-0.106	-0.073	-0.048	-0.041	-0.040	-0.041	-0.057	-0.068	-0.116
2020	-0.103	-0.107	-0.118	-0.095	-0.062	-0.042	-0.038	-0.038	-0.037	-0.048	-0.054	-0.107
2021	-0.110	-0.110	-0.109	-0.098	-0.077	-0.047	-0.042	-0.041	-0.040	-0.047	-0.054	-0.080
	Jan	**Feb**	**Mar**	**Apr**	**May**	**Jun**	**Jul**	**Aug**	**Sep**	**Oct**	**Nov**	**Dec**
Mean	**-0.114**	**-0.107**	**-0.117**	**-0.100**	**-0.071**	**-0.045**	**-0.038**	**-0.037**	**-0.036**	**-0.046**	**-0.068**	**-0.102**
St.dev.	**0.007**	**0.007**	**0.006**	**0.006**	**0.007**	**0.006**	**0.005**	**0.005**	**0.005**	**0.009**	**0.014**	**0.009**

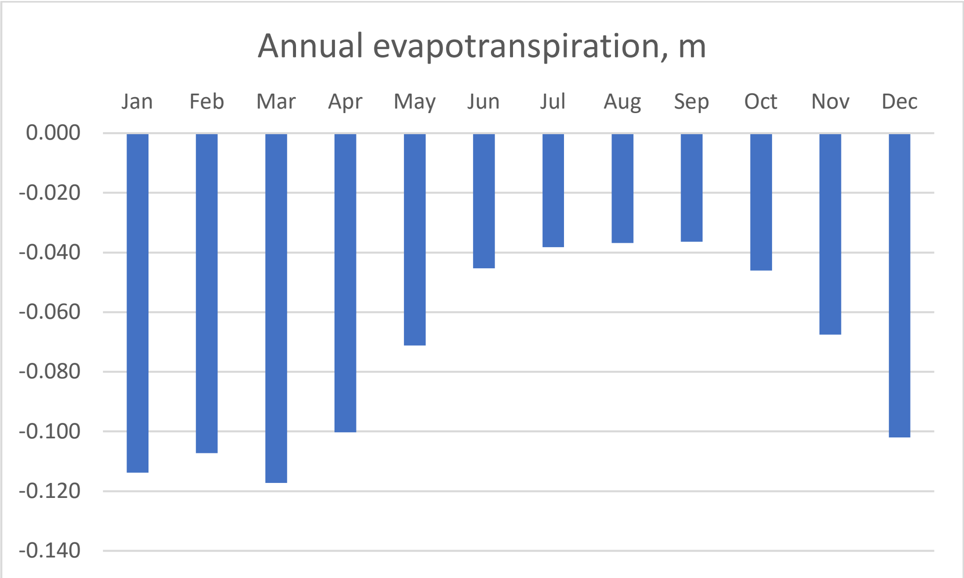

.

9. ANNEX 2C: ANNUAL SUB-SURFACE RUNOFF (ENTIRE COUNTRY)

Year	Jan	Feb	Mar	Apr	May	Jun	Jul	Aug	Sep	Oct	Nov	Dec	Total
1957	0.032	0.168	0.124	0.129	0.068	0.022	0.011	0.006	0.003	0.002	0.001	0.005	0.571
1958	0.021	0.087	0.097	0.036	0.017	0.008	0.005	0.003	0.002	0.001	0.001	0.008	0.285
1959	0.026	0.057	0.064	0.027	0.012	0.006	0.004	0.003	0.002	0.001	0.001	0.012	0.213
1960	0.017	0.024	0.048	0.020	0.010	0.005	0.003	0.002	0.001	0.001	0.001	0.001	0.134
1961	0.008	0.019	0.028	0.023	0.014	0.005	0.003	0.002	0.001	0.001	0.002	0.013	0.119
1962	0.039	0.054	0.050	0.033	0.018	0.008	0.004	0.002	0.001	0.001	0.001	0.007	0.218
1963	0.032	0.071	0.062	0.040	0.018	0.009	0.005	0.003	0.002	0.001	0.001	0.015	0.259
1964	0.028	0.036	0.047	0.026	0.011	0.006	0.003	0.002	0.001	0.001	0.001	0.001	0.164
1965	0.018	0.023	0.036	0.025	0.009	0.004	0.003	0.002	0.001	0.001	0.001	0.001	0.124
1966	0.002	0.010	0.014	0.017	0.006	0.003	0.002	0.001	0.001	0.001	0.000	0.001	0.057
1967	0.003	0.010	0.022	0.015	0.008	0.004	0.003	0.002	0.001	0.001	0.001	0.013	0.083
1968	0.022	0.033	0.036	0.018	0.010	0.005	0.003	0.002	0.001	0.001	0.001	0.004	0.136
1969	0.019	0.041	0.022	0.023	0.012	0.006	0.003	0.002	0.001	0.001	0.001	0.004	0.134
1970	0.017	0.048	0.030	0.016	0.008	0.004	0.002	0.002	0.001	0.001	0.001	0.009	0.139
1971	0.045	0.068	0.046	0.023	0.011	0.006	0.004	0.002	0.001	0.001	0.001	0.005	0.214
1972	0.017	0.024	0.036	0.023	0.013	0.007	0.004	0.003	0.002	0.001	0.003	0.015	0.149
1973	0.029	0.035	0.039	0.030	0.012	0.006	0.003	0.002	0.001	0.001	0.001	0.003	0.161
1974	0.012	0.035	0.048	0.056	0.029	0.013	0.007	0.004	0.003	0.002	0.001	0.007	0.217
1975	0.014	0.017	0.037	0.021	0.011	0.006	0.004	0.002	0.001	0.001	0.001	0.004	0.119
1976	0.019	0.030	0.049	0.040	0.020	0.010	0.006	0.004	0.002	0.001	0.001	0.002	0.184
1977	0.015	0.023	0.041	0.032	0.014	0.007	0.004	0.003	0.002	0.001	0.001	0.006	0.147
1978	0.031	0.061	0.121	0.060	0.027	0.012	0.007	0.004	0.002	0.001	0.002	0.022	0.349
1979	0.026	0.047	0.050	0.046	0.022	0.009	0.005	0.003	0.002	0.001	0.001	0.006	0.219
1980	0.023	0.018	0.037	0.038	0.017	0.007	0.004	0.003	0.002	0.001	0.001	0.010	0.161
1981	0.015	0.054	0.048	0.022	0.014	0.007	0.004	0.003	0.002	0.001	0.001	0.003	0.174
1982	0.023	0.060	0.043	0.024	0.021	0.009	0.005	0.003	0.002	0.002	0.004	0.013	0.208
1983	0.029	0.048	0.033	0.018	0.010	0.006	0.004	0.002	0.002	0.001	0.001	0.005	0.158
1984	0.023	0.043	0.044	0.021	0.010	0.006	0.004	0.003	0.002	0.001	0.001	0.012	0.170
1985	0.019	0.057	0.040	0.041	0.018	0.009	0.005	0.003	0.002	0.001	0.002	0.016	0.214
1986	0.071	0.077	0.056	0.038	0.020	0.010	0.006	0.004	0.002	0.001	0.001	0.016	0.303
1987	0.039	0.038	0.034	0.024	0.013	0.006	0.004	0.002	0.002	0.001	0.001	0.001	0.165
1988	0.011	0.031	0.032	0.019	0.009	0.005	0.003	0.002	0.001	0.001	0.002	0.003	0.119
1989	0.039	0.064	0.117	0.048	0.021	0.011	0.007	0.004	0.002	0.002	0.001	0.011	0.328
1990	0.048	0.038	0.037	0.022	0.011	0.007	0.004	0.003	0.002	0.001	0.001	0.001	0.176
1991	0.014	0.020	0.032	0.032	0.013	0.007	0.004	0.003	0.002	0.001	0.001	0.006	0.133
1992	0.014	0.014	0.016	0.012	0.009	0.005	0.003	0.002	0.001	0.001	0.001	0.003	0.081
1993	0.020	0.040	0.060	0.028	0.013	0.006	0.004	0.002	0.002	0.001	0.001	0.001	0.178
1994	0.009	0.024	0.031	0.018	0.008	0.004	0.003	0.002	0.001	0.001	0.001	0.002	0.103
1995	0.022	0.030	0.032	0.015	0.007	0.004	0.003	0.002	0.001	0.001	0.000	0.003	0.120
1996	0.009	0.040	0.059	0.029	0.013	0.007	0.005	0.003	0.002	0.001	0.001	0.005	0.173
1997	0.015	0.082	0.055	0.038	0.016	0.008	0.005	0.003	0.002	0.001	0.001	0.018	0.243
1998	0.045	0.056	0.052	0.031	0.013	0.006	0.004	0.002	0.001	0.001	0.001	0.001	0.214

Year	Jan	Feb	Mar	Apr	May	Jun	Jul	Aug	Sep	Oct	Nov	Dec	Total
1999	0.008	0.019	0.042	0.045	0.015	0.007	0.004	0.003	0.002	0.001	0.001	0.001	0.149
2000	0.003	0.018	0.045	0.024	0.011	0.006	0.004	0.002	0.002	0.001	0.004	0.013	0.134
2001	0.057	0.071	0.065	0.041	0.017	0.008	0.005	0.003	0.002	0.001	0.001	0.003	0.273
2002	0.021	0.053	0.036	0.031	0.012	0.006	0.004	0.002	0.001	0.001	0.001	0.004	0.173
2003	0.039	0.065	0.047	0.049	0.017	0.008	0.005	0.003	0.002	0.001	0.001	0.002	0.237
2004	0.009	0.019	0.032	0.021	0.011	0.006	0.004	0.002	0.001	0.001	0.001	0.013	0.120
2005	0.036	0.031	0.033	0.015	0.007	0.004	0.003	0.002	0.001	0.001	0.001	0.002	0.136
2006	0.007	0.011	0.043	0.028	0.012	0.006	0.004	0.002	0.001	0.001	0.001	0.009	0.125
2007	0.067	0.074	0.052	0.024	0.013	0.007	0.004	0.003	0.002	0.001	0.001	0.006	0.255
2008	0.049	0.072	0.040	0.021	0.010	0.005	0.003	0.002	0.001	0.001	0.001	0.006	0.212
2009	0.023	0.040	0.052	0.041	0.014	0.007	0.004	0.003	0.002	0.001	0.001	0.003	0.190
2010	0.019	0.045	0.054	0.023	0.013	0.007	0.004	0.003	0.002	0.001	0.001	0.005	0.176
2011	0.015	0.028	0.032	0.028	0.012	0.006	0.003	0.002	0.001	0.001	0.001	0.005	0.133
2012	0.027	0.025	0.050	0.032	0.013	0.006	0.004	0.002	0.001	0.001	0.001	0.005	0.168
2013	0.037	0.071	0.052	0.028	0.012	0.006	0.004	0.002	0.001	0.001	0.001	0.004	0.219
2014	0.022	0.072	0.051	0.033	0.015	0.007	0.004	0.003	0.002	0.001	0.001	0.003	0.213
2015	0.037	0.043	0.040	0.023	0.011	0.005	0.003	0.002	0.001	0.001	0.001	0.003	0.170
2016	0.026	0.034	0.028	0.032	0.011	0.005	0.003	0.002	0.001	0.001	0.001	0.001	0.146
2017	0.008	0.021	0.045	0.031	0.015	0.007	0.004	0.003	0.002	0.001	0.001	0.011	0.150
2018	0.027	0.038	0.049	0.033	0.015	0.007	0.004	0.003	0.002	0.001	0.001	0.014	0.194
2019	0.047	0.061	0.099	0.035	0.016	0.008	0.005	0.003	0.002	0.001	0.001	0.014	0.293
2020	0.077	0.077	0.072	0.025	0.012	0.006	0.004	0.002	0.001	0.001	0.001	0.003	0.281
2021	0.026	0.040	0.095	0.040	0.019	0.009	0.005	0.003	0.002	0.001	0.001	0.001	0.241
	Jan	Feb	Mar	Apr	May	Jun	Jul	Aug	Sep	Oct	Nov	Dec	
Mean	0.026	0.044	0.049	0.031	0.014	0.007	0.004	0.003	0.002	0.001	0.001	0.007	0.188
St.Dev	0.016	0.026	0.023	0.016	0.008	0.003	0.001	0.001	0.000	0.000	0.001	0.005	0.077

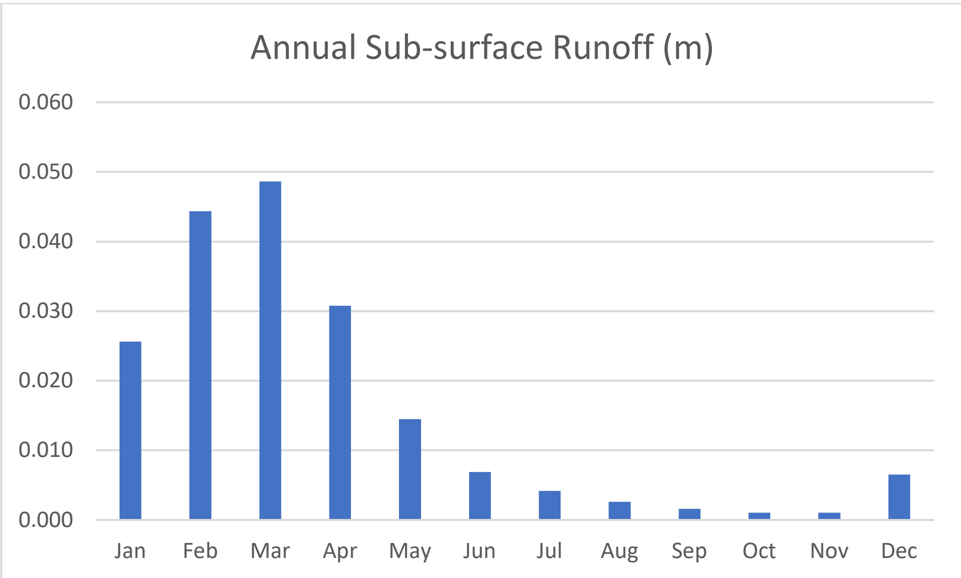

.

10.ANNEX 2D: ANNUAL SURFACE RUNOFF (ENTIRE COUNTRY)

Year	Jan	Feb	Mar	Apr	May	Jun	Jul	Aug	Sep	Oct	Nov	Dec	Total
1957	0.099	0.279	0.177	0.171	0.084	0.022	0.011	0.006	0.003	0.002	0.001	0.027	0.882
1958	0.067	0.155	0.129	0.040	0.017	0.008	0.005	0.003	0.002	0.001	0.003	0.032	0.461
1959	0.071	0.108	0.087	0.037	0.012	0.006	0.004	0.003	0.002	0.002	0.003	0.043	0.378
1960	0.037	0.050	0.073	0.026	0.010	0.005	0.003	0.002	0.001	0.001	0.001	0.009	0.219
1961	0.032	0.040	0.050	0.030	0.014	0.005	0.003	0.002	0.001	0.001	0.009	0.034	0.223
1962	0.084	0.094	0.074	0.040	0.018	0.008	0.004	0.002	0.001	0.001	0.001	0.037	0.366
1963	0.074	0.121	0.087	0.049	0.019	0.009	0.005	0.003	0.002	0.001	0.006	0.050	0.427
1964	0.054	0.068	0.069	0.031	0.012	0.006	0.004	0.002	0.001	0.001	0.002	0.009	0.259
1965	0.054	0.047	0.058	0.032	0.009	0.004	0.003	0.002	0.001	0.001	0.001	0.005	0.217
1966	0.004	0.033	0.029	0.024	0.006	0.003	0.002	0.001	0.001	0.001	0.002	0.009	0.115
1967	0.014	0.028	0.048	0.023	0.008	0.004	0.003	0.002	0.001	0.001	0.006	0.036	0.173
1968	0.048	0.067	0.053	0.025	0.010	0.005	0.003	0.002	0.001	0.001	0.005	0.023	0.241
1969	0.059	0.079	0.037	0.030	0.012	0.006	0.003	0.002	0.001	0.001	0.004	0.025	0.258
1970	0.048	0.094	0.044	0.020	0.008	0.004	0.002	0.002	0.001	0.001	0.005	0.042	0.271
1971	0.091	0.107	0.063	0.026	0.012	0.006	0.004	0.002	0.001	0.001	0.004	0.023	0.340
1972	0.052	0.048	0.061	0.030	0.014	0.007	0.004	0.003	0.002	0.002	0.013	0.041	0.277
1973	0.061	0.070	0.065	0.043	0.013	0.006	0.003	0.002	0.001	0.001	0.002	0.019	0.286
1974	0.037	0.068	0.074	0.069	0.036	0.013	0.008	0.005	0.003	0.002	0.002	0.034	0.350
1975	0.040	0.043	0.055	0.026	0.011	0.006	0.004	0.002	0.001	0.001	0.002	0.020	0.211
1976	0.048	0.059	0.081	0.051	0.021	0.010	0.006	0.004	0.002	0.002	0.001	0.015	0.300
1977	0.049	0.048	0.064	0.041	0.015	0.007	0.004	0.003	0.002	0.001	0.005	0.024	0.263
1978	0.074	0.101	0.173	0.072	0.027	0.012	0.007	0.004	0.002	0.002	0.006	0.066	0.545
1979	0.043	0.088	0.074	0.062	0.022	0.009	0.006	0.003	0.002	0.001	0.007	0.023	0.341
1980	0.055	0.029	0.069	0.055	0.018	0.007	0.004	0.003	0.002	0.002	0.002	0.045	0.290
1981	0.036	0.107	0.068	0.025	0.018	0.007	0.004	0.003	0.002	0.002	0.003	0.019	0.295
1982	0.069	0.111	0.057	0.033	0.024	0.009	0.005	0.003	0.002	0.005	0.016	0.037	0.371
1983	0.065	0.089	0.050	0.020	0.010	0.006	0.004	0.003	0.002	0.001	0.001	0.027	0.278
1984	0.055	0.086	0.065	0.024	0.011	0.006	0.004	0.003	0.002	0.001	0.006	0.042	0.304
1985	0.045	0.099	0.063	0.050	0.019	0.009	0.005	0.003	0.002	0.001	0.008	0.048	0.352
1986	0.134	0.114	0.082	0.043	0.020	0.010	0.006	0.004	0.002	0.002	0.004	0.044	0.466
1987	0.087	0.062	0.051	0.029	0.013	0.006	0.004	0.003	0.002	0.001	0.001	0.008	0.267
1988	0.042	0.066	0.060	0.020	0.009	0.005	0.003	0.002	0.001	0.001	0.006	0.012	0.229
1989	0.098	0.112	0.175	0.062	0.024	0.012	0.007	0.004	0.003	0.002	0.005	0.044	0.545
1990	0.091	0.071	0.048	0.028	0.013	0.007	0.004	0.003	0.002	0.001	0.004	0.006	0.277
1991	0.048	0.053	0.056	0.040	0.014	0.007	0.004	0.003	0.002	0.001	0.002	0.023	0.253
1992	0.033	0.031	0.028	0.014	0.011	0.005	0.003	0.002	0.001	0.001	0.006	0.016	0.150
1993	0.053	0.083	0.090	0.031	0.014	0.007	0.004	0.003	0.002	0.001	0.003	0.003	0.293
1994	0.037	0.054	0.061	0.023	0.008	0.004	0.003	0.002	0.001	0.001	0.002	0.008	0.204
1995	0.071	0.063	0.049	0.019	0.008	0.004	0.003	0.002	0.001	0.001	0.001	0.019	0.240
1996	0.040	0.092	0.091	0.032	0.014	0.008	0.005	0.003	0.002	0.001	0.001	0.024	0.312
1997	0.050	0.141	0.065	0.056	0.016	0.008	0.005	0.003	0.002	0.002	0.007	0.053	0.407
1998	0.101	0.095	0.078	0.042	0.013	0.006	0.004	0.002	0.002	0.001	0.001	0.004	0.349

Year	Jan	Feb	Mar	Apr	May	Jun	Jul	Aug	Sep	Oct	Nov	Dec	Total
1999	0.037	0.045	0.078	0.060	0.015	0.007	0.004	0.003	0.002	0.001	0.001	0.007	0.263
2000	0.020	0.056	0.079	0.031	0.012	0.006	0.004	0.003	0.002	0.001	0.022	0.039	0.275
2001	0.108	0.112	0.094	0.046	0.017	0.008	0.005	0.003	0.002	0.001	0.001	0.020	0.418
2002	0.060	0.097	0.053	0.036	0.012	0.006	0.004	0.002	0.002	0.001	0.003	0.021	0.298
2003	0.104	0.112	0.077	0.058	0.017	0.008	0.005	0.003	0.002	0.001	0.001	0.014	0.401
2004	0.032	0.045	0.054	0.029	0.011	0.006	0.004	0.002	0.002	0.001	0.005	0.046	0.237
2005	0.073	0.052	0.053	0.016	0.008	0.004	0.003	0.002	0.002	0.001	0.001	0.012	0.228
2006	0.029	0.029	0.081	0.037	0.013	0.006	0.004	0.002	0.002	0.001	0.004	0.041	0.248
2007	0.147	0.119	0.067	0.031	0.014	0.007	0.004	0.003	0.002	0.003	0.002	0.030	0.429
2008	0.110	0.110	0.056	0.021	0.010	0.005	0.004	0.002	0.001	0.001	0.003	0.028	0.352
2009	0.060	0.067	0.085	0.049	0.014	0.007	0.004	0.003	0.002	0.001	0.005	0.017	0.312
2010	0.056	0.095	0.075	0.025	0.014	0.007	0.004	0.003	0.002	0.001	0.001	0.027	0.310
2011	0.045	0.053	0.049	0.034	0.012	0.006	0.004	0.002	0.001	0.001	0.004	0.019	0.231
2012	0.075	0.053	0.077	0.040	0.013	0.006	0.004	0.002	0.001	0.001	0.003	0.026	0.302
2013	0.091	0.113	0.074	0.034	0.013	0.006	0.004	0.002	0.001	0.001	0.001	0.019	0.359
2014	0.065	0.140	0.065	0.040	0.015	0.007	0.004	0.003	0.002	0.001	0.003	0.015	0.360
2015	0.100	0.085	0.051	0.032	0.011	0.005	0.003	0.002	0.001	0.001	0.004	0.017	0.312
2016	0.074	0.066	0.056	0.042	0.012	0.005	0.003	0.002	0.001	0.001	0.002	0.010	0.274
2017	0.036	0.051	0.082	0.036	0.016	0.007	0.004	0.003	0.002	0.001	0.006	0.038	0.281
2018	0.055	0.067	0.088	0.051	0.016	0.007	0.004	0.003	0.002	0.001	0.003	0.047	0.343
2019	0.109	0.092	0.176	0.040	0.017	0.009	0.005	0.003	0.002	0.001	0.005	0.054	0.512
2020	0.166	0.122	0.099	0.026	0.012	0.006	0.004	0.002	0.002	0.001	0.001	0.020	0.461
2021	0.080	0.080	0.150	0.046	0.019	0.009	0.005	0.003	0.002	0.001	0.002	0.001	0.400
Year	**Jan**	**Feb**	**Mar**	**Apr**	**May**	**Jun**	**Jul**	**Aug**	**Sep**	**Oct**	**Nov**	**Dec**	
Mean	0.064	0.082	0.075	0.039	0.015	0.007	0.004	0.003	0.002	0.001	0.004	0.026	0.321
St.Dev	0.031	0.039	0.033	0.021	0.010	0.003	0.001	0.001	0.000	0.001	0.004	0.015	0.113

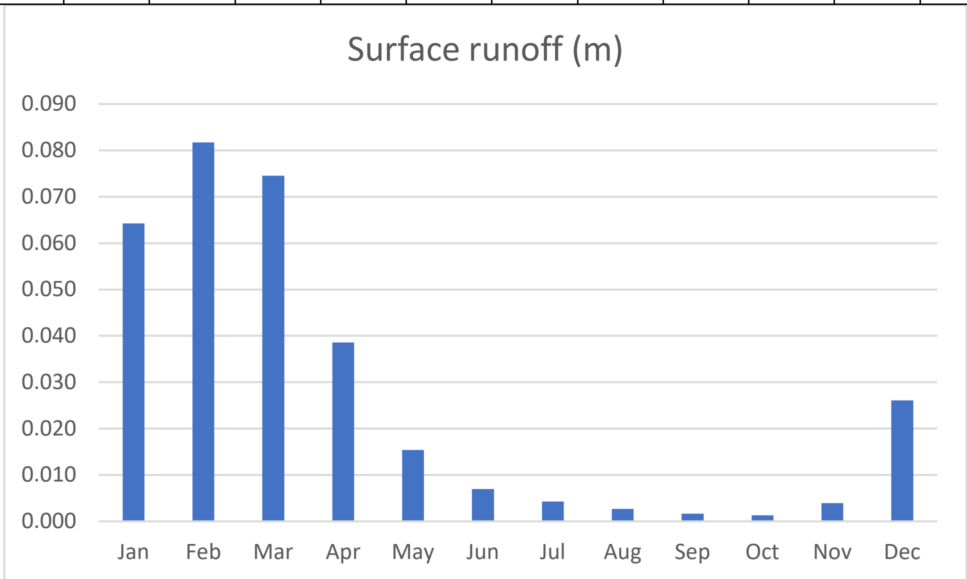

.

11.ANNEX 3 CATCHMENTS LAND COVER (SOURCE: CLIMATE DATA STORE LCCS)

South Rukuru Area (km²)

Year	Forest	Crop	Shrub	Wetland	Urban	Other	Total
1992	3093.48	6128.91	891.27	58.86	1.71	6.12	10180.35
1993	3093.48	6128.91	891.27	58.86	1.71	6.12	10180.35
1994	3093.48	6128.91	891.27	58.86	1.71	6.12	10180.35
1995	2763.54	6494.58	873.72	40.68	1.71	6.12	10180.35
1996	2786.67	6502.59	845.28	37.98	1.71	6.12	10180.35
1997	2789.28	6523.56	822.06	37.53	1.8	6.12	10180.35
1998	2750.13	6576.12	808.56	37.53	1.89	6.12	10180.35
1999	2664.18	6645.96	832.77	29.25	2.07	6.12	10180.35
2000	2658.06	6655.32	834.75	23.94	2.16	6.12	10180.35
2001	2703.33	6657.39	788.67	22.68	2.16	6.12	10180.35
2002	2710.26	6657.84	784.53	19.44	2.16	6.12	10180.35
2003	2733.39	6657.03	762.66	18.99	2.16	6.12	10180.35
2004	2754.45	6648.93	750.06	18.63	2.16	6.12	10180.35
2005	2762.64	6645.42	745.38	18.63	2.16	6.12	10180.35
2006	2762.01	6646.05	745.38	18.63	2.16	6.12	10180.35
2007	2777.4	6641.01	734.94	18.63	2.25	6.12	10180.35
2008	2788.65	6638.58	726.12	18.63	2.25	6.12	10180.35
2009	2788.2	6636.51	728.64	18.63	2.25	6.12	10180.35
2010	2786.49	6637.5	729.27	18.63	2.34	6.12	10180.35
2011	2786.67	6638.22	728.28	18.63	2.43	6.12	10180.35
2012	2787.21	6638.85	726.75	18.63	2.79	6.12	10180.35
2013	2787.66	6637.32	726.75	18.63	3.87	6.12	10180.35
2014	2794.5	6631.29	724.59	18.63	5.22	6.12	10180.35
2015	2794.5	6630.75	723.24	18.63	7.11	6.12	10180.35
2016	2831.85	6594.84	720.27	18.63	8.64	6.12	10180.35
2017	2841.12	6586.65	719.19	18.63	8.64	6.12	10180.35
2018	2858.4	6570.27	719.01	17.91	8.64	6.12	10180.35
2019	2875.95	6556.59	714.96	17.73	9	6.12	10180.35
2020	2877.57	6552.09	713.16	17.73	13.68	6.12	10180.35

Linthipe Area km²

Year	Forest	Crop	Shrub	Wetland	Urban	Other	Total
1992	2452,05	5545,8	549	83,07	30,69	17,46	8678,07
1993	2452,05	5545,8	548,46	82,98	31,32	17,46	8678,07
1994	2452,05	5545,8	548,01	82,98	31,77	17,46	8678,07
1995	2185,56	5800,05	560,52	83,79	32,85	15,3	8678,07
1996	2170,53	5814,81	560,88	84,06	33,21	14,58	8678,07
1997	2079,72	5897,43	568,62	84,15	33,57	14,58	8678,07
1998	2053,71	5922,54	569,43	84,15	33,66	14,58	8678,07

Year	**Forest**	**Crop**	**Shrub**	**Wetland**	**Urban**	**Other**	**Total**
1999	1385.73	6526.71	632.79	94.23	34.2	4.41	8678.07
2000	1364.94	6543.54	636.21	94.23	34.74	4.41	8678.07
2001	1368.36	6546.6	629.64	94.23	34.83	4.41	8678.07
2002	1368.9	6546.6	628.92	94.14	35.1	4.41	8678.07
2003	1374.75	6543	626.22	94.14	35.55	4.41	8678.07
2004	1372.41	6546.78	624.69	94.14	35.64	4.41	8678.07
2005	1377.36	6540.57	620.55	94.14	41.04	4.41	8678.07
2006	1376.91	6532.83	621.54	94.14	48.24	4.41	8678.07
2007	1376.19	6524.46	628.02	94.14	50.85	4.41	8678.07
2008	1380.87	6466.32	676.98	94.32	55.17	4.41	8678.07
2009	1383.03	6450.21	686.16	94.05	60.21	4.41	8678.07
2010	1374.48	6456.24	684.81	94.05	64.08	4.41	8678.07
2011	1375.29	6449.4	687.87	94.05	67.05	4.41	8678.07
2012	1375.83	6441.48	691.11	94.05	71.19	4.41	8678.07
2013	1374.93	6438.42	684.45	94.05	81.81	4.41	8678.07
2014	1380.06	6421.05	683.64	94.05	94.86	4.41	8678.07
2015	1379.97	6420.51	678.69	94.05	100.44	4.41	8678.07
2016	1389.87	6339.06	750.96	92.79	100.98	4.41	8678.07
2017	1394.37	6334.92	748.62	92.79	102.96	4.41	8678.07
2018	1393.38	6338.61	745.92	92.61	103.14	4.41	8678.07
2019	1396.89	6336.18	732.24	92.43	115.92	4.41	8678.07
2020	1397.61	6328.8	723.69	92.43	131.13	4.41	8678.07

Dwangwa Km^2

Year	**Forest**	**Crop**	**Shrub**	**Wetland**	**Urban**	**Other**	**Total**
1992	3812.31	3151.98	554.94	4.68	0.99	6.57	7531.47
1993	3812.22	3151.98	554.94	4.68	1.08	6.57	7531.47
1994	3812.22	3151.98	554.94	4.68	1.08	6.57	7531.47
1995	3404.25	3544.56	573.30	4.68	1.08	3.60	7531.47
1996	3271.14	3672.99	577.89	4.77	1.08	3.60	7531.47
1997	3139.11	3794.13	588.15	5.31	1.17	3.60	7531.47
1998	3059.01	3864.78	597.51	5.40	1.17	3.60	7531.47
1999	2864.88	4008.06	649.89	5.49	1.17	1.98	7531.47
2000	2850.66	4015.71	656.19	5.49	1.44	1.98	7531.47
2001	2969.91	4021.38	531.27	5.49	1.44	1.98	7531.47
2002	3116.61	4015.08	390.87	5.49	1.44	1.98	7531.47
2003	3179.16	4013.73	329.49	5.49	1.44	2.16	7531.47
2004	3188.97	4015.98	317.43	5.49	1.44	2.16	7531.47
2005	3191.22	4014.81	316.35	5.49	1.44	2.16	7531.47
2006	3192.03	4014.36	315.99	5.49	1.44	2.16	7531.47
2007	3205.35	4011.57	305.46	5.49	1.44	2.16	7531.47
2008	3211.56	4009.59	301.14	5.49	1.44	2.25	7531.47
2009	3215.16	4006.71	300.42	5.49	1.44	2.25	7531.47
2010	3214.44	4007.25	300.51	5.49	1.53	2.25	7531.47

Year	Forest	Crop	Shrub	Wetland	Urban	Other	Total
2011	3215.43	4007.25	299.52	5.49	1.53	2.25	7531.47
2012	3216.24	4006.80	299.16	5.49	1.53	2.25	7531.47
2013	3215.16	4006.62	300.33	5.49	1.62	2.25	7531.47
2014	3216.60	4005.36	300.15	5.49	1.62	2.25	7531.47
2015	3216.60	4005.36	300.15	5.49	1.62	2.25	7531.47
2016	3240.00	3975.75	306.90	4.95	1.62	2.25	7531.47
2017	3241.80	3973.32	307.53	4.95	1.62	2.25	7531.47
2018	3241.44	3974.04	307.17	4.95	1.62	2.25	7531.47
2019	3245.22	3969.81	307.26	4.95	1.98	2.25	7531.47
2020	3245.22	3968.55	307.17	4.95	3.33	2.25	7531.47

.

12. ANNEX 4: MAXIMAL DAILY RAINFALL OBSERVED EACH YEAR (ERA 5)

South Rukuru Catchment

Year	Date	max_prec(m)	surface_runoff(m)	ss_runoff(m)
1957	19570203	0.05162	0.03248	0.01029
1958	19581222	0.02875	0.00529	0.00090
1959	19591213	0.07578	0.02299	0.00438
1960	19600108	0.02666	0.00635	0.00292
1961	19611216	0.02297	0.00413	0.00096
1962	19620224	0.02141	0.01147	0.00419
1963	19630209	0.03090	0.00961	0.00340
1964	19640119	0.01582	0.00368	0.00108
1965	19650202	0.02024	0.01183	0.00102
1966	19660304	0.01962	0.00555	0.00164
1967	19671205	0.01853	0.00081	0.00023
1968	19680311	0.02776	0.01125	0.00272
1969	19691123	0.03597	0.00332	0.00017
1970	19700212	0.03299	0.01961	0.00413
1971	19710122	0.02454	0.00540	0.00207
1972	19721225	0.02515	0.00966	0.00372
1973	19730412	0.02370	0.00842	0.00369
1974	19741207	0.01799	0.00048	0.00002
1975	19750114	0.02960	0.00479	0.00139
1976	19760112	0.02853	0.00601	0.00132
1977	19770118	0.02762	0.00429	0.00102
1978	19781220	0.02461	0.00444	0.00112
1979	19790205	0.04175	0.02001	0.00625
1980	19800306	0.02165	0.00962	0.00302
1981	19811231	0.03043	0.01552	0.00193
1982	19821129	0.01731	0.00133	0.00037
1983	19830215	0.02328	0.00539	0.00139
1984	19841209	0.01903	0.00239	0.00007
1985	19850228	0.02221	0.00630	0.00340
1986	19860120	0.02301	0.00842	0.00404
1987	19870124	0.02081	0.01260	0.00325
1988	19880210	0.02487	0.01579	0.00286
1989	19891203	0.02812	0.01285	0.00212
1990	19900226	0.02320	0.00500	0.00233
1991	19910104	0.02153	0.00157	0.00031
1992	19921122	0.02097	0.00103	0.00033
1993	19930115	0.03283	0.00761	0.00270
1994	19940105	0.03262	0.00091	0.00001
1995	19950106	0.05997	0.02059	0.00556
1996	19960315	0.02207	0.00365	0.00107

Year	Date	max_prec(m)	surface_runoff(m)	ss_runoff(m)
1997	19971224	0.03432	0.01541	0.00501
1998	19980131	0.03040	0.01952	0.00277
1999	19990406	0.02856	0.01290	0.00581
2000	20000202	0.02895	0.01205	0.00162
2001	20011228	0.02367	0.01027	0.00186
2002	20020131	0.02519	0.01163	0.00163
2003	20030101	0.03514	0.00893	0.00242
2004	20040129	0.01849	0.00177	0.00043
2005	20050228	0.01905	0.00276	0.00109
2006	20061213	0.02090	0.00288	0.00040
2007	20070228	0.02841	0.00675	0.00213
2008	20080127	0.02848	0.00435	0.00170
2009	20090306	0.02819	0.00910	0.00282
2010	20100220	0.02418	0.00752	0.00286
2011	20110213	0.02298	0.00413	0.00142
2012	20121102	0.03190	0.00083	0.00002
2013	20130201	0.04183	0.01437	0.00464
2014	20140122	0.02229	0.00494	0.00083
2015	20151105	0.04143	0.00260	0.00056
2016	20160118	0.03779	0.01091	0.00280
2017	20170309	0.02450	0.00663	0.00169
2018	20180119	0.04049	0.01787	0.00707
2019	20191230	0.04426	0.01333	0.00332
2020	20200129	0.04804	0.02548	0.00783
2021	20210308	0.03093	0.01507	0.00645

Linthipe Catchment

Year	Date	max_prec(m)	surface_runoff(m)	ss_runoff(m)
1958	19581226	0.0307	0.0066	0.0026
1959	19590223	0.0559	0.0415	0.0201
1960	19600412	0.0202	0.0008	0.0001
1961	19610102	0.0406	0.0075	0.0031
1962	19620107	0.0321	0.0065	0.0020
1963	19630216	0.0363	0.0166	0.0069
1964	19640206	0.0289	0.0080	0.0037
1965	19650116	0.0246	0.0051	0.0020
1966	19660220	0.0212	0.0030	0.0005
1967	19670316	0.0482	0.0176	0.0074
1968	19680421	0.0170	0.0011	0.0001
1969	19690214	0.0210	0.0063	0.0031
1970	19700204	0.0362	0.0104	0.0048
1971	19710219	0.0405	0.0198	0.0116
1972	19720202	0.0238	0.0037	0.0012
1973	19730116	0.0279	0.0087	0.0039

Year	Date	max_prec(m)	surface_runoff(m)	ss_runoff(m)
1974	19741210	0.0450	0.0086	0.0024
1975	19751205	0.0269	0.0015	0.0000
1976	19760314	0.0703	0.0388	0.0171
1977	19771230	0.0214	0.0034	0.0010
1978	19780312	0.0231	0.0124	0.0086
1979	19790308	0.0206	0.0044	0.0020
1980	19800308	0.0613	0.0262	0.0091
1981	19811130	0.0261	0.0015	0.0000
1982	19820207	0.0528	0.0110	0.0041
1983	19830211	0.0271	0.0083	0.0036
1984	19840116	0.0263	0.0068	0.0033
1985	19850213	0.0308	0.0110	0.0048
1986	19860322	0.0251	0.0060	0.0027
1987	19870123	0.0266	0.0087	0.0028
1988	19880209	0.0291	0.0090	0.0036
1989	19890129	0.0466	0.0198	0.0074
1990	19900114	0.0322	0.0129	0.0060
1991	19910114	0.0842	0.0398	0.0156
1992	19921228	0.0273	0.0045	0.0012
1993	19930114	0.0329	0.0067	0.0030
1994	19940106	0.0378	0.0039	0.0015
1995	19950122	0.0287	0.0064	0.0031
1996	19960208	0.0263	0.0052	0.0017
1997	19970204	0.0440	0.0174	0.0072
1998	19980116	0.0374	0.0154	0.0061
1999	19991214	0.0303	0.0021	0.0000
2000	20001215	0.0259	0.0072	0.0023
2001	20010129	0.0363	0.0182	0.0098
2002	20020122	0.0304	0.0110	0.0054
2003	20030104	0.0446	0.0118	0.0057
2004	20041230	0.0212	0.0048	0.0018
2005	20050228	0.0291	0.0072	0.0031
2006	20060307	0.0573	0.0281	0.0127
2007	20070110	0.0294	0.0098	0.0042
2008	20080127	0.0456	0.0206	0.0117
2009	20090213	0.0374	0.0175	0.0087
2010	20100221	0.0444	0.0207	0.0083
2011	20110222	0.0230	0.0036	0.0009
2012	20120309	0.0295	0.0095	0.0056
2013	20130108	0.0526	0.0164	0.0066
2014	20140225	0.0581	0.0381	0.0144
2015	20150119	0.0232	0.0055	0.0017
2016	20160131	0.0375	0.0103	0.0041
2017	20170204	0.0255	0.0067	0.0028
2018	20181224	0.0644	0.0260	0.0102

Year	Date	max_prec(m)	surface_runoff(m)	ss_runoff(m)
2019	20190308	0.0781	0.0382	0.0190
2020	20200103	0.0671	0.0299	0.0113
2021	20210309	0.0656	0.0421	0.0207

Dwangwa

Year	Date	max_prec(m)	surface_runoff(m)	ss_runoff(m)
1957	19570126	0.0836	0.0601	0.0084
1958	19581222	0.0387	0.0093	0.0017
1959	19591213	0.0881	0.0251	0.0047
1960	19600320	0.0194	0.0055	0.0019
1961	19610102	0.0261	0.0020	0.0003
1962	19620130	0.0351	0.0108	0.0023
1963	19630210	0.0212	0.0060	0.0013
1964	19640114	0.0197	0.0054	0.0015
1965	19650117	0.0220	0.0034	0.0003
1966	19660220	0.0195	0.0036	0.0009
1967	19671205	0.0294	0.0015	0.0002
1968	19681212	0.0241	0.0032	0.0003
1969	19690208	0.0214	0.0068	0.0016
1970	19701205	0.0267	0.0036	0.0006
1971	19710219	0.0442	0.0217	0.0051
1972	19721220	0.0281	0.0037	0.0006
1973	19730319	0.0196	0.0023	0.0009
1974	19740331	0.0364	0.0111	0.0029
1975	19750226	0.0203	0.0061	0.0010
1976	19760217	0.0265	0.0049	0.0012
1977	19770122	0.0352	0.0124	0.0022
1978	19780118	0.0266	0.0051	0.0011
1979	19790203	0.0284	0.0041	0.0009
1980	19801209	0.0349	0.0063	0.0005
1981	19810217	0.0266	0.0053	0.0012
1982	19820208	0.0243	0.0046	0.0013
1983	19830217	0.0431	0.0203	0.0061
1984	19840205	0.0261	0.0053	0.0011
1985	19850320	0.0191	0.0038	0.0008
1986	19860110	0.0369	0.0128	0.0036
1987	19870124	0.0213	0.0080	0.0018
1988	19880121	0.0210	0.0034	0.0003
1989	19890129	0.0461	0.0214	0.0053
1990	19900114	0.0367	0.0128	0.0027
1991	19910104	0.0291	0.0037	0.0003
1992	19921119	0.0240	0.0023	0.0000
1993	19930228	0.0305	0.0146	0.0045
1994	19940106	0.0346	0.0027	0.0001

Year	Date	max_prec(m)	surface_runoff(m)	ss_runoff(m)
1995	19950106	0.0322	0.0053	0.0005
1996	19960228	0.0333	0.0167	0.0040
1997	19971220	0.0333	0.0054	0.0010
1998	19980126	0.0201	0.0057	0.0008
1999	19991214	0.0264	0.0008	0.0000
2000	20000308	0.0204	0.0040	0.0006
2001	20010107	0.0418	0.0184	0.0034
2002	20020220	0.0233	0.0057	0.0019
2003	20030101	0.0217	0.0031	0.0001
2004	20040307	0.0276	0.0059	0.0008
2005	20050301	0.0318	0.0061	0.0013
2006	20060306	0.0268	0.0044	0.0008
2007	20070228	0.0519	0.0216	0.0040
2008	20080204	0.0258	0.0095	0.0034
2009	20090404	0.0252	0.0133	0.0050
2010	20100220	0.0415	0.0157	0.0030
2011	20110211	0.0216	0.0028	0.0007
2012	20120108	0.0234	0.0038	0.0005
2013	20130108	0.0669	0.0193	0.0028
2014	20140116	0.0366	0.0108	0.0019
2015	20150219	0.0220	0.0051	0.0012
2016	20160215	0.0252	0.0037	0.0006
2017	20171229	0.0349	0.0081	0.0010
2018	20180118	0.0310	0.0097	0.0016
2019	20191230	0.0853	0.0387	0.0066
2020	20200229	0.0338	0.0193	0.0033
2021	20210308	0.0628	0.0452	0.0082

13. ANNEX 5: OBSERVED AND SIMULATED MONTHLY RAINFALL DATA AT 7 STATIONS

obs	CMCC	INM.CM5.0	ACCESS.CM2	CNRM.ESM2.1	EC.Earth3.CC	EC.Earth3.Veg.LR	MIROC	MRI.ESM2	STATION	Month
316.3	199.3	211.1	203.0	200.3	198.3	141.9	200.1	211.0	BOLERO	1
272.6	177.9	152.3	147.1	147.8	153.3	105.0	155.0	133.8	BOLERO	2
243.0	114.0	98.2	108.1	97.1	106.1	82.1	92.3	97.0	BOLERO	3
72.9	39.5	39.5	42.6	43.8	39.8	35.0	44.4	34.9	BOLERO	4
8.6	3.5	2.1	4.2	2.2	2.3	28.4	3.2	2.5	BOLERO	5
1.2	3.1	1.8	2.9	2.5	1.9	23.2	1.7	1.6	BOLERO	6
0.3	1.7	1.6	1.4	1.9	2.0	19.4	1.5	2.5	BOLERO	7
0.6	1.9	1.8	3.5	2.5	6.1	22.6	1.7	2.5	BOLERO	8
0.2	3.4	5.2	3.0	2.8	6.0	21.5	2.3	1.3	BOLERO	9
5.3	10.7	6.2	6.4	9.8	12.2	25.9	13.3	10.1	BOLERO	10
38.1	33.9	33.2	37.0	32.2	28.7	51.8	50.1	35.7	BOLERO	11

obs	CMCC	INM.CM5.0	ACCESS.CM2	CNRM.ESM2.1	EC.Earth3.CC	EC.Earth3.Veg.LR	MIROC	MRI.ESM2	STATION	Month
238.9	133.3	105.8	133.8	113.1	126.6	99.9	108.3	116.6	BOLERO	12
258.4	269.3	268.1	278.8	283.8	289.9	239.2	277.7	279.5	DEDZA	1
208.9	201.9	241.6	224.1	209.3	210.0	140.6	220.0	211.3	DEDZA	2
140.9	179.3	174.6	155.5	153.2	152.7	96.3	140.5	128.8	DEDZA	3
43.6	39.6	34.6	46.3	46.1	36.3	48.7	40.2	44.7	DEDZA	4
7.5	6.5	7.3	6.8	6.0	7.6	35.8	9.4	7.7	DEDZA	5
2.2	1.8	4.6	2.0	1.9	2.1	32.8	1.9	1.1	DEDZA	6
2.2	2.6	4.0	3.6	4.5	3.3	31.6	2.0	3.3	DEDZA	7
1.0	2.1	2.3	2.6	3.4	4.6	30.3	2.7	3.7	DEDZA	8
1.8	1.9	2.9	2.9	3.2	3.8	33.4	1.7	1.1	DEDZA	9
10.3	10.6	9.5	8.7	15.3	14.5	32.8	17.7	9.5	DEDZA	10
59.5	62.7	58.9	63.1	60.3	64.4	86.1	82.3	67.8	DEDZA	11
192.1	189.5	175.8	203.9	188.7	197.8	152.6	163.8	173.2	DEDZA	12
181.3		183.8	183.8		183.4	136.0		195.5	KARONGA	1
168.4		144.7	163.0		165.4	128.0		148.6	KARONGA	2
281.2		268.4	270.7		258.1	184.3		260.7	KARONGA	3
187.1		166.7	154.3		154.8	94.3		159.4	KARONGA	4
20.5		13.7	13.0		10.2	38.2		12.4	KARONGA	5
3.5		2.7	3.7		3.3	36.2		2.5	KARONGA	6
1.4		3.3	3.1		3.5	33.2		3.0	KARONGA	7
0.4		0.5	1.2		2.5	35.7		0.7	KARONGA	8
0.2		1.3	0.7		1.3	31.7		0.1	KARONGA	9
1.4		1.7	2.6		10.0	36.6		3.2	KARONGA	10
51.2		35.8	39.7		36.4	62.9		42.3	KARONGA	11
175.3		138.3	168.7		160.6	137.3		160.0	KARONGA	12
201.4	228.5	221.9	226.8	228.7	218.8	195.4	217.5	234.7	KASUNGU	1
193.7	202.2	239.5	197.9	205.2	202.8	127.4	211.4	189.9	KASUNGU	2
123.3	142.4	109.1	133.7	118.2	127.9	77.3	113.9	98.3	KASUNGU	3
24.2	22.7	23.2	28.8	28.5	21.5	37.8	31.5	24.5	KASUNGU	4
4.8	7.4	5.9	6.9	6.3	8.3	25.4	7.7	7.1	KASUNGU	5
0.4	6.5	6.9	4.3	5.8	5.4	28.6	4.6	2.2	KASUNGU	6
0.3	0.8	1.0	1.1	1.0	0.9	30.1	0.6	1.1	KASUNGU	7
0.1	1.3	1.6	1.7	2.4	3.7	25.7	1.3	1.5	KASUNGU	8
0.2	1.4	2.4	2.4	2.1	2.5	23.8	0.7	0.7	KASUNGU	9
5.5	9.0	6.4	6.0	7.5	8.3	28.7	11.3	8.2	KASUNGU	10
38.7	41.3	45.5	46.0	42.9	39.9	67.8	58.3	44.8	KASUNGU	11
165.3	188.2	154.7	194.3	172.6	188.8	143.2	148.4	162.4	KASUNGU	12
267.7	299.9	283.9	309.1	309.6	313.8	249.3	307.1	314.5	NAMINJIWA	1
205.9	199.9	258.1	232.1	210.8	212.7	150.7	210.4	205.9	NAMINJIWA	2
140.5	187.5	180.6	165.9	158.2	166.4	107.7	153.7	145.6	NAMINJIWA	3
45.2	53.3	43.0	59.3	62.6	52.5	49.6	63.1	52.5	NAMINJIWA	4
13.5	18.9	20.1	18.9	19.2	17.7	48.3	24.2	19.0	NAMINJIWA	5
9.2	13.5	17.4	14.3	16.4	15.0	47.6	13.3	12.5	NAMINJIWA	6
11.4	16.2	17.5	17.5	20.3	18.2	42.6	14.3	18.3	NAMINJIWA	7

obs	**CMCC**	**INM.CM5.0**	**ACCESS.CM2**	**CNRM.ESM2.1**	**EC.Earth3.CC**	**EC.Earth3.Veg.LR**	**MIROC**	**MRI.ESM2**	**STATION**	**Month**
6.1	9.6	10.2	9.1	9.1	10.3	35.4	9.0	10.5	NAMINJIWA	8
6.2	11.0	12.2	11.8	10.3	11.2	38.6	11.1	9.5	NAMINJIWA	9
25.0	35.5	30.9	28.6	35.3	38.3	55.8	36.2	30.5	NAMINJIWA	10
71.6	82.3	69.1	77.0	70.8	80.3	80.6	92.7	74.7	NAMINJIWA	11
202.9	200.9	206.0	193.6	196.2	201.8	171.2	187.7	183.3	NAMINJIWA	12
195.3	209.4	208.1	257.9	219.8	226.6	172.0	215.5	214.4	NGABU	1
139.1	134.4	153.1	161.5	149.0	150.6	107.8	145.4	145.6	NGABU	2
111.3	121.1	138.4	98.6	104.2	110.4	78.1	101.6	95.1	NGABU	3
34.0	43.1	33.7	41.7	45.9	38.6	34.4	49.1	36.1	NGABU	4
12.7	13.6	14.8	15.7	14.2	14.5	32.4	19.8	15.6	NGABU	5
11.0	14.2	18.1	15.5	18.8	15.6	36.0	12.3	12.2	NGABU	6
10.9	10.7	11.2	11.9	13.4	15.2	35.5	9.4	11.4	NGABU	7
4.1	5.0	7.0	5.5	6.5	6.0	23.7	5.1	6.2	NGABU	8
4.8	8.7	10.9	8.8	8.8	9.2	25.9	9.5	10.3	NGABU	9
15.6	22.7	23.7	20.6	22.2	23.3	36.9	22.7	21.3	NGABU	10
58.5	59.7	71.7	67.0	62.3	66.2	77.5	78.1	63.7	NGABU	11
161.3	181.2	185.0	161.2	164.9	164.9	139.8	157.3	153.2	NGABU	12
316.3	341.8	328.2	332.0	325.1	331.3	301.5	322.5	335.9	SALIMA	1
272.6	253.8	295.3	292.0	271.7	265.0	203.0	276.4	270.7	SALIMA	2
243.0	299.8	286.1	280.5	274.7	278.0	152.8	265.9	250.2	SALIMA	3
72.9	67.7	59.1	74.1	76.1	64.8	70.9	73.9	84.4	SALIMA	4
8.6	10.7	7.9	9.3	8.3	10.4	40.4	10.2	10.1	SALIMA	5
1.2	1.6	4.3	1.5	0.9	1.6	52.0	0.9	0.7	SALIMA	6
0.3	0.7	2.4	1.6	1.2	1.7	48.7	0.6	1.2	SALIMA	7
0.6	1.2	1.6	1.3	3.1	2.9	43.9	1.5	1.9	SALIMA	8
0.2	0.8	2.0	2.2	1.5	2.3	36.0	0.7	0.4	SALIMA	9
5.3	9.2	6.6	7.1	8.4	8.4	47.3	11.7	7.7	SALIMA	10
38.1	32.4	29.1	31.0	28.6	28.7	67.1	50.7	33.7	SALIMA	11
238.9	241.8	236.3	268.0	253.7	245.4	210.0	227.1	235.3	SALIMA	12